The Impact of Aluminum on the Initiation and Development of $MnO_{x(s)}$ Coatings for Manganese Removal

Gary Stephen Hinds

Thesis submitted to the faculty of the Virginia Polytechnic Institute and State University in partial fulfillment of the requirements for the degree of

Master of Science
In
Environmental Engineering

William R. Knocke
Mitsuhiro Murayama
John E. Tobiason

May 4th, 2015
Blacksburg, VA

Keywords:
Manganese, Aluminum, $MnO_{x(s)}$ Coating

The Impact of Aluminum on the Initiation and Development of $MnO_{x(s)}$ Coatings for Manganese Removal

Gary Stephen Hinds

ABSTRACT

Many treatment facilities remove soluble Mn by an autocatalytic adsorption-oxidation process involving manganese oxide ($MnO_{x(s)}$)-coated filter media and a free chlorine residual known as the natural greensand effect (NGE). In recent years, significant amounts of aluminum (Al) have been found integrated into $MnO_{x(s)}$ coatings on media from drinking water treatment facilities worldwide. The primary objective of this study was to characterize $MnO_{x(s)}$ coatings developed in the presence and absence of Al, and to further define the role played by Al in the coatings' initiation and development. A secondary objective of the study was to examine the potential for pre-filter oxidation of Mn and formation of nano-size $MnO_{x(s)}$ particles, which would be destabilized by $Al(OH)_{3(s)}$ and captured in the filter. This material could act as a seed for coating formation and help explain the integration of Al into $MnO_{x(s)}$ coatings. Bench-scale column tests were conducted to examine Mn removal and backwash composition, while centrifugation and ultrafiltration were utilized to examine the potential for rapid Mn oxidation. Results indicate that the presence of Al augments the initiation and development of $MnO_{x(s)}$ coatings. The backwash solids of columns loaded with Al were composed of a mixture of Mn and Al, suggesting that active adsorption-oxidation sites were present in the $Al(OH)_{3(s)}$ floc captured by the filter. These results suggest at least a small amount of pre-filter $MnO_{x(s)}$ formation by contact with free chlorine; further, that $Al(OH)_{3(s)}$ solids present may destabilize these negatively charged solids into a form that is important to $MnO_{x(s)}$ coating formation.

ACKNOWLEDGEMENTS

I would like to extend thanks to several people for their assistance and involvement in this research project. First and foremost, I would like to thank my advisor Dr. William Knocke, whose guidance, insight, and funding have made this project possible. The lessons and experiences I gained as a result of working with Dr. Knocke make up the most valuable portion of the degree I received from Virginia Tech. Additionally, I would like to thank Dr. Mitsu Murayama and Dr. John Tobiason for their time and efforts spent on my graduate advisory committee.

Many thanks are also owed to Jeff Parks, who taught me to use the ICP-MS and helped me analyze the hundreds of samples produced by my experiments. From the first day, Julie Petruska proved indispensable to this project; her knowledgeability and readiness to help in all aspects of lab work were much appreciated. Thanks also to Michel Vargas, who provided the SEM data contained in this report.

Finally, I would like to thank the Via Department of Civil and Environmental Engineering for generously providing me with Via Fellowship support during my time in Blacksburg.

TABLE OF CONTENTS

TABLE OF FIGURES

TABLE OF TABLES

1.0 INTRODUCTION

1.1 Background

The removal of soluble manganese (Mn) (defined in this study as truly soluble Mn(II), and not by ability to pass through a given filter size) from surface and groundwater sources by the adsorption-oxidation process known as the natural greensand effect (NGE) has been practiced at water treatment facilities worldwide for decades. The NGE involves the adsorption of soluble Mn(II) ions to manganese oxide ($MnO_{x(s)}$) coatings developed on the media surface. These adsorbed ions are rapidly oxidized in a surface-catalyzed reaction by a free chlorine residual added prior to the filter and maintained across the bed depth, and become part of the $MnO_{x(s)}$ coating structure. These sites are subsequently available for adsorption of additional Mn(II) ions, resulting in a continuous process of adsorption and oxidation. The NGE takes advantage of the catalytic properties of $MnO_{x(s)}$ surfaces to enhance the kinetics of Mn(II) oxidation by free chlorine, which is a slow process in bulk solution at neutral pH (Knocke et al. 1987). The process also eliminates concerns associated with the capture of particulate $MnO_{x(s)}$ formed by oxidizing Mn(II) prior to filtration, another common method of Mn control (Knocke et al. 1991).

Tobiason et al. (2008) discovered consistent levels of aluminum (Al) incorporated into $MnO_{x(s)}$ coatings at several utilities participating in a case study. The authors noted that these findings may indicate a relationship between deposition of Mn and Al on the media surface. In a subsequent study, Jones (2012) examined the interactions between Mn and Al during NGE filtration, concluding that Al was in fact incorporated into $MnO_{x(s)}$ coatings at both the soluble and particulate level. However, the specific mechanisms of interaction between Mn and Al during the development of a $MnO_{x(s)}$ coating were not elucidated.

1.2 Research Objectives

This study further explores the mechanisms by which Al is incorporated into $MnO_{x(s)}$ coatings, and addresses questions regarding the initiation and development of $MnO_{x(s)}$ coatings. Specific research objectives for the project include:

1. To evaluate the impact of Al on the initiation and formation of $MnO_{x\,(s)}$ coatings on virgin media, specifically regarding rate of coating development, Mn removal performance, and surface characteristics of the coatings; and,

2. To explore the potential for pre-filter oxidation by free chlorine of Mn(II) into nano-sized $MnO_{x(s)}$ particles, which may subsequently be destabilized by $Al(OH)_{3(s)}$ floc, be captured by the media bed, and seed the formation of $MnO_{x(s)}$ coating on NGE media.

2.0 LITERATURE REVIEW

2.1 Issues Associated with Mn in Drinking Water

The presence of untreated Mn in finished drinking water is undesirable for a number of reasons. This section outlines the aesthetic and health issues associated with Mn in drinking water, and reviews the applicable regulations for finished water Mn levels.

2.1.1 Aesthetic Issues

Concerns of Mn levels in finished drinking water are currently largely driven by aesthetic issues such as taste and discoloration (AWWA 2011). The US Environmental Protection Agency (EPA) regulates Mn by a non-enforceable secondary maximum contaminant level (SMCL) of 0.05 mg/L (EPA 1979). This level is set as a guideline to prevent water discoloration, stained fixtures, and taste issues, but legal enforcement is left to the discretion of individual states. The issues associated with elevated Mn levels in a distribution system are well documented. Soluble Mn(II) allowed into the distribution system will be oxidized by disinfectant residuals, resulting in buildup of brown and black $MnO_{x(s)}$ deposits on distribution pipe interiors (Kothari 1988; Peng et al. 2010; Sly et al. 1990). These buildups can decrease effective pipe diameter, leading to higher head loss through pipes and increasing operational energy costs (Kothari 1988). In high-flow conditions, built-up $MnO_{x(s)}$ deposits have been observed to slough off pipe walls, leading to water discoloration at customers' taps (Sly et al. 1990). These events are known as black water events, and can be responsible for serious public perception issues about water quality. Biofilms of Mn-feeding bacteria can also develop as a result of elevated Mn levels, which result in their own attendant pipe clogging and taste and odor issues (Kothari 1988; Sly et al. 1990). Certain authors have noted that the current SMCL of 0.05 mg/L may not be low enough to eliminate these problems (Casale et al. 2002; Sly et al. 1990), and Sly et al. recommended that the SMCL be lowered to 0.01 mg/L to address the situation (1990).

2.1.2 Health Issues

Mn is required in trace amounts for human metabolic health, but is toxic at excessive levels. Damage from Mn overexposure is largely neurological in nature, with symptoms comparable to those seen from Parkinson's disease. Mn poisoning in adults is typically associated with inhalation of Mn dust in industrial settings, as adult humans are capable of excreting excess Mn

ingested orally; however, recent studies have suggested that Mn poisoning can occur from prolonged exposure to high-Mn food and water sources, specifically in at-risk populations (Agency for Toxic Substances and Disease Registry 2012).

Health issues attributed to Mn in drinking water are generally considered minimal, since most Mn uptake is assumed to come from food. The World Health Organization (WHO) has set a health-based guideline for Mn concentration in drinking water at 0.4 mg/L based on an assumed no observed adverse effect level equal to their maximum observed daily Mn diet, since no adverse effects were observed from even the largest studied Mn intake (WHO 2011). It has been suggested that the WHO guideline be revised to reflect the effect of oral Mn intake by at-risk populations, notably infants, who excrete excess Mn less effectively than adults (Ljung & Vahter 2007). One study linked drinking water Mn content in excess of the WHO guideline to a decrease in children's scores on mathematics exams (Khan et al. 2012). A later study of children in South Korea examined the effect of blood Mn level on children's performance on a range of cognitive, attention, and behavioral tests. The study linked the highest 5^{th} percentile of blood Mn level with reduced scores on thinking, reading, and calculation-based tests; the lowest 5^{th} percentile also struggled with certain neurological assessments (Bhang et al. 2013).

2.2 Mn Chemistry and Sources

Mn undergoes a wide range of complex oxidation reactions, making control of Mn in drinking water complicated and sometimes difficult. This section reviews the oxidation chemistry of Mn and provides an overview of the sources of Mn in drinking water. The factors affecting seasonal and chronic Mn issues are discussed, and their impacts on water treatment facilities described.

2.2.1 Mn Oxidation States

Manganese can exist in up to 11 oxidation states, but only a few are consistently important to water treatment processes. In its reduced state of Mn(II), which is one state in which Mn is commonly found in natural waters, Mn is highly soluble (Brezonik & Arnold 2011). Soluble Mn^{2+} is a stable species in the absence of an oxidant such as dissolved oxygen. Mn^{2+} does form a complex with natural carbonate in waters ($MnCO_{3(s)}$), but this salt is quite soluble for pH values below approximately 8; based on solubility constants reported by Brezonik and Arnold (2011), at a pH of 7 and a Mn concentration of 0.2 mg/L, alkalinity would need to be present at values in

excess of 15 meq/L in order for $MnCO_{3(s)}$ to precipitate, compared with approximately 1.5 meq/L at pH 8. Accordingly, this compound is generally not important for natural systems and most water treatment processes (those which require elevated pH, such as lime-soda ash softening, precipitate $MnCO_{3(s)}$). When Mn is oxidized, either in a natural setting by dissolved oxygen or in a water treatment setting by an applied strong oxidant, typically the two states formed are Mn(III) and Mn(IV), which are both highly insoluble. Mn(III) generally takes the form of the stable oxyhydroxide manganite (γ-$MnOOH_{(s)}$), whereas Mn(IV) is typically present in natural and engineered systems as $MnO_{2(s)}$. Permanganate (MnO_4^-), which contains Mn(VII), is occasionally used to oxidize Mn(II) and can be formed when Mn(II) is oxidized by ozone, but is not naturally formed (Brezonik & Arnold 2011).

2.2.2 Sources of Mn

Mn is found in both surface water and groundwater sources, and can be either a chronic or a seasonal problem. Mn is contributed to groundwater sources from the earth's crust, approximately 0.1% of which is composed of Mn in various mineral forms (National Academy of Sciences 1973). These Mn-containing minerals, which often have Mn(II) adsorbed to their surfaces, are reduced and dissolved by the reducing conditions common to groundwater sources and biological activity in the soil. Mn concentrations in groundwater tend to be relatively stable over time, but can vary substantially over relatively small geographical areas. Utilities drawing from multiple wells might find that their influent Mn concentration varies significantly based on which wells are currently being drawn from (Brandhuber et al. 2013). A 2011 nationwide survey of groundwater sources by the USGS found that approximately 34% of wells sampled had natural Mn concentrations in excess of the EPA SMCL of 0.05 mg/L (USGS 2011).

Mn can be found in surface water from lakes and reservoirs and from streams and rivers. A 2006 study of utilities nationwide found that although utilities using surface water sources generally reported lower annual average Mn concentrations than those using groundwater sources, the maximum concentrations reported from both types of sources were comparable (Kohl & Medlar 2006). This reflects the seasonal nature of Mn issues experienced by many surface water sources, particularly lakes and reservoirs.

Impounded water bodies tend to contain Mn deposits in their sediments, which participate in the metabolic cycles of microorganisms. Mn reducing bacteria reduce Mn(IV) to the soluble

Mn(II) in deeper layers of the sediments, where anaerobic conditions exist. At higher layers where oxygen is available, Mn(II) is converted back to Mn(IV) by Mn oxidizing bacteria, preventing Mn(II) from diffusing upwards. When a lake or reservoir is well mixed, the aerobic zone often penetrates into the sediment-water interface, preventing the release of Mn(II) into the water column.

However during periods of thermal stratification, typically experienced during the summer months, the colder bottom layer of a lake or reservoir (known as the hypolimnion) is isolated from atmospheric oxygen. Dissolved oxygen is frequently consumed entirely in the hypolimnion, resulting in anaerobic conditions at the sediment-water interface. Under these conditions, Mn oxidizing bacteria must migrate to higher levels in the water column which are still aerobic, resulting in the release of Mn(II) from lake sediments into the water column. Utilities drawing water from the hypolimnetic layer of a lake or reservoir often see high levels of Mn during the summer months for this reason (Brandhuber et al. 2013). Even utilities which draw water from higher layers in the water column may see a spike in Mn concentration during the fall overturn, when cooling of the upper lake or reservoir layers breaks the thermal stratification and the water body mixes thoroughly. These seasonal Mn issues can be problematic for utilities which may not need to practice Mn control for the majority of the year, but might be required to do so for a few months or weeks each year.

Stream and river sources can experience high Mn levels as a result of their watershed geology. Rivers fed by Mn-laden groundwater flows or by runoff contaminated by mine drainage may have chronic Mn problems (Hem 1992; Missouri Department of Natural Resources 2007). Rivers fed by reservoirs or lakes can also be impacted by seasonal variations in Mn content in the lake (Brandhuber et al. 2013).

2.3 Mn Treatment by Strong Oxidants

The treatment of soluble Mn typically consists of oxidizing the metal from its soluble, reduced form of Mn(II) to the insoluble Mn(III) and/or Mn(IV) forms. One way to approach the problem is to use a strong oxidant to oxidize Mn(II) directly in solution to precipitate solid $MnO_{x(s)}$. This material can then be removed from solution by solid-liquid separation techniques such as sedimentation and filtration. This section describes the use of some common strong oxidants.

Oxidants such as permanganate (MnO_4^-) and chlorine dioxide (ClO_2) have been shown to oxidize Mn(II) in solution almost completely in a matter of seconds to a few minutes, depending on solution pH (Knocke et al. 1991). The rate of oxidation exhibits well-documented responses to changing water parameters; oxidation rate increases with increasing initial Mn(II) concentration, pH, and temperature. Knocke et al. (1991) also noted that soluble Mn(II) removal exceeded the levels expected based on oxidant stoichiometry; this extra removal was attributed to the fact that solid $MnO_{x(s)}$ adsorbs soluble Mn(II) out of solution. More recent concerns about the effects of residual Mn levels below the SMCL have led to additional research of the use of these oxidants at low (≤ 0.05 mg/L) initial Mn(II) levels. Gregory and Carlson (2003) showed that the kinetics of MnO_4^- oxidation at initial Mn(II) levels of 0.05 mg/L may be too slow for effective treatment, whereas ClO_2 provides rapid oxidation at even low initial Mn(II) concentrations. Ozone can also be very effective for Mn(II) oxidation (El Araby et al. 2009; Weng et al. 1986; Wilczak et al. 1993).

This approach is subject to concerns with dosing of the strong oxidant, as excess MnO_4^-, ClO_2, and ozone result in undesirable consequences in a distribution system. Dissolved MnO_4^- imparts a pink color to water, and a residual in the distribution system forms $MnO_{x(s)}$ precipitate on pipe walls (Brandhuber et al. 2013). This results in the same aesthetic concerns associated with untreated Mn(II) in a distribution system. Excess ozone can oxidize Mn(II) to Mn(VII), generating MnO_4^- and resulting in the same issues experienced with overdosing MnO_4^- directly (Wilczak et al. 1993). Additionally, on-site generation and destruction of ozone can prove costly. Oxidation of Mn(II) by ClO_2 can yield chlorite (ClO_2^-) as a byproduct, which is a harmful compound and is regulated by the EPA with a maximum contaminant level (MCL) of 1.0 mg/L (EPA, 1979; Knocke et al. 1991). Additional issues may be encountered from the use of any of these strong oxidants in the capture of the particulate $MnO_{x(s)}$ formed, which is often negatively charged and colloidal in nature and may require destabilization and aggregation into larger particles (Knocke et al. 1991). These authors suggested that addition of a strong oxidant should occur prior to a coagulation step if possible to mitigate issues associated with the capture of $MnO_{x(s)}$ colloids. In general, issues associated with dosing strong oxidants to precipitate $MnO_{x(s)}$ may render this method of Mn control undesirable under certain water treatment conditions.

2.4 Treatment of Mn by the NGE

The NGE is a process which involves the adsorption of soluble Mn(II) ions to $MnO_{x(s)}$-coated filter media and subsequent surface-catalyzed oxidation to Mn(IV) by free chlorine added prior to filtration. The NGE has been shown to be extremely effective for Mn removal over a wide range of raw water conditions (Knocke et al. 1988). An understanding of the NGE requires knowledge of Mn sorption and oxidation by free chlorine. This section describes the chemistry of the process and how it is affected by water quality parameters.

2.4.1 Mn Adsorption and Oxidation

The oxidation of Mn by free chlorine in solution has been shown to be a slow reaction at pH values below 8-9 (Hao et al. 1991; Knocke et al. 1987). Hao et al. examined the impacts of changing stoichiometry, pH, and inhibitor conditions on Mn(II) oxidation by free chlorine. Modeling work performed by the authors confirmed that oxidation by free chlorine takes place in two distinct steps: a slow "homogeneous" oxidation of Mn(II) to Mn(IV) in solution, and a fast "heterogeneous" adsorption-oxidation reaction of Mn(II) adsorbed to the surface of already formed $MnO_{x(s)}$ (Hao et al. 1991).

$$HOCl + Mn^{2+} + H_2O \rightarrow MnO_{2(s)} + Cl^- + 3H^+ \quad [1]$$

Slow homogeneous reaction (from Hao et al. 1991)

$$Mn^{2+} + MnO_{2(s)} \rightarrow Mn{\cdot}MnO_{2(s)} \quad [2]$$

$$Mn{\cdot}MnO_{2(s)} + HOCl + H_2O \rightarrow 2MnO_{2(s)} + Cl^- + 3H^+ \quad [3]$$

Fast heterogeneous reaction (from Hao et al. 1991)

These theoretical reactions express stoichiometry for full oxidation of Mn(II) to Mn(IV); typically, the solids formed consist of $MnO_{x(s)}$ where the variable x represents a number which can vary depending upon the mix of Mn oxidation states in the precipitated solid (Morgan & Stumm 1964). These same reactions are the driving force for the NGE; due to the typically short contact times of free chlorine and Mn(II) in solution and the abundance of $MnO_{x(s)}$ sites present in a coated media bed, the fast heterogeneous step dominates Mn(II) oxidation in an oxide-

coated filter bed. As long as a free chlorine residual is maintained through the filter bed to oxidize adsorbed Mn(II) and regenerate adsorption sites, the process continuously builds a coating of $MnO_{x(s)}$ on the filter media.

Solution pH has a profound effect on the kinetics of the NGE, as it impacts both the adsorption and oxidation processes. Morgan & Stumm (1964) showed that at a pH of 7.5, approximately 0.5 moles of Mn^{2+} could be adsorbed per mole of $MnO_{x(s)}$ colloids but at pH values of approximately 9.0, $MnO_{x(s)}$ colloids could adsorb in excess of 2 mol Mn^{2+} per mol. This dependency reflects the ability of active surface sites to adsorb H^+ ions, which renders these sites unable to adsorb Mn^{2+}. Alkaline pH values are defined by lower H^+ concentrations, yielding a higher concentration of available surface sites and enhancing the adsorption of Mn^{2+} from solution. Higher pH values are also associated with faster Mn(II) oxidation. These two effects combine to enhance Mn removal in oxide-coated filter media beds with increasing pH, a phenomenon which has been thoroughly demonstrated in practice by past work (Anjuman et al. 2010; Knocke et al. 1988; Knocke et al. 2010; Tobiason et al. 2008).

Tobiason et al. (2008) identified several factors, including pH, which impacted the uptake of soluble Mn(II) in the absence of free chlorine. Experimentation found that adsorption was enhanced by higher Mn(II) feed concentrations, lower hydraulic loading rates (HLR), and lower concentrations of organic matter. Water hardness was not found to impact the adsorption of Mn; further, no specific link could be established between Mn adsorption and amount of $MnO_{x(s)}$ coating present on the media. This can be attributed to the fact that adsorption occurs almost exclusively on surface sites, and heavily coated media with a thicker coating may not have significantly more available surface sites than lightly coated media since much of the $MnO_{x(s)}$ coating may be covered by outer layers of coating (Anjuman et al. 2010). Additionally, the average oxidation state of the coating surface affects Mn adsorption. Knocke et al. (1988) found that significantly less adsorption occurred on a media sample with an average surface composition of $MnO_{1.4\text{-}1.6(s)}$ compared with two samples whose coatings were composed of $MnO_{1.8\text{-}2.0(s)}$, even though the first sample had more than twice the amount of extractable Mn in its coating. Once the sample with a low oxidation state was regenerated by soaking in $KMnO_4$, its adsorptive capacity was significantly increased.

The importance of using an oxidant to regenerate the adsorptive capacity of the filter has been thoroughly demonstrated, either through continuous free chlorine addition in the influent or

by periodic regenerative backwashing. Knocke et al. (1988) noted that even under a relatively high HLR of 5.1 gpm/ft^2, effective Mn removal was maintained by an oxide-coated media bed with concurrent free chlorine residual. A minimum residual of 1 mg/L as Cl_2 was recommended following filtration.

Cerrato et al. (2011) used X-ray photoelectron spectroscopy (XPS) to illustrate the effect of continuous regeneration by free chlorine on the characteristic valence state of the Mn present in NGE filters. XPS detected significant amounts of Mn(II) on the surface of media after exposure to dissolved Mn(II) and no chlorine; most of this Mn(II) could be released from the media by elution with a mildly acidic (pH 5.0) backwash. Identical samples subjected to a combination of Mn(II) and free chlorine yielded surfaces composed mainly of Mn(IV), from which very little Mn was recovered by acidic elution.

The necessity of free chlorine for effective NGE treatment has been observed in practice as well. A case study by Tobiason et al. (2008) found that eliminating pre-filter free chlorine resulted in elevated soluble Mn levels in the filtered water within a few hours. The study also showed that although the adsorptive capacity of coatings was exhausted in the absence of free chlorine, the $MnO_{x(s)}$ coatings were maintained on the filter media. Further, Mn(II) adsorptive capacity of the coating was restored once free chlorine was reintroduced to the filter-applied water.

2.4.2 Pre-Filter Oxidation & Backwashing

When utilizing oxide-coated filter media to promote Mn removal, it is generally desirable to prevent oxidation of Mn(II) directly prior to filtration. Any $MnO_{x(s)}$ generated directly upstream of an oxide-coated media bed must be removed as particulate matter, which can be difficult due to small size and highly negative surface charge density (Knocke et al. 1991). Pre-formed $MnO_{x(s)}$ particles have also been shown to not contribute to the formation of $MnO_{x(s)}$ coating (Merkle et al. 1997). Very little work has been performed on the pre-filter oxidation of Mn in oxide-coated media settings, since the kinetics of Mn oxidation by free chlorine are known to be extremely slow and in any engineered oxide-coated media removal system the vast majority of Mn removal occurs by adsorption and oxidation. However, the presence of pre-oxidized Mn has been documented as a byproduct of some studies and has been shown to contribute to Mn breakthrough issues in oxide-coated media filters. Hargette & Knocke (2001) monitored the

soluble and particulate (defined in the study as caught by a 0.2 µm filter) Mn input to two filter columns at pH 6.0 and 7.3 after mixing free chlorine and Mn for a short time period (a few minutes). The higher pH filter had approximately four times as much particulate oxidized Mn in the filter-applied water, and removed less total Mn due to particulate Mn breakthrough. Although the vast majority of applied Mn was soluble (the column influents averaged 1.6% particulate Mn at pH 6.0 and 5.9% particulate Mn at pH 7.3), the short contact time of Mn and free chlorine was sufficient to produce a small fraction of pre-oxidized $MnO_{x(s)}$ at both pH values.

Hargette & Knocke (2001) also performed backwash experiments at various rates on these columns and examined the contents of the material recovered during backwash. Backwash Mn content was found to be composed entirely of $MnO_{x(s)}$, indicating that the source of this material was either sheared off coating, pre-formed $MnO_{x(s)}$ particles, or $MnO_{x(s)}$ formed by adsorption-oxidation on pre-formed $MnO_{x(s)}$ particles captured in the filter bed. Not surprisingly, the authors found that increased backwash rates corresponded to greater amounts of Mn released from the bed, as more turbulent backwash enhances scouring of particles from a bed and results in more coating sheared from media. Additionally, the authors found that backwash from the columns operated under higher pH conditions yielded more Mn, which was attributed to the presence of more $MnO_{x(s)}$ particles in the column influent. Interestingly, in almost all cases less than 20% of the $MnO_{x(s)}$ recovered in backwash could be attributed to influent $MnO_{x(s)}$, indicating a significant effect from some combination of adsorption-oxidation on these captured particles and sheared off coating. The authors also generally observed that greater amounts of Mn were recovered with each successive backwash of a column.

Unpublished data by Archana Subramanian also seem to indicate the potential for oxidation of Mn(II) by free chlorine in relatively short periods of time. Subramanian prepared samples with 0.1 mg/L dissolved Mn(II), then filtered them through a parallel range of ultrafilters to obtain a size fractionation. Samples were then exposed to 2 mg/L free chlorine for ten minutes, at which time the samples were once again analyzed by ultrafiltration. The results (shown in Figure 1) indicate that exposure to free chlorine for ten minutes oxidized a small fraction of Mn and created particulate $MnO_{x(s)}$ which was detected at all membrane sizes (Subramanian).

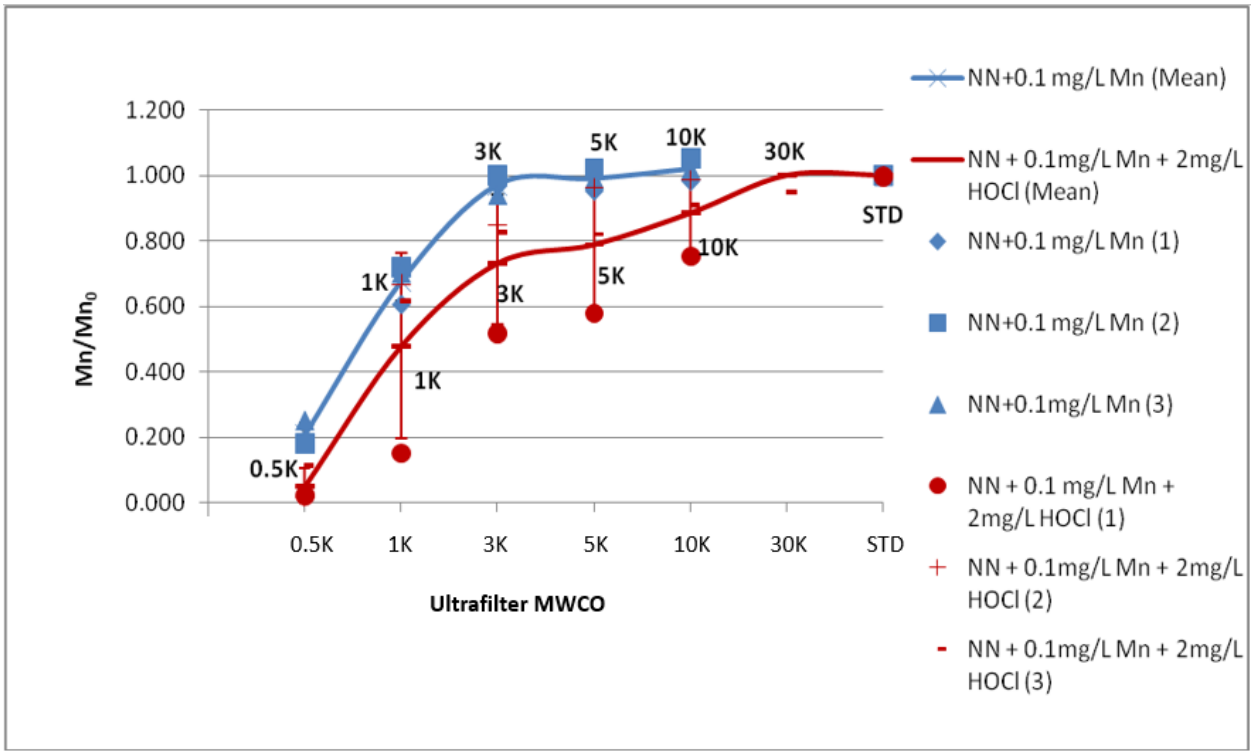

Figure 1: Mn Removal by Ultrafilter Molecular Weight Cutoff Before and After Chlorination. Subramanian, Archana. Unpublished Data, Used under Fair Use, 2015.

2.4.3 Coating Initiation and Development

The initiation mechanism of $MnO_{x(s)}$ coating on uncoated (virgin) media is not precisely known. Merkle (1996) suggested that native mineral deposits (calcium, aluminum, and iron) present on virgin anthracite coal media might have been responsible for initial sorption of Mn(II) and subsequent oxidation, seeding the formation of a $MnO_{x(s)}$ coating. Merkle (1997) also suggested that silanol groups (Si-OH) (which can be present on the surface of media or on clay particles retained in the bed) may play a role in initial adsorption of Mn(II). Regardless of the initiation mechanism, the literature agrees that significant adsorption of Mn(II) only occurs on $MnO_{x(s)}$, and until a coating is developed with sufficient surface area, removal of soluble Mn is ineffective.

Junta & Hochella (1994) used electron microscopy techniques to examine the development of $MnO_{x(s)}$-based coatings on iron-based minerals in the presence of dissolved oxygen. The authors found that the $MnO_{x(s)}$ coatings tended to initiate at surface features (such as ridges and steps) and either propagated horizontally across a surface to form a thin coating along the entire

surface or grew vertically and along features to form large precipitate patches depending upon the characteristics of the base surface.

Formation of oxide coatings on filter media has been shown to occur in layers, often resulting in the creation of ring-like stratification in the coating reflecting temporal changes in influent composition over time (Tobiason et al. 2008; Jones 2012). Tobiason et al. (2008) noted the tendency of coatings to smooth out large-scale features on the surface of sand media from full-scale filters, reflecting the tendency of adsorption and oxidation to occur at such surface features.

It has been theorized that the layered formation of coating has the ability to entrain particulates, effectively cementing them into the coating. Merkle (1996) used microscopic imaging of a surface formed in an active treatment plant to observe a diatom cemented into the $MnO_{x(s)}$ coating formed on the media. Jones (2012) discovered that in filter column experiments with particulate levels of Al applied in the feed waters, columns subjected to higher Mn loading exhibited improved capture of Al particles at all sizes. Jones later examined the resulting surfaces using scanning electron microscopy (SEM), and found a matrix of crystalline material and amorphous material which was suggested to be Al floc entrained in $MnO_{x(s)}$ coating.

Indirect evidence of this phenomenon was also presented by Goodwill (2006), who correlated the apparent Brunauer-Emmett-Teller (BET) surface area of $MnO_{x(s)}$-coated media samples with the amount of extractable Mn found in these coatings. Goodwill found that samples taken from filters responsible for particle removal as well as soluble Mn removal yielded a roughly linear relationship of approximately 0.84 m^2 of surface area gained per mg additional Mn in the coating; conversely, samples from filters and second-stage contactors which were not subject to significant particulate loading generally were found to have significantly less surface area per mg extractable Mn and exhibited a much lower regression slope of surface area gained per mg extractable Mn in the coating. Goodwill's data from particle filters and second-stage filters can be found in Figure 2, along with previous data from Merkle (1997) reflecting samples from particle filters.

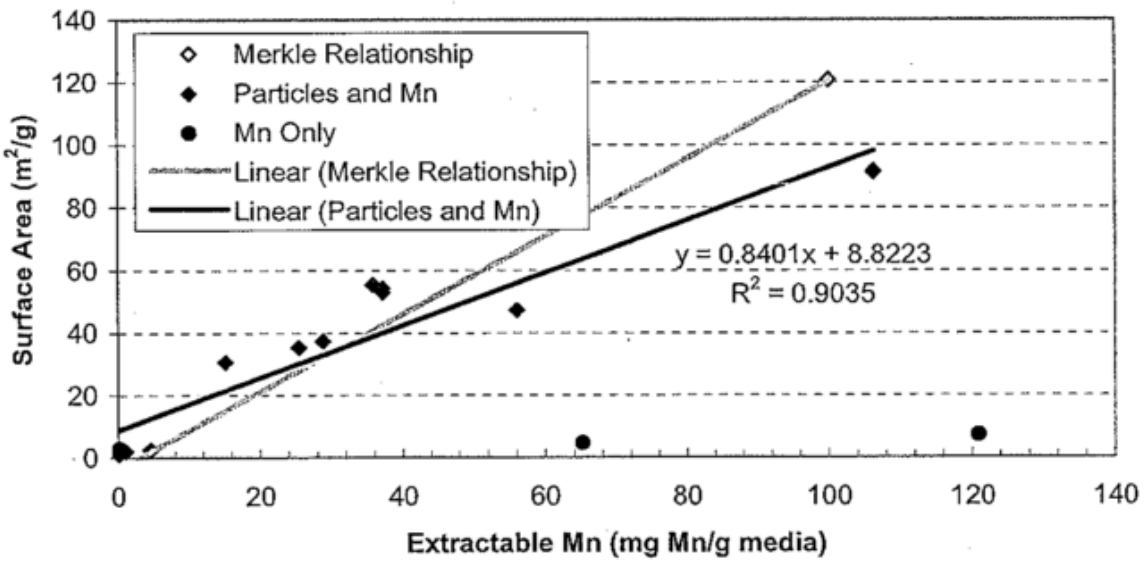

Figure 2: BET Surface Area of Oxide-Coated Media by Coating Extractable Mn. Goodwill, J., 2006. *Characterization of Manganese Oxide Coated Filter Media*. Master's Thesis, University of Massachusetts Amherst; Used with Permission of Joseph E. Goodwill, 2015.

(Circular data points represent samples from second-stage (post-filter) contactors; diamond-shaped points (including data from Merkle (1997)) represent samples taken from single-stage particle filters also practicing adsorption-oxidation of soluble Mn)

2.5 Al Incorporation in $MnO_{x(s)}$ Coatings

Several studies of $MnO_{x(s)}$ coatings developed in active water treatment plants have reported significant amounts of Al incorporated in the coatings (Goodwill 2006; Jones 2012; Merkle 1996; Tobiason et al. 2008). Results obtained by Tobiason et al. (2008) yielded a surprisingly consistent molar ratio (between 1.0 and 2.0 mol Al/mol Mn) of Al to Mn within $MnO_{x(s)}$-coated media from full-scale filter beds, even within one plant which used ferric-based coagulants as opposed to the Al-based coagulants used at other facilities in the study. These results led the authors to suspect that a relationship may exist between Mn and Al which is responsible for this incorporation. This section examines the role of Al in water treatment and describes past work on interactions between Mn and Al under conditions typical of NGE filters.

2.5.1 Al Chemistry and Sources

Al is present in its Al(III) state in virtually all settings of importance to water treatment. Al does not participate in any oxidation or reduction reactions except in extreme conditions (Brezonik & Arnold 2011). Aqueous Al^{3+} typically hydrolyzes and precipitates as aluminum

hydroxide ($Al(OH)_{3(s)}$), which has low solubility in the neutral pH ranges typically encountered in water treatment plants. $Al(OH)_{3(s)}$ is an extremely low-density amorphous solid (Brezonik & Arnold 2011). Most natural waters contain at least low levels of Al, but Al levels in surface water treatment settings are typically augmented by the addition of treatment chemicals. Many utilities use Al-based coagulants to treat waters for turbidity and dissolved organic carbon removal. In the case of a single-stage filter for turbidity removal and soluble Mn treatment, the precipitates of these chemicals are applied directly to oxide-coated media; in the case of a two-stage process where a $MnO_{x(s)}$-coated bed is operated for Mn removal after a conventional particle filter removes turbidity, only soluble Al is present during Mn treatment.

2.5.2 Interactions between Mn and Al

Soluble Mn is not known to adsorb to $Al(OH)_{3(s)}$ floc significantly at pH values under 7.5. A study by Wang et al. (2012) suggested that chemical adsorption of Mn^{2+} onto $Al(OH)_{3(s)}$ occurred at pH 8.5, but at pH values of 7.5 and 6.5 any sorption that occurred was likely physical and very weak. Unpublished data by Jones (2012) demonstrated no enhanced Mn^{2+} capture on a range of filter sizes with the addition of incrementally greater Al concentrations at pH values between 6.1 and 6.3, suggesting that adsorption of Mn^{2+} to $Al(OH)_{3(s)}$ is not common under conditions typically present in drinking water filtration. $Al(OH)_{3(s)}$ is known to aggregate colloidal $MnO_{x(s)}$, and as mentioned previously is recommended to aid capture of $MnO_{x(s)}$ solids formed by the use of strong oxidants.

Jones (2012) examined potential interactions between Mn and Al during the NGE process, studying the effects of soluble and particulate Al on the adsorption of Mn. Jones found that soluble Al is adsorbed by $MnO_{x(s)}$ coatings, but does not affect the concurrent uptake of soluble Mn; similarly, the uptake of soluble Mn does not appear to affect the uptake of soluble Al. The total mass of accumulated soluble Al uptake Jones observed in laboratory-coated samples was not sufficient to account for the Al levels reported incorporated into coatings by Tobiason et al. (2008). As a result, Jones conducted experiments with particulate $Al(OH)_{3(s)}$ to determine the potential for integration of particulate Al into $MnO_{x(s)}$ coatings. The results indicated that integration of $Al(OH)_{3(s)}$ does occur, but only with simultaneous deposition of Mn^{2+}. Interestingly, Jones reported that higher Mn loadings (and therefore greater Mn deposition) appeared to enhance the capture of $Al(OH)_{3(s)}$ particles of all sizes. Transmission electron

microscopy (TEM) conducted on Jones' samples coated in the presence of particulate Al revealed a coating composed of nano-sized $MnO_{x(s)}$ crystals interspersed with larger (20-30 nm) amorphous material, which Jones hypothesized to be $Al(OH)_{3(s)}$.

Although the role of Al in the NGE process has not been studied in depth, the integration of particulate Al into $MnO_{x(s)}$ coatings certainly seems to agree with previous observations by Merkle (1996) and Goodwill (2006), indicating that particles can become encapsulated in $MnO_{x(s)}$ coatings and potentially contribute to measured surface area. Additional evidence for this phenomenon was provided by Merkle (1997), who notes that one sample of anthracite coated in a water treatment plant which contained significant levels of Al in its coating exhibited a surface area approximately 10 times higher than samples from other facilities which did not contain high Al levels.

While some recent research has been performed examining the presence of Al on media samples taken from water utilities practicing soluble Mn removal, very little work has been performed to document the initiation and development of coatings in the presence and absence of Al in controlled laboratory settings and to outline the implications of such interactions. The need for additional insight into the role of Al in potentially enhancing $MnO_{x(s)}$ coating development became the primary driving force for this research study.

3.0 EXPERIMENTAL DESIGN & METHODS

This section describes the experimental design used to accomplish the research objectives, and details the methods used in conducting experiments and analyzing data. Experimental work for this research project can be divided into two distinct types of experiments: bench-scale column experiments and batch experiments involving centrifugation/ultrafiltration. The design of both types of experiments is explained, and experimental procedures and equipment used are described.

3.1 Bench-Scale Filter Column Experiments

3.1.1 Experimental Design

The bench-scale column experiments were modeled after the experimental design used by Jones (2012). Feed water was prepared in plastic five-gallon buckets and stored in large plastic reservoirs. Two separate feeds and reservoirs were required: a primary feed which was drawn at a higher rate and a secondary feed which was dosed at a lower rate into the primary feed before introduction to the columns. These feeds were prepared such that the mixing of the two solutions yielded the desired source water characteristics. Preparation of the feed water is discussed in Section 3.1.2.

Water was drawn from the two reservoirs through ¼-inch interior diameter (ID) plastic tubing at prescribed flow rates by two separate peristaltic pumps. For all experiments, one larger set of pump heads drew from the primary feed reservoirs at a rate of 13 mL per minute while a smaller set drew from the smaller secondary feed reservoirs at a rate of 3 mL per minute. The combined 16 mL per minute resulted in a hydraulic loading rate (HLR) of 4 gpm/ft^2 for the filter columns and an empty-bed contact time (EBCT) of 0.9 minutes. The pumps each held four heads, enabling the operation of four columns simultaneously. Feed waters were combined in a plastic tee fitting and the resulting influent allowed to drip directly into the top of the columns.

The columns used were 7/16 inch ID glass tubes obtained from the Chemistry Department on campus at Virginia Tech. Columns were mounted to metal rod stands using burette clamps. A small glass wool plug was inserted into the bottom of the columns to support the media bed. The bottom of the columns were coupled using a short sheath of ½ inch ID plastic tubing to a ½ X ¼ inch plastic coupling, which directed column effluent into a ¼ inch ID tube for discharge. The effluent tube was positioned so that effluent would drip into a funnel at an elevation above the

top of the media bed to maintain standing water and positive hydraulic head across the entire depth of the media. This funnel directed effluent water into a sink. The pumps and columns were kept contained in a plastic tub which drained to the sink for spill protection. Figure 3 presents a process flow diagram for the benchtop column experiments.

Unless otherwise noted, all column experiments described in this paper were conducted using a six-inch bed of initially uncoated filter sand. The sand used was FilterSil 0.50 manufactured by Unimin Corporation (New Canaan, CT), which has the characteristics presented in Table 1. Uncoated media was chosen as opposed to precoated media in order to be able to specifically observe the initiation of $MnO_{x(s)}$ coatings on the media surface under a variety of controlled experimental conditions.

Table 1: Virgin Filter Media Characteristics

Parameter	Value
Effective Size	0.5 mm
Uniformity Coefficient	1.63
Specific Gravity	2.65
Extractable Mn	< 0.001 mg/g dry media
Extractable Al	< 0.001 mg/g dry media

A series of experiments were performed using this experimental setup to ascertain the impact of precipitated Al solids on the formation and development of $MnO_{x(s)}$ coatings on the sand media. Several experiments were conducted with and without added Al. Throughout these experiments, both pH and free chlorine concentration were monitored in the column effluent to ensure the desired conditions were being maintained. Samples were collected frequently at the column influent tee fitting and effluent discharge tube to monitor Mn and Al removal through the column.

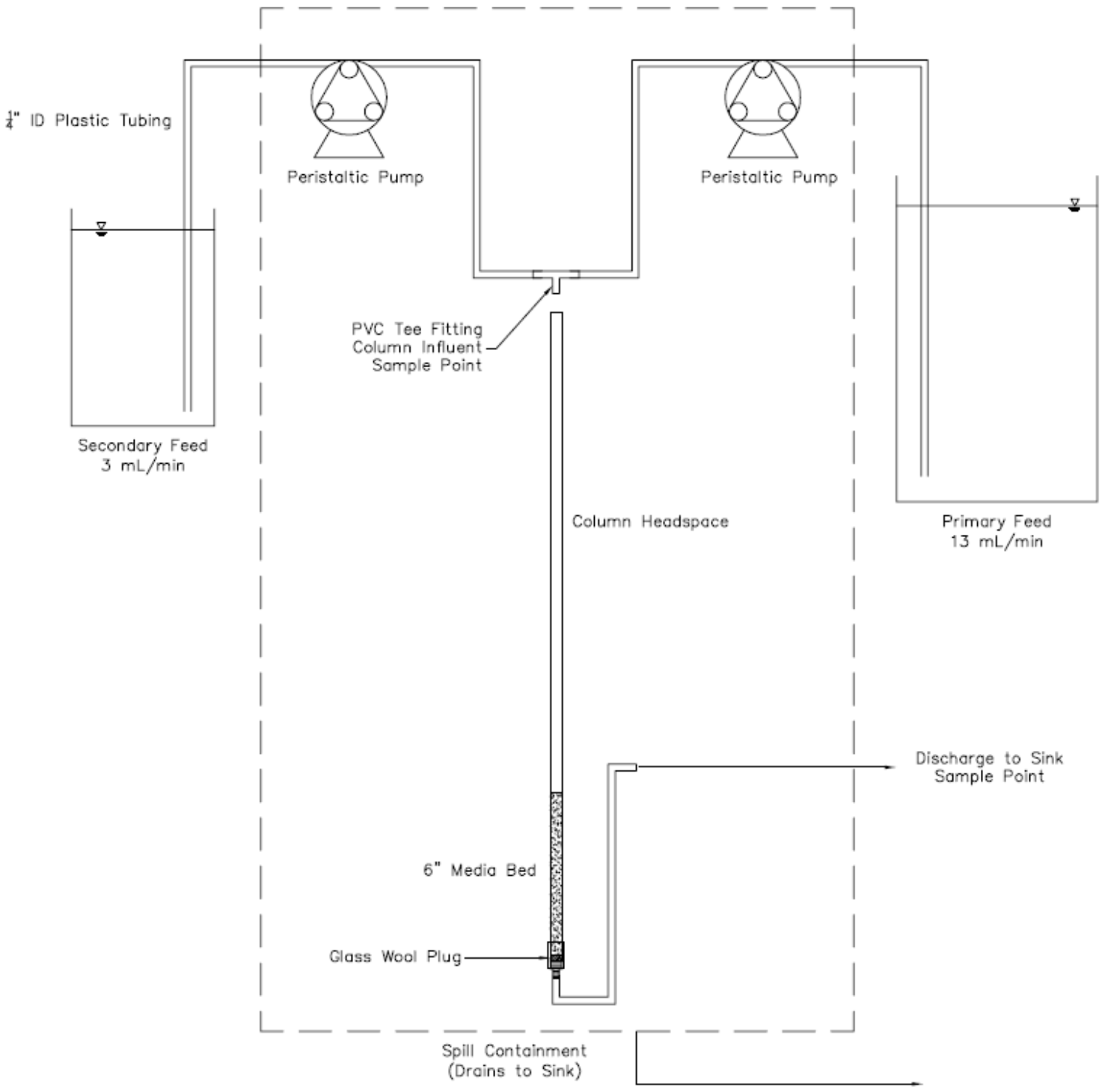

Figure 3: Schematic of Bench-Scale Column Experimental Layout

3.1.2 Manganese-Only Experiments

Deionized water (DI) was used as the base for all prepared feeds in order to maintain control over the composition of the feed water. Mn stock solutions were prepared from powdered manganese chloride tetrahydrate ($MnCl_2 \cdot 4H_2O$) and nanopure water. The manganese chloride was dissolved in nanopure water to achieve 1 g/L as Mn(II). This stock was prepared at least once per week to minimize the slow oxidation of Mn by dissolved oxygen. For all experiments performed prior to June 16, 2014, manganese was added via the secondary feed (drawn at 3 mL/min). This feed was prepared by dosing DI with soluble Mn(II) from the prepared stock to 1.067 mg/L, which was subsequently diluted by the primary feed to the required 200 µg/L Mn(II). The primary feed for these experiments (drawn at 13 mL per minute) was prepared with alkalinity added from sodium bicarbonate powder, free chlorine added from bleach, and pH adjustment by hydrochloric acid addition. These feed waters, when mixed at their respective rates, yielded a column influent with the typical characteristics presented in Table 2.

Table 2: Combined Feed Characteristics for Manganese-Only Experiments

Alkalinity (meq/L)	0.8
Free Chlorine (mg/L as Cl_2)	2.5 - 3
Manganese (µg/L)	200
pH	7.0-7.3

Starting on June 16, 2014, the points of addition of Mn and free chlorine were switched to more accurately resemble how free chlorine would typically be dosed in a full-scale water treatment plant. The primary feed was prepared with approximately 250 µg/L Mn instead of free chlorine, and the secondary feed now consisted of 16 mg/L as Cl_2 free chlorine with pH adjustment from hydrochloric acid to prevent localized high pH conditions when the two feed solutions mixed. The combined characteristics of the column influent remained identical to all previous experiments, and no observable difference in column performance was noted as a result of the switch.

3.1.3 Manganese/Aluminum Experiments

Experiments involving added Al were performed under similar conditions to Mn-only experiments to isolate the effects of Al on the formation of $MnO_{x(s)}$ coatings. Feed solutions were prepared in identical fashion to the method described in Section 3.1.2, with the addition of the desired level of Al from a stock solution of alum to the primary feed. The Al stock was prepared by dissolving alum (aluminum sulfate octadecahydrate, $Al_2(SO_4)_3 \cdot 18H_2O$) in nanopure water to achieve 6 g/L as alum. The resulting solution of $Al(OH)_{3(s)}$ was shaken vigorously before dosing the feed solutions to ensure dosing was performed with a homogenous stock solution. The volume of stock prepared and the rate at which it was used necessitated that the stock be prepared approximately every week, similarly to the Mn stock.

The two feeds were combined to achieve the column influent described in Table 3. As with the Mn-only condition, on June 16, 2014 the addition points of Mn and chlorine were switched to more accurately represent typical water treatment plant conditions. No change in column performance was noted. Two concentrations of Al were tested: a particulate condition and a soluble condition. For the particulate condition, 220 µg/L was chosen as a value at which aluminum hydroxide ($Al(OH)_3$) precipitates at the pH values of interest and which might be observed in the influent to a full-scale filter following alum coagulation and sedimentation (Jones 2012). The soluble condition was achieved by maintaining a concentration of 10 µg/L, which is below the solubility limit of Al^{3+} for the pH range of interest (Brezonik & Arnold 2011).

Table 3: Combined Feed Characteristics for Manganese/Aluminum Experiments

Alkalinity (meq/L)	0.8
Free Chlorine (mg/L as Cl_2)	3
Manganese (µg/L)	200
Aluminum (µg/L)	220 or 10
pH	7.0-7.3

3.1.4 Alternating Feed Experiment

Data collected from the Mn-only and Mn/Al experiments led to the design of an experiment using variable feeds to elucidate how the presence of Al impacts the Mn removal performance of media. Two columns (Column A and Column B) were operated in parallel; three combinations of influent conditions were applied to the two columns, as laid out in Table 4. During

Combination I, Column B received particulate Al and Column A did not. Once steady-state conditions were established with respect to effluent Mn in Column B, particulate Al addition was discontinued to observe the effect on Mn removal. Column A continued to receive an identical Mn-only feed during this combination (Combination II) for comparison with Column B. After several days, when both columns had reached steady-state conditions with respect to effluent Mn, particulate Al was added to the feed for Column A, which had not yet been exposed to Al. Column B continued to receive a Mn-only feed during this last period (Combination III).

Table 4: Alternating Feed Experimental Conditions

	Combination I		**Combination II**		**Combination III**	
	Column A	**Column B**	**Column A**	**Column B**	**Column A**	**Column B**
Mn (µg/L)	200	195	194	197	198	202
Al (µg/L)	0	160	0	0	104	0
pH	6.9-7.2	7.0-7.3	7.1-7.4	7.1-7.4	7.1-7.3	7.0-7.3
Free Chlorine (mg/l as Cl_2)	2.5-2.8	2.1-2.7	2.3-2.6	2.2-2.6	1.7-2.0	2.3-2.5

3.1.5 Backwashing Procedure

For experiments involving particulate Al, the capture of particulates by the filter media resulted in head loss buildup and necessitated backwashing. The glass columns were cut with approximately 18 inches of available headspace above the top of the media bed to accommodate standing water from the head loss generated by anywhere between one and two days of consecutive column operation. Once available headspace was consumed by head loss across the filters, flow was stopped and backwash initiated. Standing water was drained to near the top of the media bed in the column being backwashed. The discharge end of the drainage tube was then connected to a larger separate peristaltic pump which was capable of drawing DI from a jar at approximately 100 mL/min (25 gpm/ft^2), a flow rate sufficient to fluidize the media by 25-30% of its original depth. The influent tee fittings were removed so that a tube could be coupled to the top of the column and directed to the sink such that backwash waste would drip from an elevation close to the top of the glass column into the sink. For experiments in which backwash composition was of interest, backwash was captured in a Nalgene bottle and a representative portion filtered through a 0.45 µm filter. The samples were subsequently analyzed for metals content.

The column was backwashed for approximately ten minutes, allowing approximately one liter of DI to pass through the bed. By this time, no particulate matter was visually observable in the backwash water. The flow of backwash water was then stopped and the effluent tube disconnected from the pump and replaced above the effluent funnel. Backwash water suspended in the column above the media bed which had not been washed out the top drained through the filter until the standing water level was reestablished just above the top of the media bed. The influent tee fitting was replaced and the flow of feed water restarted.

A backwash rate sufficient to produce 25-30% bed expansion, hereafter referred to as "fluidizing backwash rate," has the potential to remove not only captured particulates within the filter but also to shear off some small amounts of coating established on the media by the fluidization and scouring of media (Hargette & Knocke 2001). This material would contribute to the overall Mn content measured in backwash solids, as solid $MnO_{x(s)}$ from sheared off pieces of coating is indistinguishable from solid $MnO_{x(s)}$ formed pre-media and integrated into Al floc. Therefore for some experiments, a sub-fluidizing backwash rate was used prior to the fluidizing backwash rate with the intent of recovering only materials formed pre-media and captured as particulates. For this procedure, the discharge end of the drainage tube was coupled to a small peristaltic pump head which drew water at a rate of approximately 22 mL/min or a hydraulic loading rate of approximately 6 gpm/ft^2. This rate was chosen as the highest flow which produced no visible movement of media grains; as such, this was expected to minimize the potential for dislodging Mn from the media coating.

3.1.6 Cleaning Procedure

At the conclusion of an experiment, a quantity of oxidized Mn was typically visible on the glass and plastic column components which were exposed to the combined feeds. This material had to be removed before beginning a new experiment to mitigate soluble Mn(II) removal from the development of $MnO_{x(s)}$ coatings on the glass and plastic components. Cleaning of the columns was achieved by soaking in a solution of the reducing agent hydroxylamine sulfate (HAS) and an acid bath. The columns were emptied of media but the glass wool plug retained, and the effluent tube clamped shut. A solution containing several grams per liter of HAS was poured in and allowed to soak overnight. The next morning, the solution was drained and retained for future cleanings and the columns rinsed and set into a 10% nitric acid bath. After an

overnight soaking period, the columns were rinsed three times with distilled water and replaced in the burette clamps for future experiments. The combination of reducing agent and acid provided conditions allowing the dissolution and removal of both precipitated $MnO_{x(s)}$ and $Al(OH)_{3(s)}$ solids.

3.2 Centrifugation/Ultrafiltration Experiments

3.2.1 Experimental Design

The centrifugation experiments were designed to replicate the range of conditions created in the column tests and examine the composition of solids formed under the varying conditions. A primary feed water containing soluble Mn(II) (with background ionic constituents) was prepared in a similar fashion to the column experiments and dosed with a concentrated free chlorine solution under pH-controlled conditions. A control solution was simultaneously prepared containing identical conditions, but was not dosed with chlorine. Preparation of these solutions is discussed in Section 3.2.2. Comparison between these two solutions could be used to isolate any fraction of Mn which was oxidized by the added chlorine. Following a prescribed reaction time between the Mn and free chlorine, an excess stoichiometric dose of sodium thiosulfate was added to both solutions to quench the free chlorine residual and stop the oxidation reaction. Sodium thiosulfate was used because it has been shown to instantaneously react with chlorine and stop further oxidation, but to not reduce and dissolve any of the solid $MnO_{x(s)}$ which had already been oxidized (Knocke et al. 1991). The quenched solution and control solution were then subjected to centrifugation and ultrafiltration (UF) for physical separation of solid-phase components.

Six 30 mL Nalgene centrifuge tubes were filled to equal weight with solution. These samples were loaded into an IEC Centra MP4R centrifuge equipped with a six-slot fixed-angle rotor with a maximum rotational speed of 13,400 rpm (15,050 G). A set of samples was typically centrifuged three times, with one pair being removed for measurement after each time increment. The metals content of each sample's supernatant was measured by gently removing the tube's cap and slowly withdrawing 1 mL of supernatant from the top surface of the sample. This aliquot was diluted ten times by addition of 9 mL of nanopure water and the resulting sample acidified for analysis using an inductively coupled plasma mass spectrometer (ICP-MS). The supernatant concentration of Mn or Al was considered to be approximately equal to the truly dissolved

portion of these metals in the sample, and any difference between the centrifuged supernatant concentration and the concentration measured in the original solution prior to centrifugation could be attributed to the formation and subsequent centrifugal separation of solid-phase material. Experiments were carried out using feeds containing Mn only and a combination of Mn and Al to determine any effect of particulate Al on the formation and settling of any solid $MnO_{x(s)}$ formed by free chlorine oxidation of Mn(II).

One experiment was subjected to high-speed ultracentrifugation to enhance separation of solids from supernatant. Samples were collected and balanced in open-top thick-wall polycarbonate Nalgene UltraPlus tubes which were cleaned with soap and water. The samples were then loaded into a Beckman Coulter Optima L-90K centrifuge equipped with a type 50.2 Ti fixed-angle rotor. The centrifuge was operated at a rotational speed of 45,000 rpm, which corresponded to approximately 240,000 G. Samples were centrifuged for eight hours, and supernatant drawn from each sample at the conclusion of the experiment for analysis.

Samples from the same batch of each solution were taken for UF analysis. These results could be compared with the centrifugation results to assess how effectively solid-phase material was removed by centrifugation. Solution was filtered through 30K, 10K, 5K, 3K, and 1K molecular weight cut-off (MWCO) sized Amicon ultrafiltration membranes (EMD Millipore Corporation) to obtain a size distribution of solid particles being formed. Prior to use, the filter membranes were soaked for over one hour in nanopure water which was changed three times during the soak. At least 20 mL of nanopure water were then filtered through the membrane to flush out any organic substance on the membrane which could interfere with measurement. The UF cell was filled with approximately 120 mL of sample and pressurized. The first milliliter of filtrate was wasted, then filtrate was collected in 10 mL samples for ICP analysis. Generally 30-50 mL of filtrate (3-5 ICP samples) were collected to assess any variability of filtrate metals concentration over time with the increasing concentration of metals in the feed. Filter membranes were stored and refrigerated in a 10% ethanol solution after each use.

3.2.2 Feed Water Preparation

Feed waters for the centrifugation and UF experiments were prepared in a similar fashion to the feed solutions for the column experiments, except that a higher concentration free chlorine solution was used to dose the primary Mn solution. The primary solution (which contained all

components except for free chlorine), prepared with DI in a one liter Nalgene container, had the composition detailed in Table 5 (both Mn-only and Mn/Al conditions shown).

Table 5: Primary Feed Characteristics for Centrifugation/UF Experiments

Alkalinity (meq/L)	1
Mn (ug/L)	200
Al (ug/L)	220 or 0
pH	7.0

As with the column feeds described earlier, alkalinity was added as powdered sodium bicarbonate, Mn and Al from stocks prepared as described earlier, and pH adjustment as hydrochloric acid. The secondary solution consisted of DI water and 800 mg/L as Cl_2 of free chlorine added from bleach, with pH adjustment to 7.0 to avoid the creation of localized high-pH conditions upon the addition of the free chlorine solution. The solutions reacted for the prescribed time under the conditions summarized in Table 6, and were then quenched with excess thiosulfate. Control solutions contained the same characteristics and were also dosed with thiosulfate, but received no free chlorine.

Table 6: Dosed Centrifugation/UF Solution Characteristics

Alkalinity (meq/L)	1
Mn (ug/L)	200
Al (ug/L)	220 or 0
Free Chlorine (mg/L as Cl_2)	3
pH	7.0

3.2.3 Cleaning Procedure

After centrifugation by the low-speed Centra centrifuge, tubes were cleaned to remove any $MnO_{x(s)}$ or particulate $Al(OH)_{3(s)}$ adhered to the walls. A weak acid bath of DI acidified to 2% nitric acid was prepared, and the tubes allowed to soak overnight. Tubes were then rinsed thoroughly with DI and allowed to dry. This method was shown to remove leftover $MnO_{x(s)}$ and $Al(OH)_{3(s)}$ particulates which could otherwise contaminate the next sample poured into the tube.

3.3 Analytical Methods

3.3.1 Media Extraction

The method for extracting coatings from $MnO_{x(s)}$-coated media, described in Jones (2012), was adapted from a procedure used by Knocke et al (1990). An aluminum pan was weighed and approximately one gram of media placed in it. The sample was dried overnight at 105°C in an oven, and the dry weight of the media recorded. The media was then placed in 250 mL of nanopure water, to which was added 300 mg of HAS. The solution was then acidified to 2% nitric acid. After at least six hours, ten mL of the solution were withdrawn for ICP analysis. From the dissolved metals concentration in solution, the metals content of the original coating could be calculated in mg metal per gram dry media by the following method:

$$\left(\frac{\text{mg metal}}{\text{g dry media}}\right) = \frac{\text{Concentration in Extraction Solution} \times \text{Volume Extraction Solution}}{\text{Dry Weight Media}}$$

Where the concentration in the extraction solution was determined by ICP analysis of a small sample. This procedure was typically performed on a sample from the top inch and bottom inch of a column bed after the conclusion of an experiment. It was also used to dissolve backwash material caught on glass fiber filters to determine the content of backwash solids in select experiments.

3.3.2 Surface Analysis

Samples of media from the top and bottom of certain column experiments were retained and analyzed using SEM. SEM enables the examination of the physical features of a surface, and was used in this case to search for observable differences between the physical compositions of coatings formed under different conditions. The SEM machine also allows for the performance of energy dispersive spectroscopy (EDS), which involves using a high-energy electron beam to excite electrons in the atoms of the sample itself. The resulting release of the sample electron produces an x-ray pattern unique to that element, which can be detected and used to determine the relative counts of an element. This method enables the identification of chemical compositions of coatings formed under various conditions. More detailed descriptions of SEM technology and methodology can be found in the literature (Goldstein et al. 1981).

The SEM machine used was a FEI Quanta 600 FEG equipped with a Schottky field-emission gun and a Bruker Silicon Drift EDS Detector (model XFlash 4010). Samples were sputter-coated to a thickness of 10 nm with a gold/palladium mixture and analyzed with an acceleration voltage of 10 kV at a working distance of 10 mm.

3.3.3 Leucoberbelin Analysis

Leucoberbelin Blue (LBB) is a blue dye which darkens when exposed to oxidized forms of Mn, allowing for a colorimetric response measurement. An attempt was made to quantify the amount of Mn(II) that was oxidized in Mn(II)-containing samples exposed to free chlorine. The method used was adapted from Cerrato et al (2010). A solution of 0.04% LBB in 0.45 mM acetic acid was prepared and dissolved overnight in the refrigerator. Since the LBB method is incapable of distinguishing between Mn(III), Mn(IV), and Mn(VII), standards were prepared by making a fresh stock solution of $KMnO_4$ in nanopure and diluting to 10, 50, and 100 µg/L as Mn(VII). When considered on an oxidizing equivalence basis, these standards correspond with 25, 125, and 250 µg/L as Mn(IV), which was the species of interest in the experiments (assuming full oxidation to Mn(IV) was accomplished by the free chlorine). The standards, along with a blank sample, were mixed at a 1:5 ratio with the LBB solution and allowed to react for 15 minutes. Samples were then loaded into a 10 cm path length spectrophotometer cell and measured using a Beckman Coulter DU 640 Spectrophotometer at wavelength 620 nm. No distinguishable response could be measured at a concentration below 100 µg/L as Mn(VII) (250 µg/L as Mn(IV)). Since any reaction taking place in the centrifugation experiments appeared to oxidize only a small fraction of the 200 µg/L Mn(II) in solution (likely on the order of 10 µg/L as Mn(IV) or below), it was determined that the LBB method was not feasible for studying Mn(II) oxidation at the low concentrations being tested in this research study.

3.3.4 ICP-MS

Samples were analyzed for concentrations of elements in solution using a Thermo Electron Corporation X-Series inductively coupled plasma mass spectrometer (ICP-MS). Ten mL of sample were collected in capped plastic ICP sample tubes and acidifed to 2% nitric acid. Samples were analyzed using the laboratory procedure, which uses standard SM-1517-014.

3.3.5 pH

Sample pH was measured using an Accumet pH Meter 910 and probe (Fisher Scientific). The meter was calibrated before each use with buffers of pH 4, 7, and 10. The probe was cleaned with nanopure water and dried between each sample measurement to prevent cross contamination. After use, the probe was stored in a pH 4.0 buffer solution.

3.3.6 HACH Benchtop Spectrophotometer

A HACH DR/2400 benchtop spectrophotometer was used to measure free chlorine and to make real-time measurements of manganese and aluminum concentration, especially during column experiments. Free chlorine was measured using the DPD method (HACH method 8021) and reagents. The method has a maximum detection limit of 2.0 mg/L as Cl_2; concentrations higher than this limit were measured by diluting 1:1 with nanopure to halve the free chlorine concentration. Mn and Al were monitored periodically using the HACH procedures to track daily column performance between analyses of ICP sample batches, and to verify the content of solutions prepared for centrifugation and UF. The PAN method (Method 8149) was used to measure Mn, and the ECR method (Method 8326) was used to measure Al. Sample cells were cleaned thoroughly between measurements.

4.0 EXPERIMENTAL RESULTS

This section presents the results of the experiments described in Section 3.0. Results from bench-scale column tests are presented first, including Mn removal data and media coating extractions. Next, results obtained from examination of the content of backwash material from the columns are presented. Data from centrifugation/UF studies are presented last.

4.1 Bench-Scale Column Performance

The development of $MnO_{x(s)}$ coatings on media was documented in part by monitoring the performance of the column regarding Mn removal. Multiple experiments were conducted to ascertain column performance in the presence and absence of Al, and further experiments were designed to examine phenomena observed. Table 7 (located in Appendix A) provides a summary of all experiments which are included in this thesis.

4.1.1 Mn-Only Experiments

The normalized effluent Mn curves for all experiments performed in the absence of Al (Mn-only experiments) are shown in Figures 4 and 5. Results have been plotted on two charts for ease of viewing. For all experiments, the target influent Mn was 200 µg/L; due to small variations in influent concentration between experiments, data points have been normalized to reflect the percent of measured influent Mn concentration exiting the column in the effluent. Specific conditions for each experiment are summarized in Table 7 (Appendix A). Although conditions such as pH and free chlorine concentration varied slightly between experiments, overall trends in the data are apparent. In all cases, effluent Mn concentrations began decreasing within hours of experiment initiation as $MnO_{x(s)}$ coating gradually developed on the media. The rate at which effluent Mn concentration decreased generally appeared to become more gradual over the course of several days, eventually resulting in a quasi-steady-state condition where a relatively constant level of approximately 40% – 60% of influent Mn passed through the media beds. This condition was reached at some point between four and six days in most of the experiments conducted, although Experiments 5 and 6 appeared to reach steady-state effluent Mn conditions earlier. Additionally Experiment 2, which did not remove as much Mn as the other experiments, never reached steady-state effluent Mn conditions. This experiment showed an increase in effluent Mn levels after day eight, followed by improvement in Mn removal over the next three days.

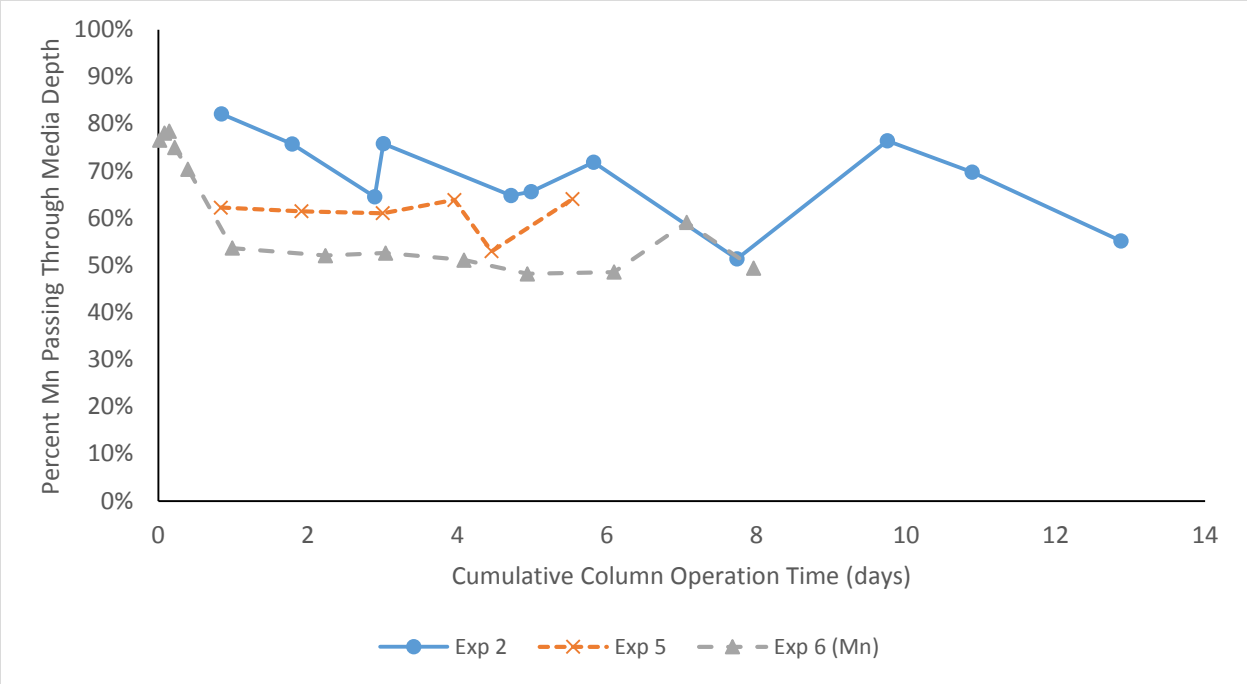

Figure 4: Normalized Mn Removal Curves for Mn-Only Experiments (200 µg/L Mn, 2.5 – 3.0 mg/L free chlorine, pH 7.0-7.3)

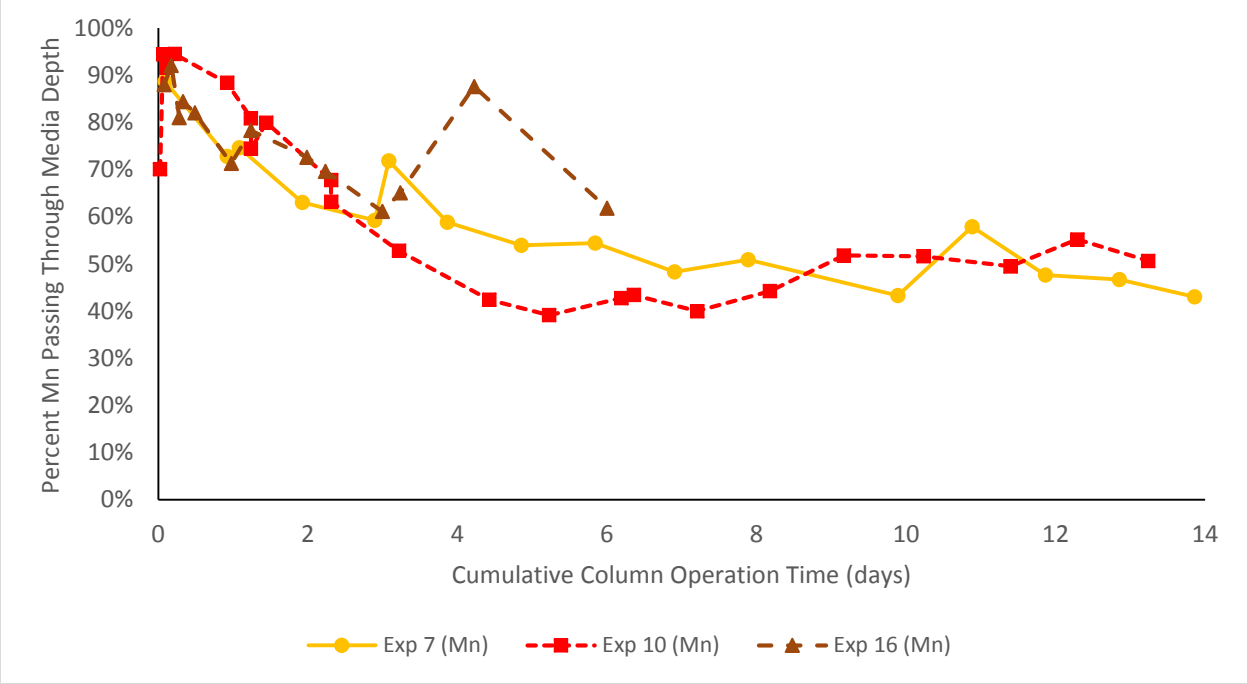

Figure 5: Normalized Mn Removal Curves for Mn Only Experiments, Continued (200 µg/L Mn, 2.5 – 3.0 mg/L free chlorine, pH 7.0-7.3)

4.1.2 Mn/Al Experiments

Normalized effluent Mn curves for all experiments which included both Mn and particulate Al (Mn/Al experiments) are presented in Figures 6 and 7. Data are once again plotted on two separate charts, and are presented on the basis of percent of influent Mn passing through the media bed. Specific conditions for each experiment are summarized in Table 7, which can be found in Appendix A.

In the presence of particulate Al, effluent Mn concentration decreased very rapidly and completely. For all experiments, effluent Mn concentration was below detection limit within one day of experiment initiation. The columns were able to maintain full removal of influent Mn over the entire duration of the experiments, even immediately following backwashing.

A comparison between the Mn removal curves of select Mn-only experiments and Mn/Al experiments can be found in Figure 8. Two of each type of experiment were chosen as representative samples. The most striking differences between the two conditions are the rate of coating formation, discernable in the figure as the rate at which effluent Mn decreases, and the steady-state conditions reached in the effluent Mn levels from each type of column. These differences in coating performance reflect differences in the properties of the coatings.

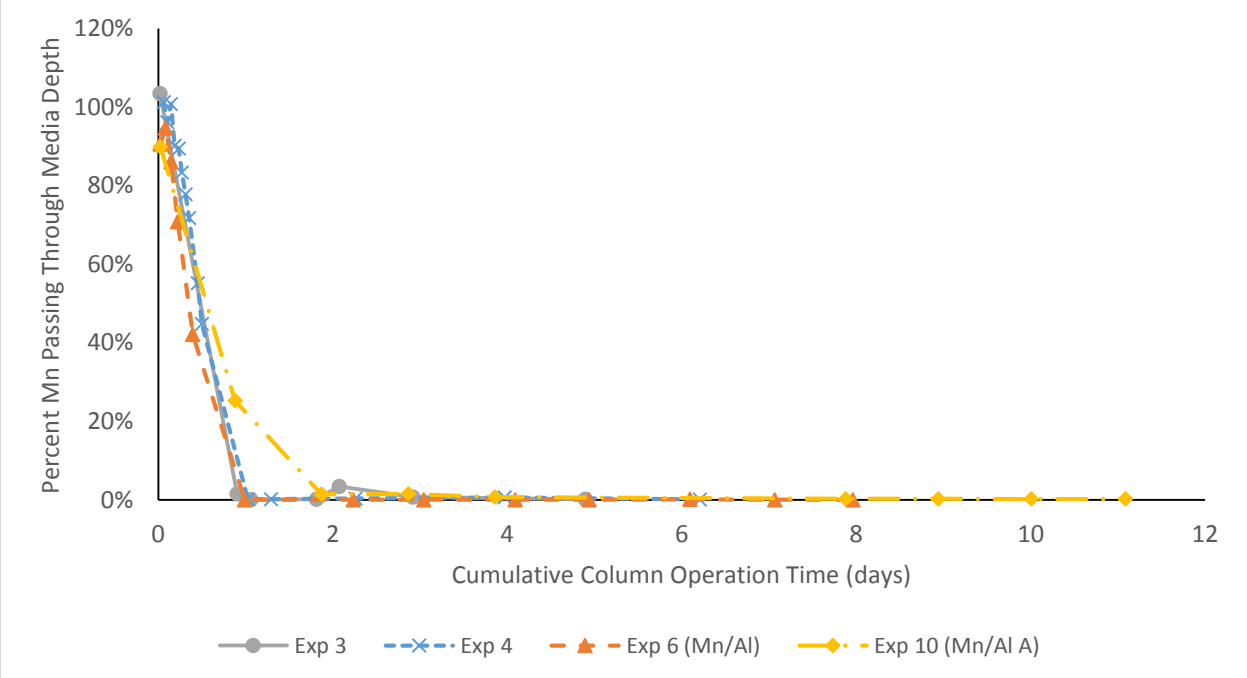

Figure 6: Normalized Mn Removal Curve for Mn/Al Experiments (200 µg/L Mn, 220 µg/L Al, 2.5 – 3.0 mg/L free chlorine, pH 7.0-7.3)

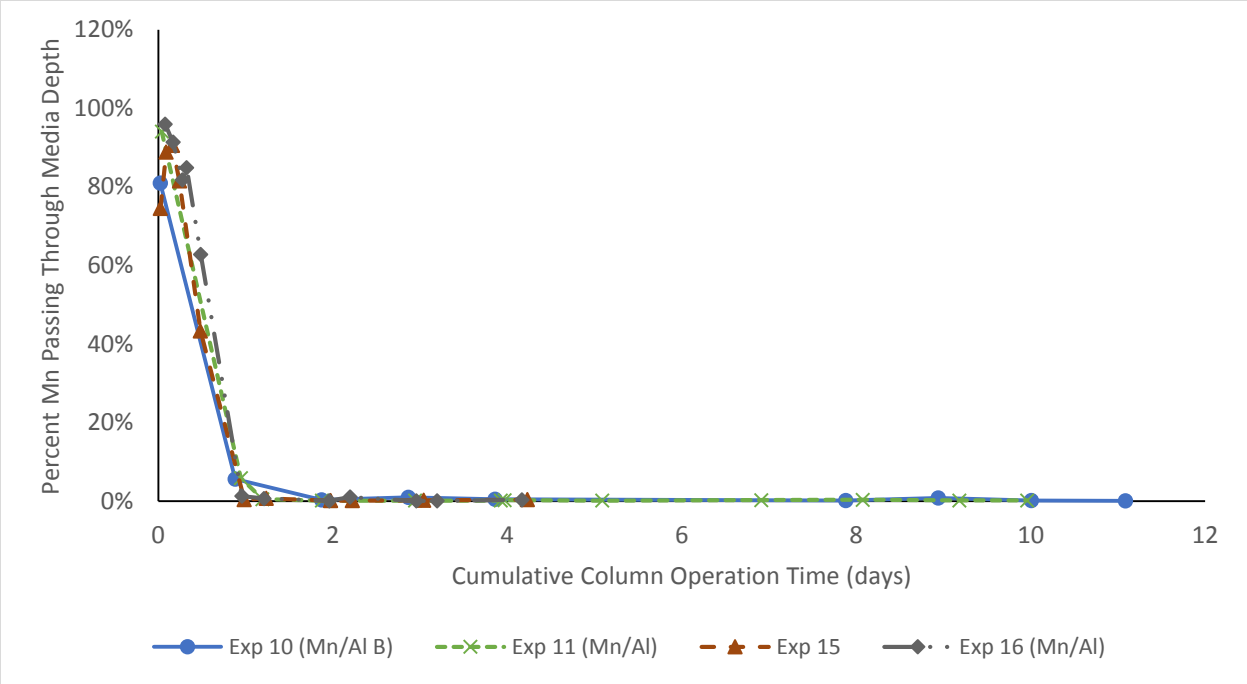

Figure 7: Normalized Mn Removal Curve for Mn/Al Experiments, Continued (200 µg/L Mn, 220 µg/L Al, 2.5 – 3.0 mg/L free chlorine, pH 7.0-7.3)

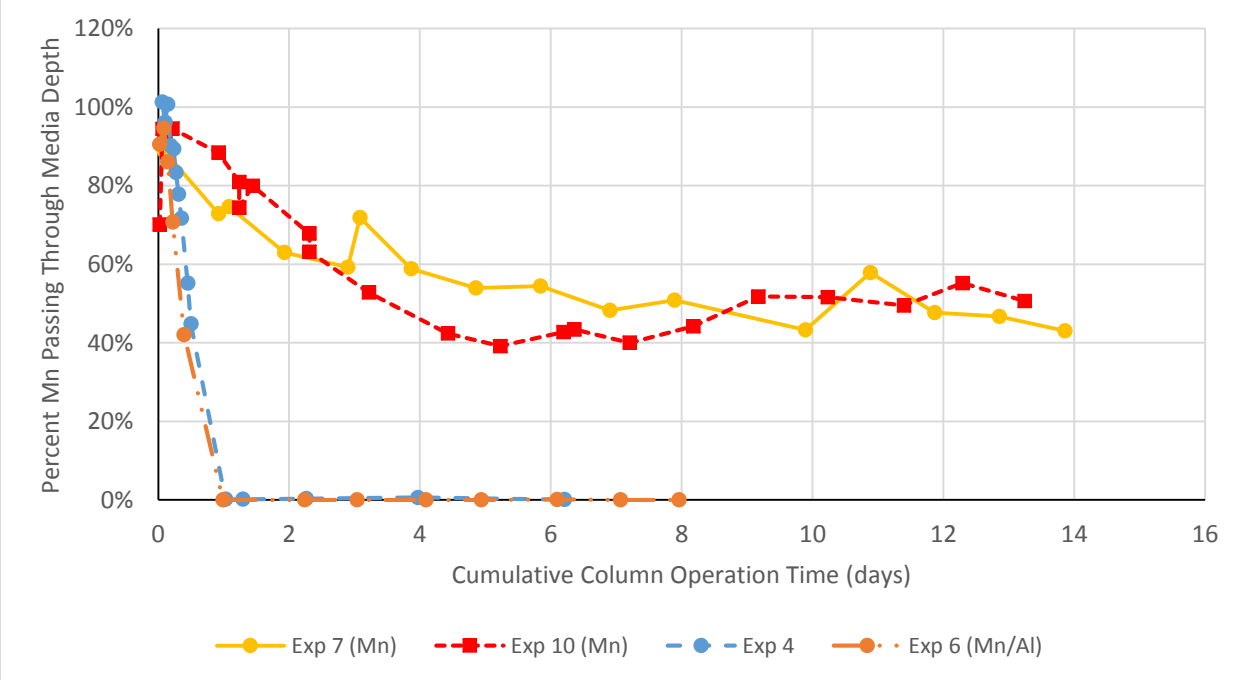

Figure 8: Comparison of Mn Removal Curves for Mn Only and Mn/Al Conditions

Also of interest for the Mn/Al experiments are the Al removal curves, found in Figures 9 and 10. These curves present the effluent Al concentration from the media bed over time. Al passing through a media bed consists of some soluble Al species (concentration determined by pH) and some particulate species which are not captured by the media. The plots were not normalized to influent concentration because the percent of Al passing through the bed is likely to be heavily influenced by the soluble Al portion, which is not a function of the influent Al concentration. Initially, between 40 and 80 µg/L of Al passed through the media, which equates to between approximately 20% and 35% of the target Al concentration of 220 µg/L. Throughout the course of the first day of each experiment, when the capture of Mn was still improving over time (before influent Mn removal reached steady state at 100%), capture of Al improves and appears to reach a steady-state condition coincidentally with the Mn removal curve. This behavior is illustrated in Figure 11, which presents the overlaid Mn and Al removal curves from one experiment for comparison. Typically during the steady-state condition reached by the effluent Al level, between 20 and 60 µg/L of Al exited the columns in the effluent, which equates to between approximately 10% and 30% of the total target influent Al concentration.

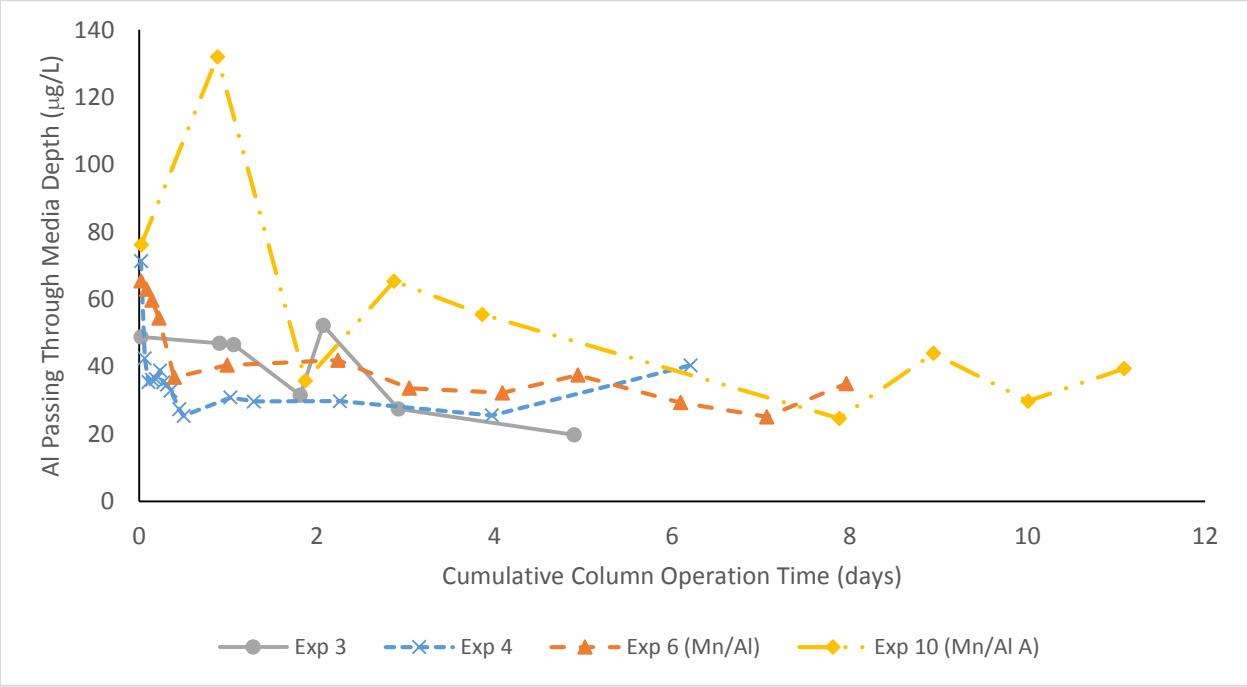

Figure 9: Al Removal Curves for Mn/Al Experiments (200 µg/L Mn, 220 µg/L Al, 2.5 – 3.0 mg/L free chlorine, pH 7.0-7.3)

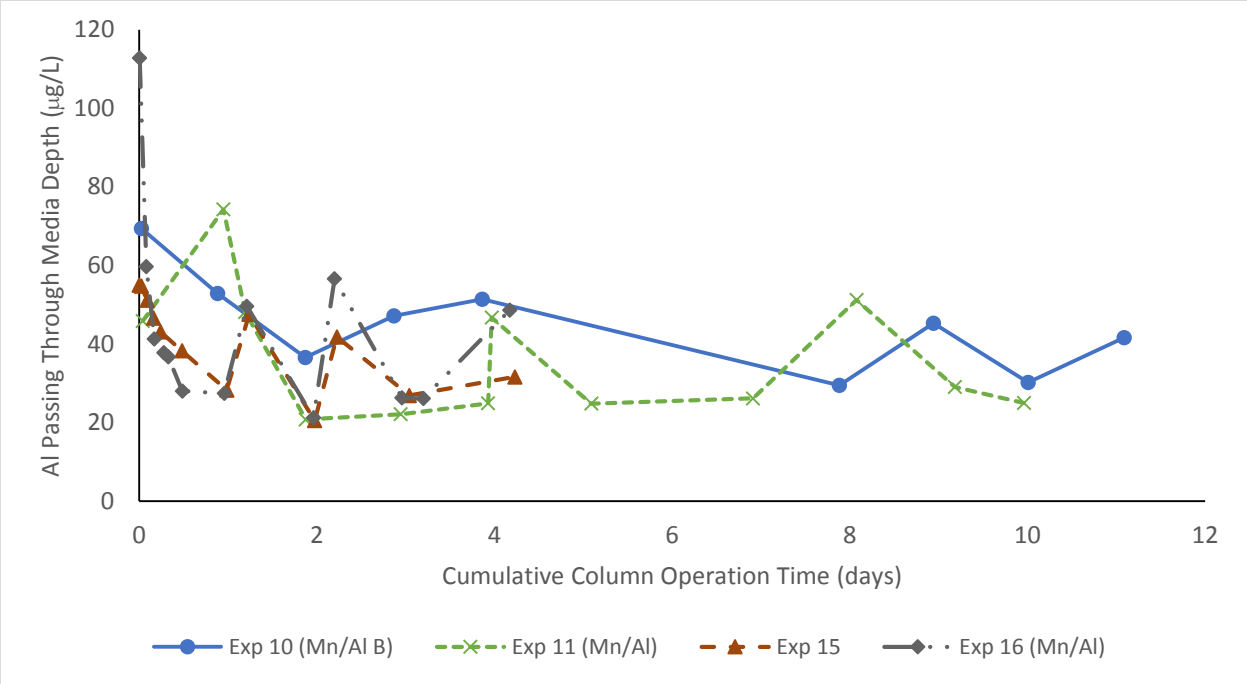

Figure 10: Al Removal Curves for Mn/Al Experiments, Continued (200 µg/L Mn, 220 µg/L Al, 2.5 – 3.0 mg/L free chlorine, pH 7.0-7.3)

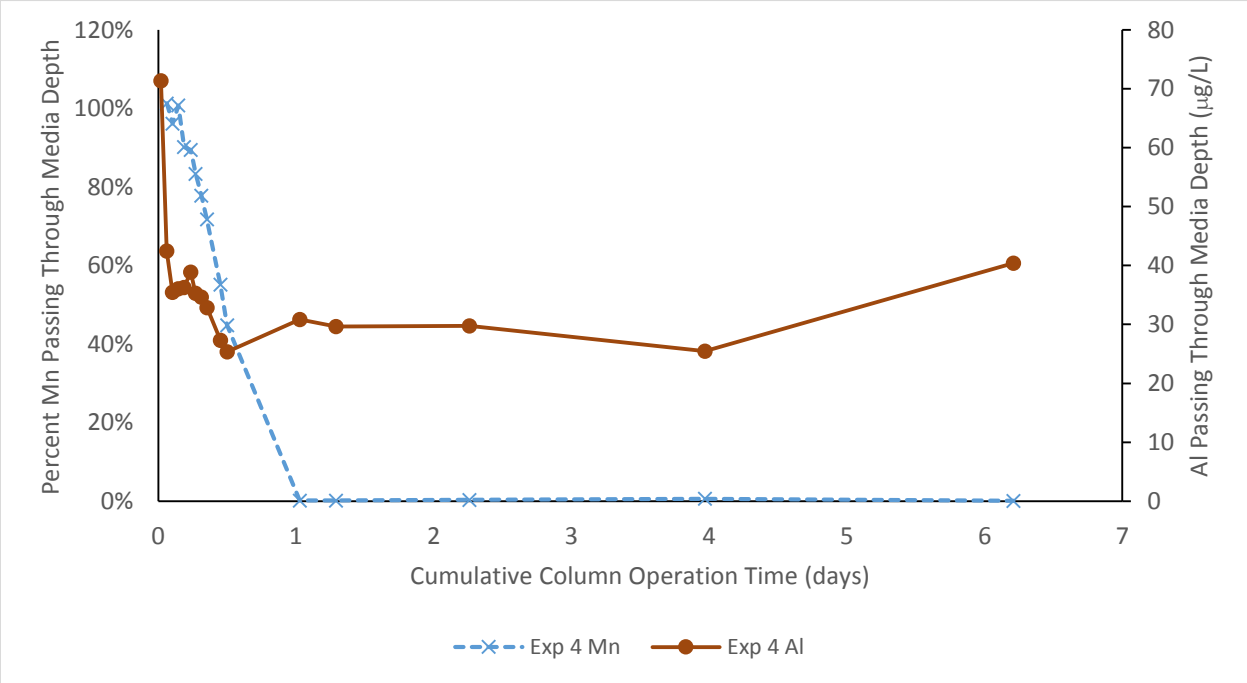

Figure 11: Overlaid Mn and Al Removal Curves for Experiment 4 (to illustrate relationship betwen capture of Mn and Al)

4.2 Comparison of Coatings Formed With and Without Al

Clearly observable differences in the performance of $MnO_{x(s)}$ coatings formed in the presence and absence of Al indicate a distinction in the properties of these coatings. The coatings were examined visually and through extractable metals content to illuminate the effects of particulate Al on the development of coating on media.

4.2.1 Comparison of Media Appearance

For Experiment 16, conducted 11/3/14 – 11/9/14, a time-series of pictures was taken to document the physical appearance of media over time for both Mn-only and Mn/Al conditions. Results are shown in Figure 12. The image consists of six pictures of each column taken between 0 and 144 hours of operation, with a white sheet of paper as background. Images are presented side-by-side for comparison, with the Mn-only condition occupying the left-hand side of each pairing. Significant coloration of both columns can be seen at 24 hours as a brownish-black $MnO_{x(s)}$ deposit begins to form on media in each bed. The Mn/Al column appears to be slightly darker-colored at this stage, indicating greater levels of Mn coating. This is consistent with the Mn removal curves, which show greater amounts of Mn being removed by the Mn/Al columns in the first 24 hours of operation compared with the Mn-only columns. For all Mn/Al columns, 24 hours of operation marked the point at which essentially 100% of the influent Mn was being removed. At subsequent times, the Mn/Al column appears darker than the Mn-only column and individual grains are more difficult to see, again corresponding with the greater Mn removal documented by the removal curves.

Another interesting trend observable in these pictures is the coating gradient between the top and bottom of each column. Because media at the top of the column comes into contact with the highest possible concentrations of Mn and free chlorine, these grains develop more coating and color quicker than the grains at the bottom of the column (Hargette & Knocke 2001). This phenomenon is best seen in the hour 50 pictures in Figure 12. For ease of viewing, these pictures have been enlarged and presented in Figure 13. The gradient appears more pronounced for the Mn/Al column, suggesting that more Mn is removed in the upper layers of the bed in the presence of Al and less Mn is available to coat the bottom layers. This is confirmed by the extractable Mn content found in the top and bottom layers of each column after the full 144-hour experiment, which reveal more Mn coating in the top layers of the Mn/Al column than in the top

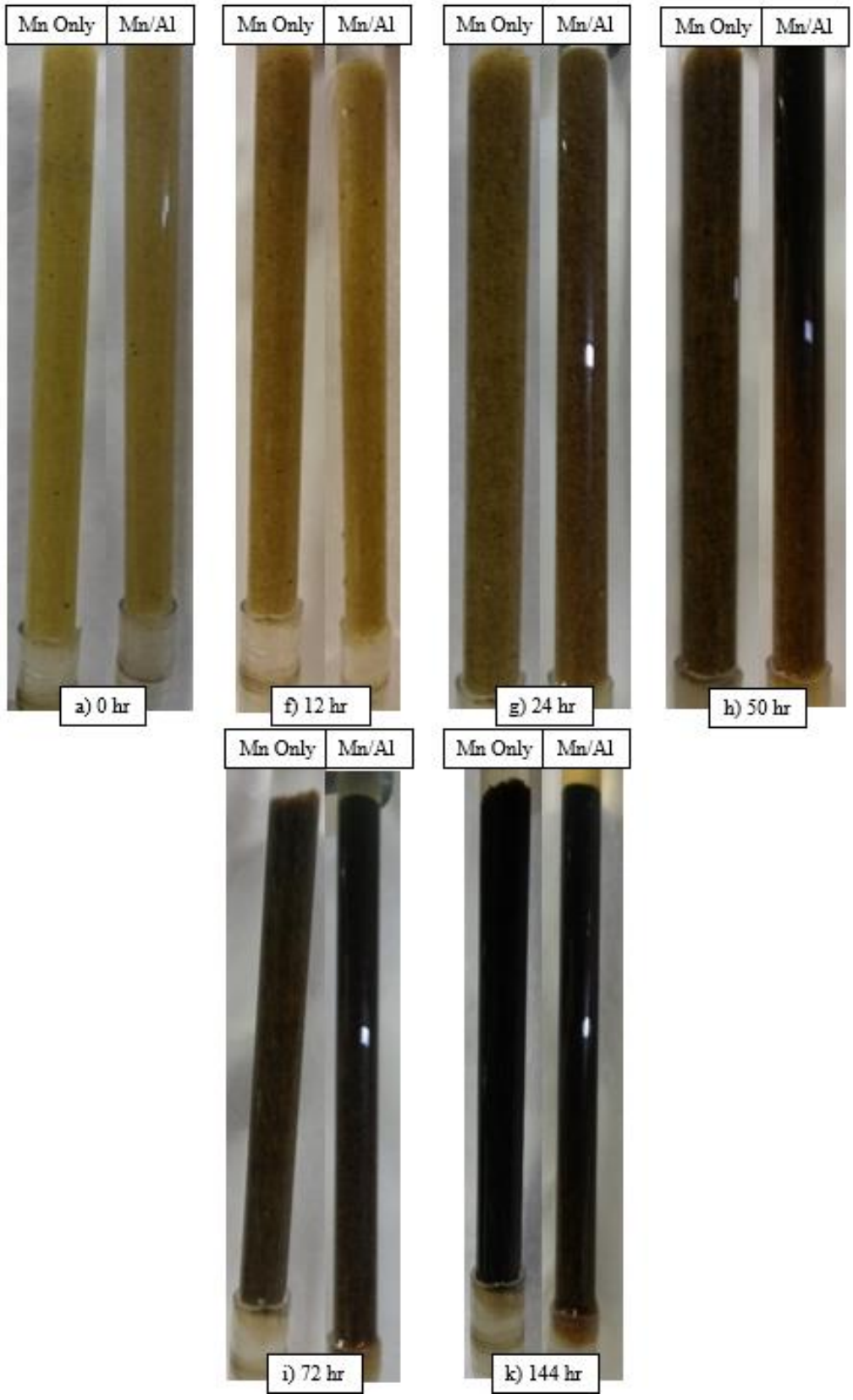

Figure 12: Time-Series of Column Appearance for Experiment 16

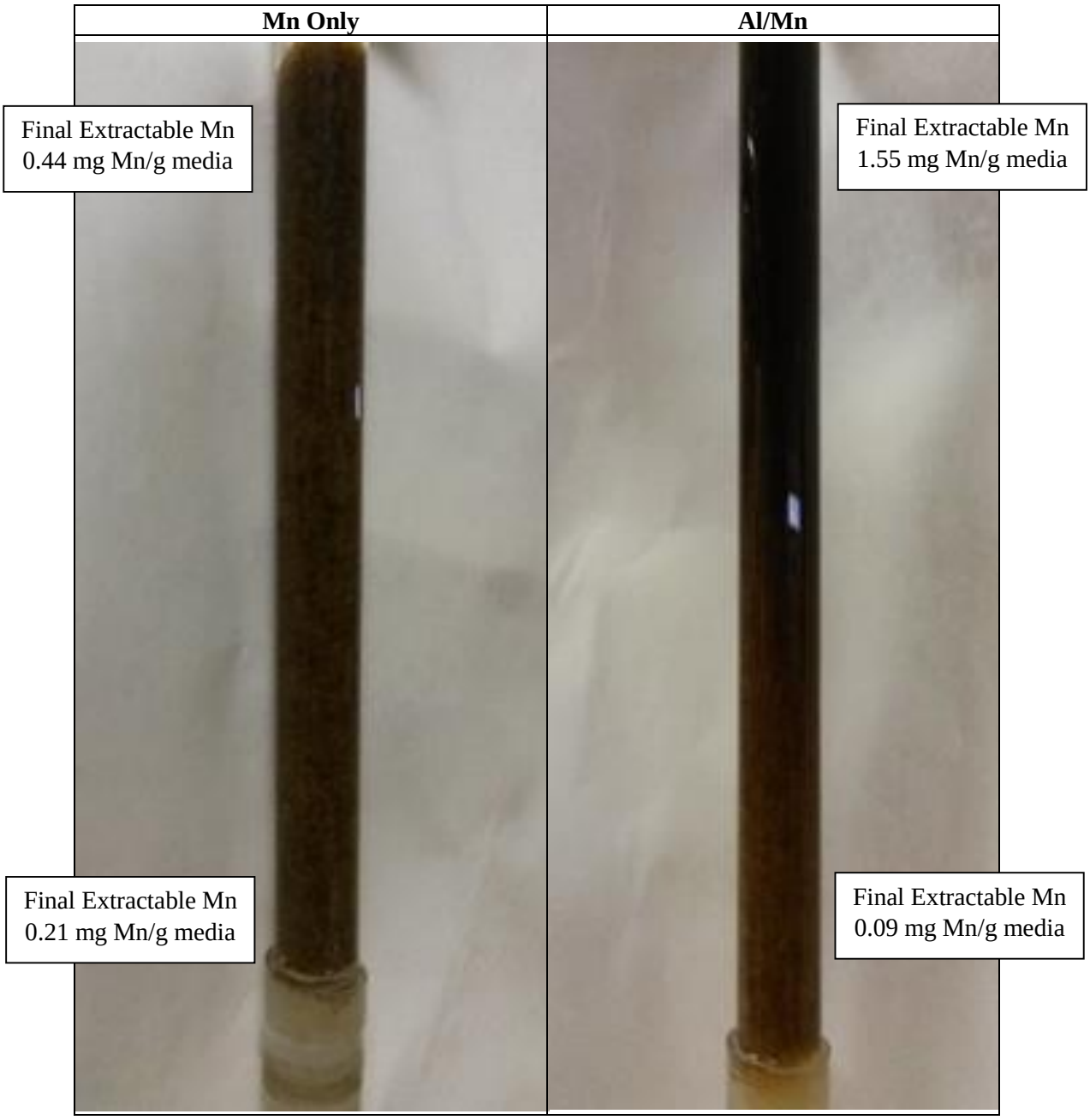

Figure 13: Enlargement of Hour 50 Images from Experiment 16 (Extraction data presented reflects results obtained after full 144-hour duration of experiment)

layers of the Mn-only column and less Mn coating in the bottom layers of the Mn/Al column compared with the Mn-only column. The specific values are presented in Figure 13 for reference. These measurements confirm that Al (presumably particulate Al) enhances the capacity of the media to adsorb Mn, which is also reflected in the fact that the Mn/Al columns achieved full removal of influent Mn whereas the Mn-only columns were only able to remove 40% - 60% of influent Mn.

SEM images of media coated under both Mn-only and Mn/Al conditions can be found in Figure 14. Images of media coated under Mn-only conditions can be found on the left, with images of media coated under Mn/Al conditions on the right. Both images in the top row were prepared at a magnification level of 10,000X, whereas the bottom row contains images prepared at a magnification level of 100,000X. Immediately apparent at the 10,000X level is the difference between the physical appearances of each type of surface. The image of the Mn-only sample shows a relatively smooth surface which follows the general contours of the surface features on the media itself. There is no appearance in this image of discrete particles in the coating, but instead a relatively smooth surface with small ridges. However, the image of the Mn/Al sample reveals a much rougher, more complex surface with contours dominated by smaller features on the order of 0.5 – 1 µm in size (presumably reflecting the incorporation and possible encapsulation of particulate Al). The contours of the coating seem to indicate the incorporation of particulate matter, contributing to the roughness and porosity of the surface. At the 100,000X magnification level, the structure of the $MnO_{x(s)}$ coatings are visible. Both the Mn-only and Mn/Al surfaces appear to follow the same general structure, with fairly pointed topography and ridges forming between successive peaks. The major physical differences between the two coating samples appears to be in the underlying topography, with the addition of particulate Al contributing significantly to the roughness and porosity of the coating.

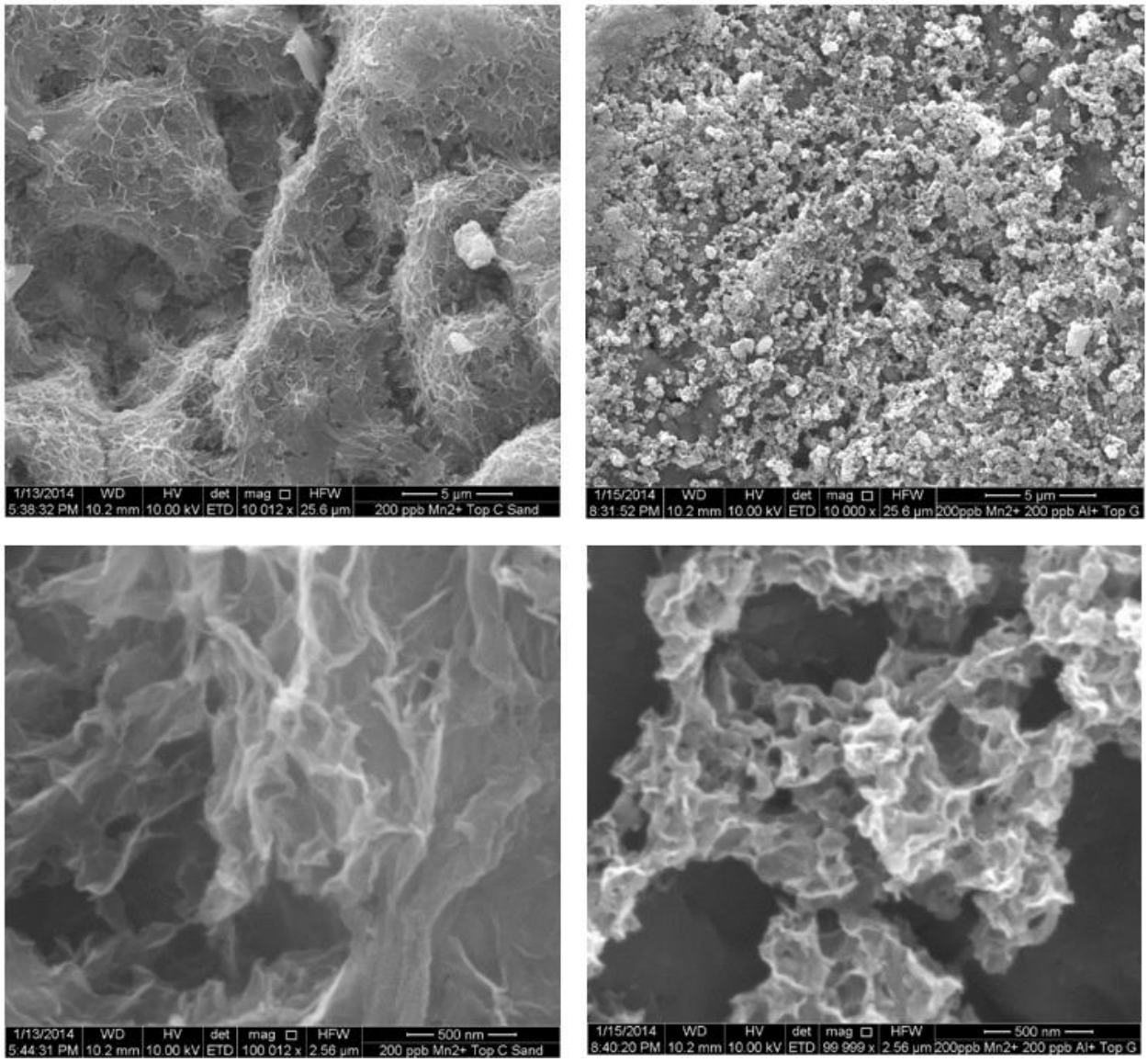

Figure 14: SEM Images of MnOx(s) Coating (Clockwise from top left: Mn Only Coating, 10,000X Magnification; Mn/Al Coating, 10,000X Magnification; Mn/Al Coating, 100,000X Magnification; Mn Only Coating, 100,000X Magnification)

4.2.2 Comparison of Media Extraction Data

The extractable metals content measured at the conclusion of each experiment provides insight regarding the performance of $MnO_{x(s)}$ coatings formed in the presence and absence of Al. The final extractable Mn contents found on samples collected from Mn-only experiments are presented in Table 8**,** found in Appendix A. Samples were collected from both the top and bottom layers of the column to capture the effects of coating gradient through the column depth.

The amount of extractable Mn (expressed in mg Mn per g dry media) varies between experiments based primarily on the duration of the experiment; longer experiment durations provide more time for coating to develop in all layers of the bed, yielding higher extractable Mn content. This phenomenon is illustrated in Figure 15, which presents the extractable Mn content from the top and bottom samples of all experiments (Mn-only and Mn/Al) against experiment duration. As duration increases, the amount of extractable Mn recovered from both the top and bottom layers of the Mn-only media beds increases. However, the top to bottom ratios of extractable Mn content presented in Table 8 tended to remain relatively constant between experiments.

Table 9 (Appendix A) presents the coating extraction data from all Mn/Al experiments. Because the uptake of Al was of interest in these experiments, extractable Al values are included in the table. For each experiment, the molar ratio of Al to Mn was calculated for the top and bottom media layers; similarly, the top to bottom ratio was calculated for both Al and Mn. As with the Mn-only experiments, longer experiment durations tended to yield greater amounts of extractable Mn and Al from the media. Extractable Mn for the Mn/Al experiments is plotted against experiment duration in Figure 15; extractable Al is plotted against experiment duration in Figure 16. The data from the two plots follow a similar trend, indicating high correlation between extractable Mn and Al in these coatings.

These plots reveal two key differences between media collected from the Mn/Al experiments and media collected from the Mn-only experiments. First, media collected from Mn/Al experiments tended to yield greater total amounts of extractable Mn than media from Mn-only experiments of similar durations. This reflects the tendency of media coated in the presence of Al to remove and accumulate larger amounts of Mn than media coated in the absence of Al. Second, whereas the Mn-only media showed increasing extractable Mn content in both the top and bottom layers with longer experiment duration, only the media collected from the top layers of the Mn/Al columns showed dramatically increasing extractable Mn and Al with longer experiment durations. The media collected from the bottom of these beds did not yield appreciably larger extractable Mn and Al content with increasing experiment duration. This fact indicates that the upper media layers in these beds contained sufficient capacity to remove essentially all of the influent Mn, and resulted in a much wider range of top to bottom Mn ratios among the Mn/Al experiments than among the Mn-only experiments.

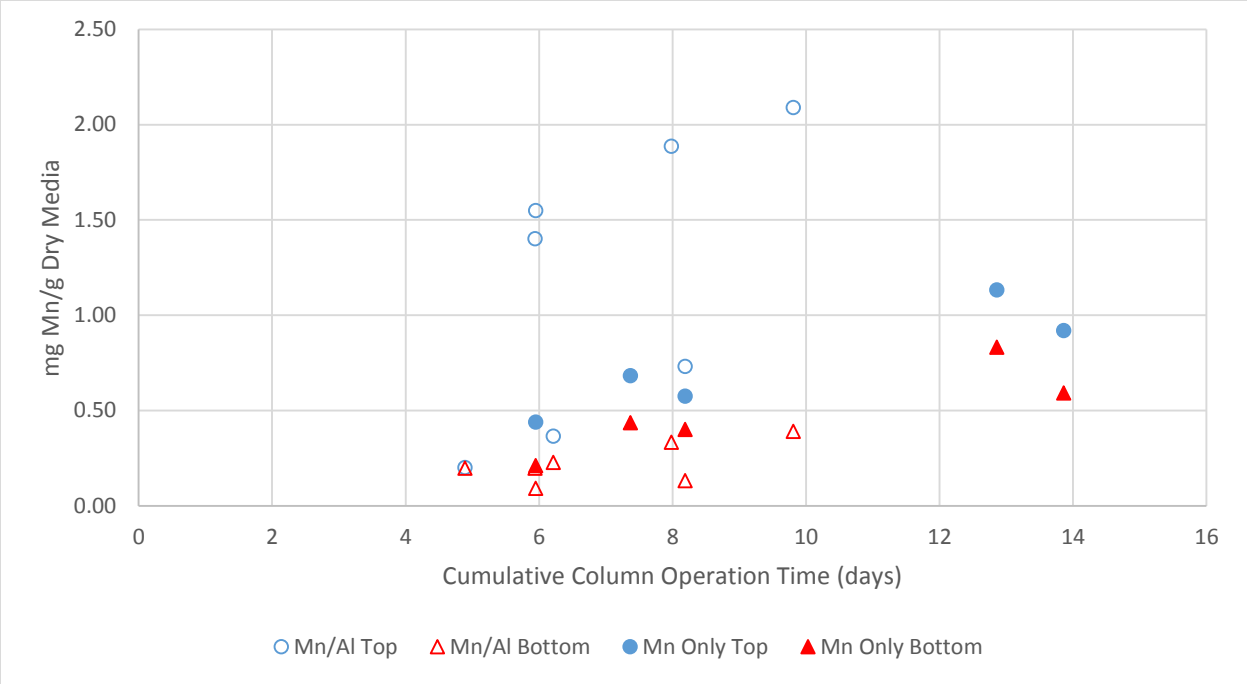

Figure 15: Extractable Mn Content in Top and Bottom Media Samples, All Experiments

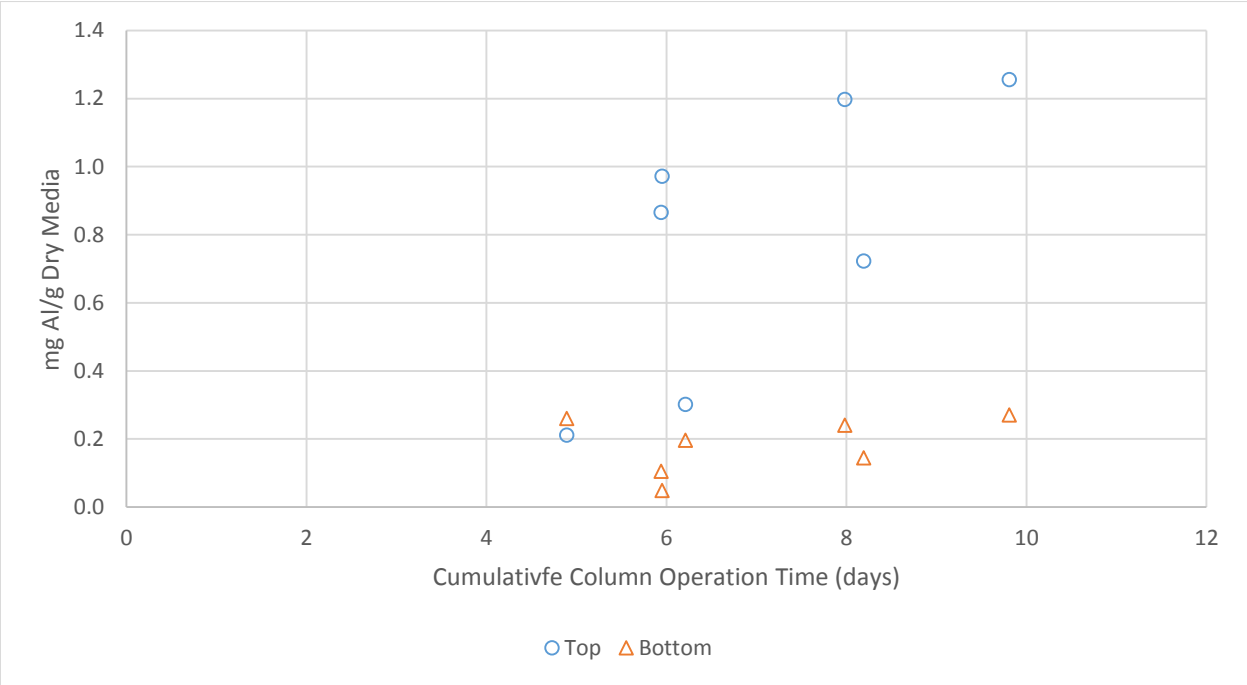

Figure 16: Extractable Al Content in Top and Bottom Media Samples of Mn/Al Experiments

The relationship between top to bottom Mn ratios and experiment duration is compared between both Mn-only and Mn/Al conditions in Figure 17. As noted previously, the Mn-only columns yielded a relatively constant ratio with experiment duration, resulting in a generally flat trend. The ratio is much more variable for the Mn/Al experiments. Two experiments (Experiment 15 and Experiment 16 (Mn/Al)) yielded unexpectedly high ratios given their relatively short operation time. These high ratios suggest that these two experiments removed Mn and Al at specifically high rates in the topmost levels of the beds.

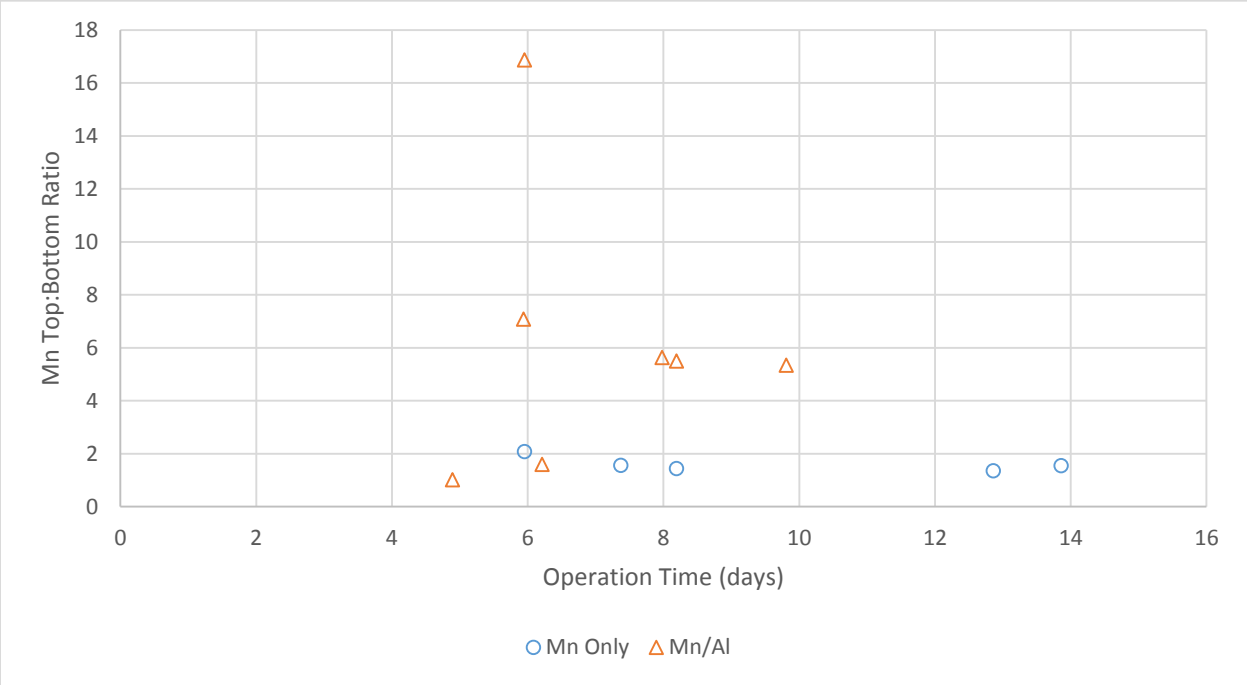

Figure 17: Mn Top:Bottom Ratios vs. Operation Time for Both Mn-Only, Mn/Al Conditions

The incorporation of Al into coatings formed in the Mn/Al experiments was consistent between experiments. Figure 18 correlates the extractable Mn from each sample with the extractable Al, separated into top and bottom samples. The data describe an approximately linear pattern with a regression slope equivalent to 1.2 mol Al/mol Mn, which is comparable to the overall average Al:Mn molar ratio across all samples of 1.6 (the regression slope is heavily influenced by the highest Mn values, some of which yielded lower molar ratios). The consistency of Al incorporation across the depth of media beds between identical experiments corroborates findings by Tobiason (2008) and Jones (2012) that Al incorporation tends to be consistent across a media bed; the exact molar ratios of Al to Mn in these experiments differ from those observed

by Tobiason and Jones due to differences in influent conditions. As seen in Table 9 (Appendix A), the Al:Mn molar ratio was higher on average for bottom samples than for top samples; this is consistent with the explanation of high levels of Mn being removed in the upper layers of the column. This rule held true for each individual experiment except for Experiment 15 and Experiment 16, which as noted before appear to have been specifically effective at removing both Mn and Al in the top layer.

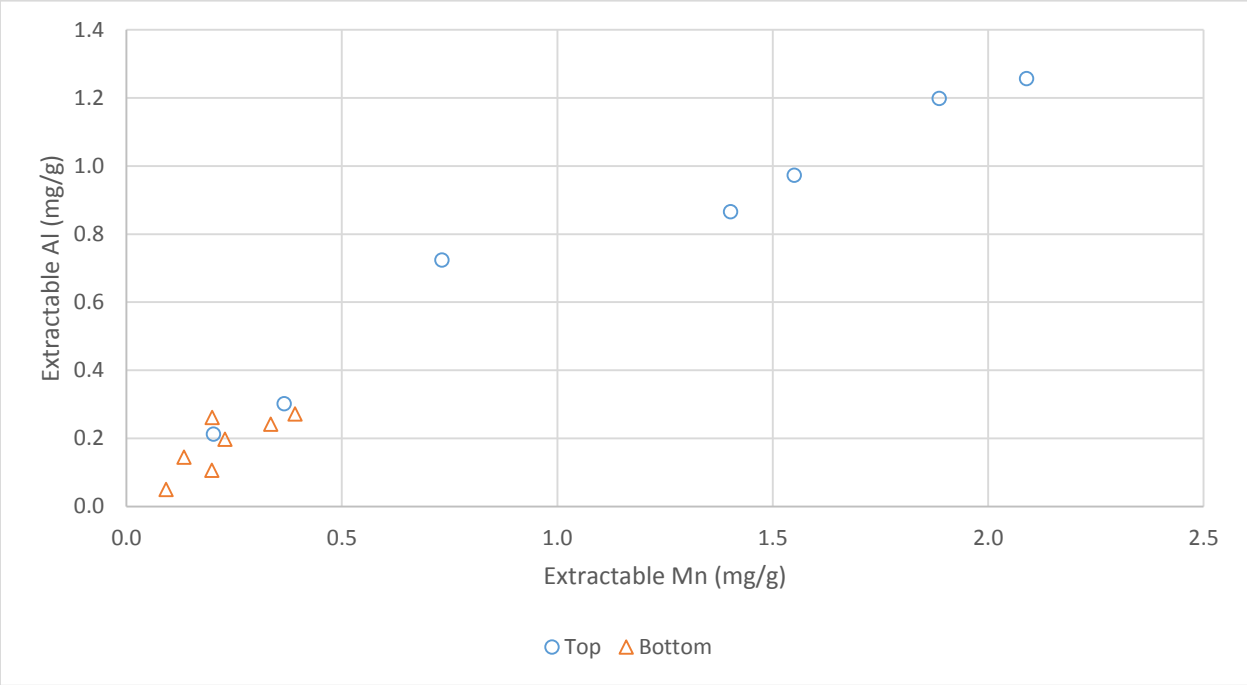

Figure 18: Correlation between Extractable Mn, Extractable Al, All Mn/Al Experiments

4.2.3 Alternating Feed Experiment

In an effort to further explore the effect of Al on the development of $MnO_{x(s)}$ coating, two parallel columns of uncoated filter sand were variably exposed to feeds with and without Al. The experiment consisted of three combinations of influent conditions; a description of the experimental design may be found in Section 3.1.4. The Mn removal curves for this experiment are presented in Figure 19. Changes in the experimental feed combinations are delineated by vertical dashed lines and the combinations are labelled in the figure to correspond with Table 4. For the individual data series, data points taken during Mn-only feed conditions are shown with no fill and data points taken during Mn/Al conditions are shown as solid. Combination I yielded results typical of previous experiments for both the Mn only and the Mn/Al feeds, with Column

B achieving full removal of influent Mn in approximately 24 hours. During Combination 2, Column A continued to show behavior typical of Mn-only columns in other experiments, gradually approaching steady-state conditions with approximately 50 – 60% of the influent Mn being removed. Column B, which had developed a coating in the presence of particulate Al but no longer received Al in the feed water, continued to remove all influent Mn for the remainder of the experiment. Once Column A, which reached steady-state conditions with a Mn-only feed, received particulate Al, the effluent Mn quickly dropped below detection limit.

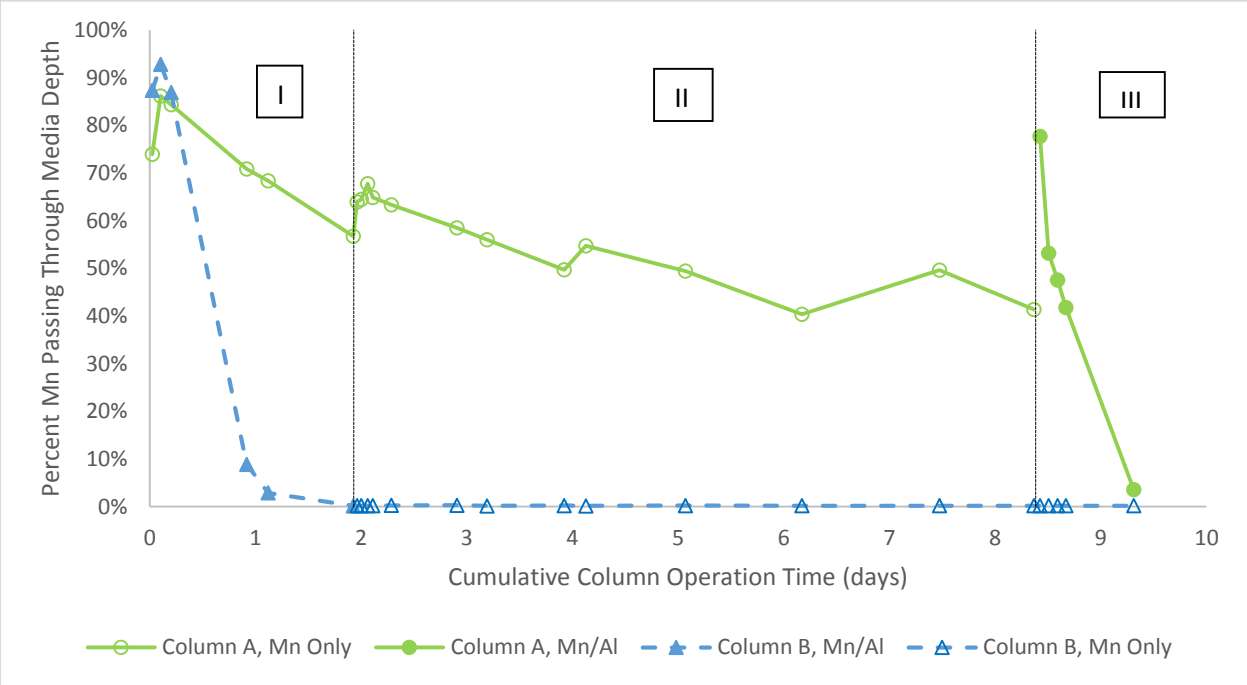

Figure 19: Alternating Feed Experiment (Hollow Points = Mn only, Solid Points = Mn/Al)

The results of this experiment underscore the contribution of Al to enhanced formation of a $MnO_{x(s)}$ coating. The fact that Column B remained capable of removing all influent Mn even after influent Al was discontinued demonstrates that the presence of Al during $MnO_{x(s)}$ coating development contributes to formation of coating sufficient to remove greater levels of influent Mn than coating developed in the absence of Al. The behavior of Column A confirms that the addition of particulate Al at any time rapidly enhances Mn removal, even when a $MnO_{x(s)}$ coating already exists on the media. As this coating, which previously was not subjected to any Al loading, continued to develop in the presence of particulate Al, effluent Mn levels rapidly dropped in a fashion typical of previously observed Mn/Al experiments.

Media extractions from the alternating feed experiment are presented in Table 10, located in Appendix A. Column A, which was operated with a Mn-only feed for the majority of the experiment, has similar Mn extraction levels to other Mn-only experiments. Although the column was loaded with particulate Al for a period of approximately 24 hours before the end of the experiment, resulting in enhanced removal of influent Mn, the effects of this period on coating composition were negligible and the top to bottom Mn ratio is comparable to ratios from other Mn-only experiments. Column B, on the other hand, was initially operated with particulate Al. Even though addition of Al was discontinued after two days, enhanced capture of Mn continued (as evidenced by the Mn removal curve). Accordingly, the Mn top to bottom ratio for Column B is comparable to ratios from Al/Mn experiments, despite the fact that Column B was operated with a Mn-only feed for the majority of the experiment. The disparity between the Mn top to bottom ratios for Column A and Column B indicates that addition of Al aided in the capture of Mn and the development of a $MnO_{x(s)}$ coating capable of removing all influent Mn in this experiment.

The Al extraction data from the two columns are consistent with one another. Column B, which was exposed to Al for approximately twice the duration of Column A, yielded approximately twice the extractable Al content in both the top and bottom samples. The top to bottom Al ratios are similar between both columns, which makes sense because both columns were subjected to the same levels of Al.

4.2.4 Soluble Al Experiment

After prior experiments demonstrated a significant impact of particulate Al on $MnO_{x(s)}$ coating formation, an experiment was conducted using soluble levels of Al (soluble Al experiment) to determine whether coating formation would be affected. Based on solubility and speciation constants reported in Brezonik & Arnold (2011), the solubility of Al at pH values of 7.0 and 7.5 are approximately 15 and 40 µg/L, respectively; for the soluble Al experiment, a target value of 10 µg/L was chosen. While this Al concentration yielded soluble Al in conditions present in the feed solution, localized conditions at the media surface were not able to be measured. The Al in this experiment was assumed to remain soluble throughout the experiment. Exact experimental conditions can be found in Table 7, located in Appendix A.

Figure 20 presents the Mn removal curve observed during the soluble Al experiment. The decrease in effluent Mn concentration occurs at a somewhat slower rate than seen in the particulate Al experiments, reaching detection limit after approximately four or five days (compared with 24 hours for all particulate Al experiments). However, the effluent Mn does decrease below detection limit, indicating that the enhanced Mn removal capacity exhibited by coatings formed in the presence of particulate Al over coatings formed in the absence of Al occurred under soluble Al conditions as well. The reduced rate of coating formation compared with particulate Al conditions can be partially explained by the lower mass loading of Al. The fact that soluble levels of Al enhanced the Mn removal capacity of $MnO_{x(s)}$ coatings strongly indicates that the destabilizing effects of Al are partially responsible for the improved $MnO_{x(s)}$ coating formation. This comports with the theory that some amount of $MnO_{x(s)}$ particles are formed prior to filtration, the capture of which are improved by destabilization and aggregation by Al. Enhanced capture of $MnO_{x(s)}$ in an uncoated media bed would lead to faster adsorption-oxidation, quicker coating development, and ultimately improved soluble Mn removal.

Figure 21 presents the Al removal curve observed during the soluble Al experiment. A higher percentage of Al passed through this media bed compared with columns operated with particulate Al, which is to be expected since retention of particulate Al floc in the media bed was not a factor for the soluble Al experiment. Initially, approximately 60% of influent Al passed through the media bed; this value decreased slightly as the $MnO_{x(s)}$ coating developed. After approximately four days, when effluent Mn decreased below detection limit, Al removal through the column also reached a steady-state condition with 30-40% of influent Al passing through the column. The slight decrease in effluent Al as the coating developed can likely be attributed to an increase in the amount of coating available for adsorptive uptake of Al (Jones 2012).

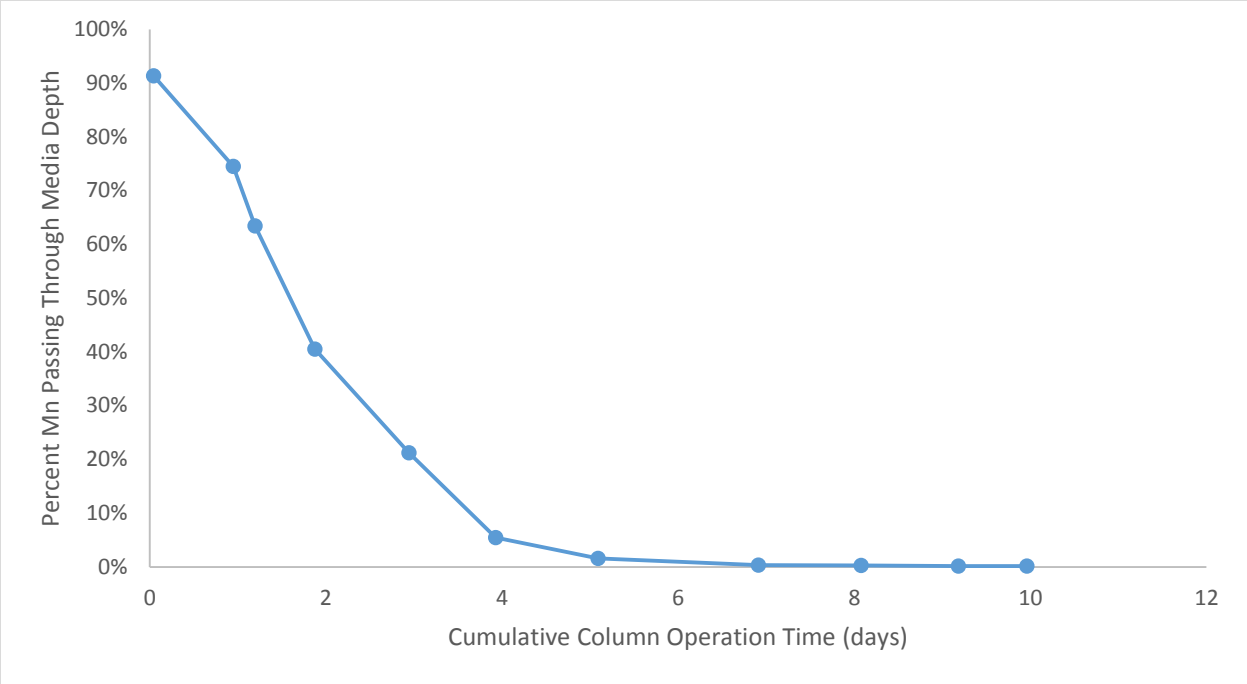

Figure 20: Mn Removal Curve for Soluble Al Experiment (200 µg/L Mn, 10 µg/L Al, 2.5 – 3.0 mg/L as Cl_2, pH 7.3-7.5)

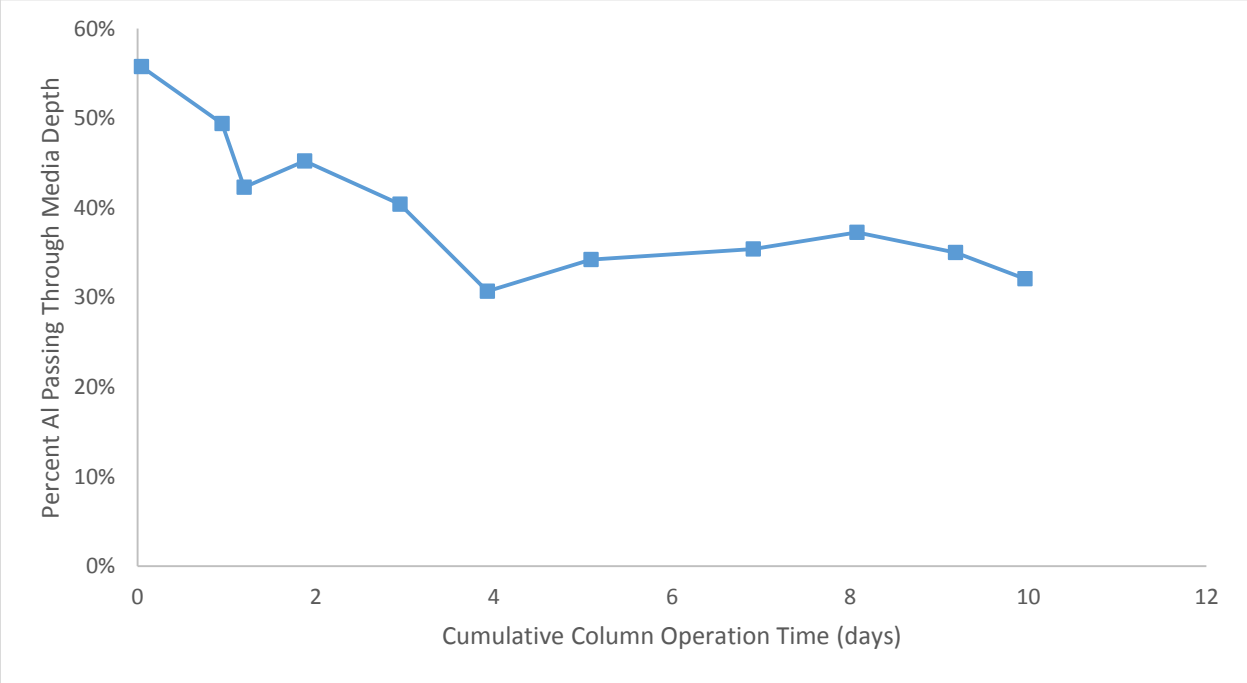

Figure 21: Al Removal Curve for Soluble Al Experiment (200 µg/L Mn, 10 µg/L Al, 2.5 – 3.0 mg/L as Cl_2, pH 7.3-7.5)

Media extraction data for the soluble Al experiment are presented in Table 11 (Appendix A). Samples from both the top and bottom of the soluble Al bed yielded more extractable Mn than was found on media samples from Mn only and particulate Al/Mn experiments of similar durations. Since the soluble Al column removed more cumulative Mn over the experiment than the Mn only columns, this result reflects the tendency of soluble levels of Al to enhance coating formation. The particulate Al columns captured more cumulative Mn over the course of an experiment than the soluble Al column; however, particulate Al columns required backwashing, which resulted in a significant loss of captured Mn. The soluble Al column was not backwashed, and so extractable Mn values reflect the total cumulative Mn removed during the experiment. Predictably, media samples from the soluble Al column yielded much lower extractable Al content than media samples from the particulate Al columns. This result was expected, as a much lower mass loading rate of Al was applied to the soluble Al column.

The top to bottom ratio of extractable Mn proved to be significantly higher than the ratios observed from Mn only columns. This confirms that the capacity of the $MnO_{x(s)}$ coating for Mn removal was improved such that the top layer of media in the soluble Al column captured significantly more Mn than the top layer of media in the Mn only columns. However, the Mn top to bottom ratio was lower than that found in columns loaded with particulate Al. This indicates that enhanced coating formation was not as pronounced in the soluble Al column as in the particulate Al columns, which comports with the slower rate of coating formation observed in the soluble Al column. The top to bottom ratio of extractable Al found in the soluble Al column was higher than the ratio measured in the particulate Al column, indicating that Al was removed more effectively by the top layers of the soluble Al column media than the particulate Al column media. This result contrasts with previous experiments, the results of which would suggest that the Mn and Al top to bottom ratios should increase or decrease together (on account of the observation that increased Mn deposition correlated with increased Al deposition). However, this contrast may be attributable to differences in how soluble and particulate Al are captured and incorporated into the coatings; whereas the capture of soluble Al is an adsorption reaction, the capture of particulate Al is a physical process and may also have been susceptible to effects of backwashing.

4.2.5 Ferric Iron Experiment

Ferric iron (Fe) was substituted for Al during one experiment to assess the effect of an alternative coagulant on the formation of $MnO_{x(s)}$ coatings. The target Fe concentration was kept at 220 µg/L as Fe, identical to the target Al concentration of previous experiments; exact experimental conditions can be found in Table 7 in Appendix A. For this experiment, backwashing was performed as necessary based on head loss development. Fe salts perform similarly to Al(III), hydrolizing when dissolved and forming amorphous hydroxide floc ($Fe(OH)_{3(s)}$). Because the solubility of $Fe(OH)_{3(s)}$ is several orders of magnitude less than $Al(OH)_{3(s)}$ (ranging between 0.1 – 0.2 µg/L in the pH range of 7.0 – 7.3 based on constants reported in Brezonik & Arnold (2011)), Fe coagulants can be used at pH values as low as 5 or as high as 9, at which the solubility of $Al(OH)_{3(s)}$ would render Al coagulants ineffective (AWWA 2011). Tobiason et al. (2008) extracted media collected from several treatment plants, including one which applied Fe coagulant to its feed water. This sample showed elevated levels of extractable Fe compared with plants applying an Al coagulant or no coagulant, indicating that Fe may be incorporated into $MnO_{x(s)}$ coatings in a similar manner to Al.

The Mn removal curve for the Fe experiment is shown in Figure 22. As with the Al/Mn experiments, this column achieved an effluent Mn level below detection limit. The effluent Mn concentration decreases at approximately half of the rate observed from the particulate Al/Mn experiments, which can be attributed to the difference in molecular weight between Fe and Al. The molecular weight of Fe is approximately twice the molecular weight of Al, so 220 µg/L of Fe represents approximately half the molar concentration of 220 µg/L of Al. However, the addition of 220 µg/L Fe yielded a more rapid decrease in effluent Mn than the addition of soluble Al did.

The Fe removal curve for the Fe experiment is presented in Figure 23. The pattern of this curve is markedly different than the curves typical of particulate Al, in which initially only 30% of influent Al passed through the column and capture improved as $MnO_{x(s)}$ coating developed. The Fe curve shows that 90% -100% of influent Fe passed through the media bed for the first four days; only once effluent Mn concentration had reached the detection limit did capture of Fe improve, reaching a steady-state condition wherein approximately 50% - 60% of influent Fe was passing through the media. It is possible that the high levels of breakthrough observed in this

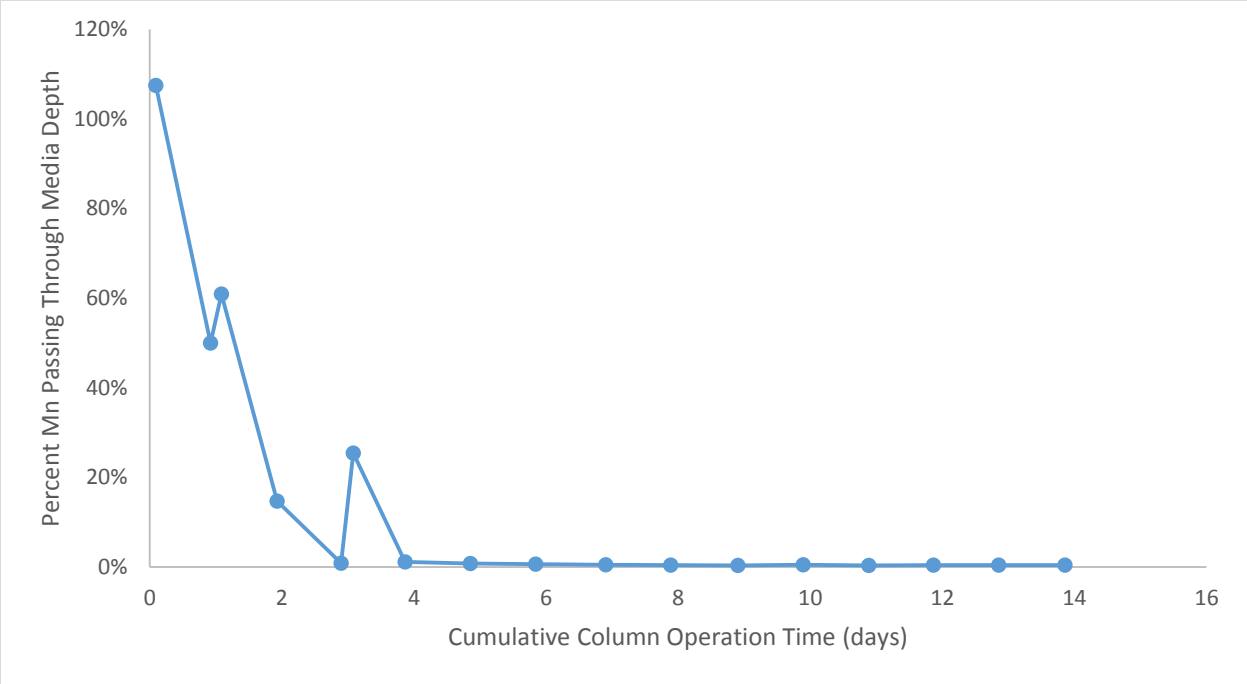

Figure 22: Mn Removal Curve for Fe Experiment (200 µg/L Mn, 220 µg/L Fe, 2.1-2.5 mg/L as Cl_2, pH 7.0-7.3)

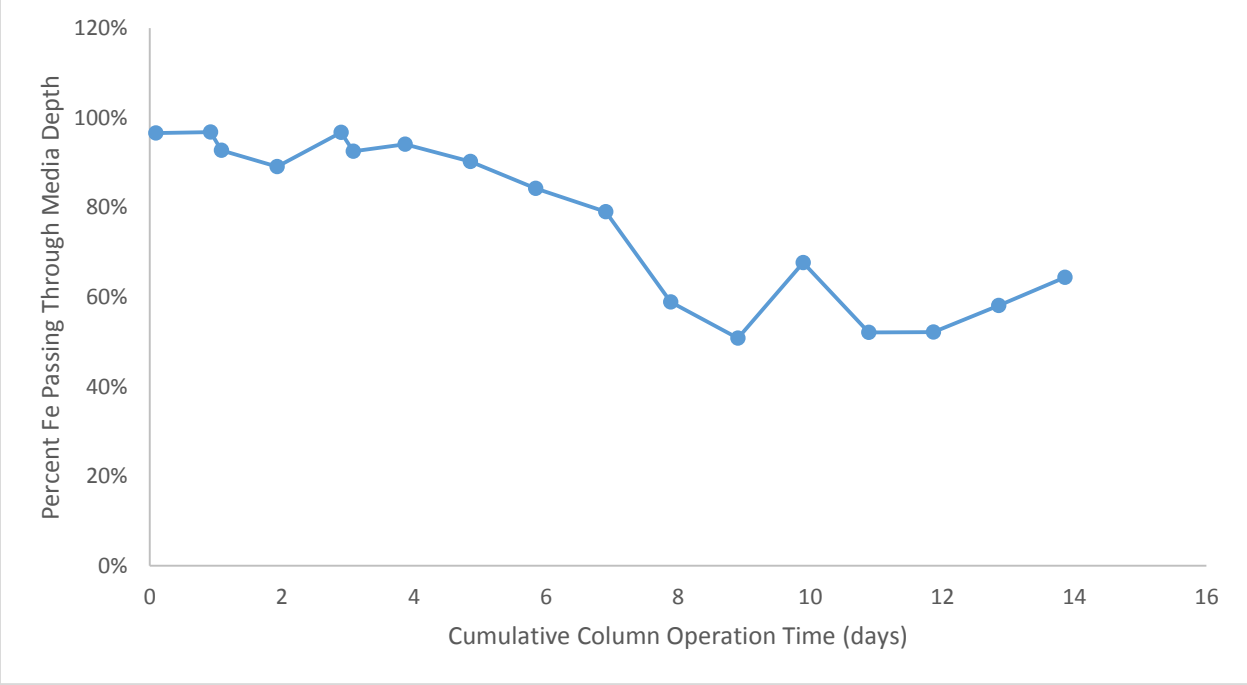

Figure 23: Fe Removal Curve for Fe Experiment (200 µg/L Mn, 220 µg/L Fe, 2.1-2.5 mg/L as Cl_2, pH 7.0-7.3)

experiment compared with the particulate Al experiments may reflect Fe floc breaking up in the media bed; additionally, due to the low solubility of Fe compared with Al, much less soluble Fe would have been available for adsorptive uptake compared with soluble Al. Despite the ineffective capture of Fe, head loss was observed to develop in the column (although at a slower rate than most particulate Al experiments), and the first backwash occurred after approximately two days of operation. Interestingly, in the case of Al studies, enhanced Mn deposition was correlated with more effective capture of Al at the particulate level; this correlation was not observed in the Fe experiment despite a similar enhancement of Mn deposition.

Table 12 (Appendix A) presents media extraction data from samples collected after the conclusion of the Fe experiment. These data include results of extracted Mn, Al, and Fe. As anticipated, higher concentrations of each element were found in samples from the top of the bed. No Al was added to the feed water, but small amounts may have been introduced by impurities in the ferric sulfate used to ad Fe, accounting for the small amount of Al found in the top layer of the bed. The top to bottom ratio of Mn content is higher than the ratio of top to bottom Mn seen in most of the particulate Al experiments; however, the duration of this trial was longer than any particulate Al trial, yielding more opportunity for additional Mn capture in the top of the bed and inflating this ratio.

The top to bottom Fe ratio from this experiment is noticeably large when compared with the top to bottom Al ratios from the particulate Al experiments, which indicates that most of the Fe capture (and subsequent integration into $MnO_{x(s)}$ coating) occurred in the topmost layer of the bed. The steep gradient in Fe concentration is consistent with the low solubility of Fe; since almost all of the influent Fe was particulate, it would be most likely to be captured in the top layer of the bed, which would contain the smallest media due to backwash stratification. Very little soluble Fe would remain to penetrate the media bed and become adsorbed in $MnO_{x(s)}$ coatings in the bottom layers.

4.3 Backwash Content from Particulate Aluminum Studies

Visual inspection of the solids recovered from backwashing columns loaded with particulate Al yielded an interesting result. In the feed water, Al solids formed prior to contact with the media were white, which is typical of $Al(OH)_{3(s)}$ floc. However, at the conclusion of a period between subsequent backwashes, the solids recovered during backwash were brown, suggesting

that they contained some oxidized Mn. For several Mn/Al experiments, backwash solids were collected on glass filters and dissolved using the media extraction method to establish the composition of the solids. This section contains results of these experiments.

4.3.1 Sub-Fluidization Backwash Rate Solids Composition

Solids recovered from backwash contain particulate matter captured in the media bed, but can also contain pieces of coating which have been sheared off media by the flow of water or by the scouring action of fluidized media grains colliding with one another. In an effort to eliminate or at least mitigate the contribution of sheared-off media coating to solids composition measurements, a select number of backwash trials used a flow rate which was not sufficient to produce any visual disturbance of the media (termed a sub-fluidization rate). Solids collected during this portion of the backwash were assumed to consist only of pre-formed particulates which were captured in the media bed, and were not associated with the $MnO_{x(s)}$ coating on the media.

Table 13 (located in Appendix A) contains data for solids recovered from all sub-fluidization backwashes. Sub-fluidization backwashes were performed for two Mn/Al experiments. Extremely low levels of both Al and Mn were released from the bed during these backwashes, with some backwashes yielding less than 1 µg of one or both metals. The detection of Mn in the samples indicates the presence of particulate Mn in the backwash solids, which as noted previously were initially assumed to be the result of $MnO_{x(s)}$ particles aggregated into Al floc. Subsequent testing on fully formed $MnO_{x(s)}$ coatings demonstrated that even in the absence of free chlorine (which would eliminate any pre-media Mn oxidation and new coating formation), sub-fluidization backwashes still yielded trace amounts of Mn comparable to the lower Mn levels found in Table 13. Since the only source of particulate Mn in the backwash of a column operated in the absence of free chlorine would be previously formed coating, the assumption that sub-fluidization backwashes eliminate coating loss may not be accurate.

As the experiment progressed, sub-fluidization backwashes tended to yield progressively greater amounts of Mn. This trend was apparent from visual examination of the glass fiber filters used to capture backwash solids. Pictures of filters for sub-fluidization backwashes from Experiments 15 and 16 are presented in Figure 24, with appropriate dates labelled; the brown coloration of oxidized Mn becomes increasingly noticeable with each successive filter. This

trend is also borne out by the molar ratios of Al to Mn found in each backwash, presented in Figure 25. Earlier backwashes released solids which tended to favor Al, with later backwashes producing lower ratios. The application of any pre-media oxidized particulate Mn to the column would be expected to be relatively constant over time, as the influent conditions did not change during the experiment. Therefore, the trend of progressive backwashes yielding lower Al to Mn ratios may be related to the disruption of $MnO_{x(s)}$ coating on the media, which further supports the assertion that even sub-fluidization flow rates may be sufficient to shear off small amounts of $MnO_{x(s)}$ coating.

Because backwash solids represent the accumulation of material only for a specific duration between successive backwashes, examining these data in the context of time between backwashes is useful. Figure 26 presents the molar ratio of Al to Mn in the backwash solids by time between backwashes, as opposed to cumulative operation time. These durations ranged from 12 hours to 48 hours between the two experiments. As duration between backwashes increased, the molar Al to Mn ratio shifted in favor of Mn. This trend suggests that the longer solids are retained in the media bed, the more Mn they tend to accumulate relative to Al. Since the loading of particulate Al and any pre-media oxidized Mn can be assumed to be constant, the molar ratio of any applied solids should be constant; therefore, a decrease in the ratio with increased time between backwashes may reflect active Mn adsorption-oxidation sites entrained in Al floc, which would likely be the result of captured $MnO_{x(s)}$ particles formed prior to filtration. These particles would act like $MnO_{x(s)}$ coating on media, collecting soluble Mn(II) and increasing the Mn content of captured solids with longer durations between backwash.

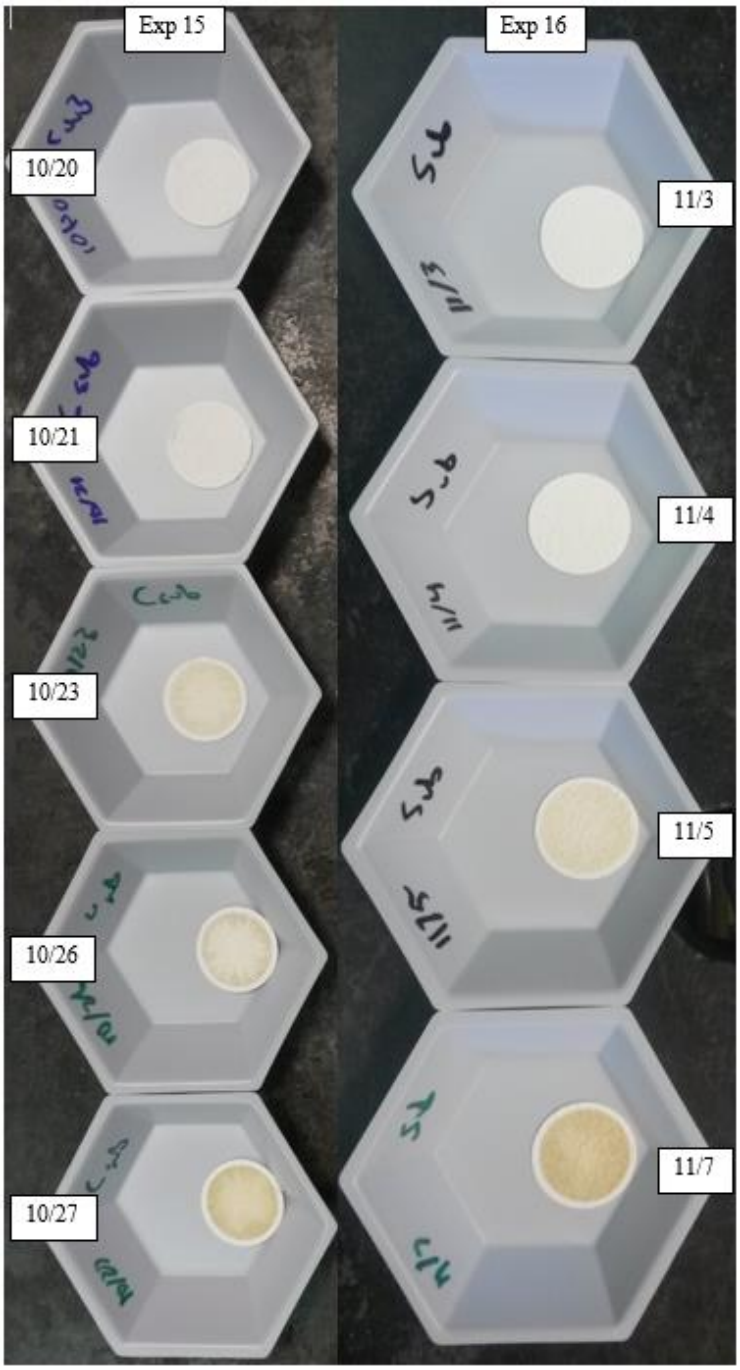

Figure 24: Glass Fiber Filters with Solids from Sub-Fluidization Backwashes (Experiments 15 and 16)

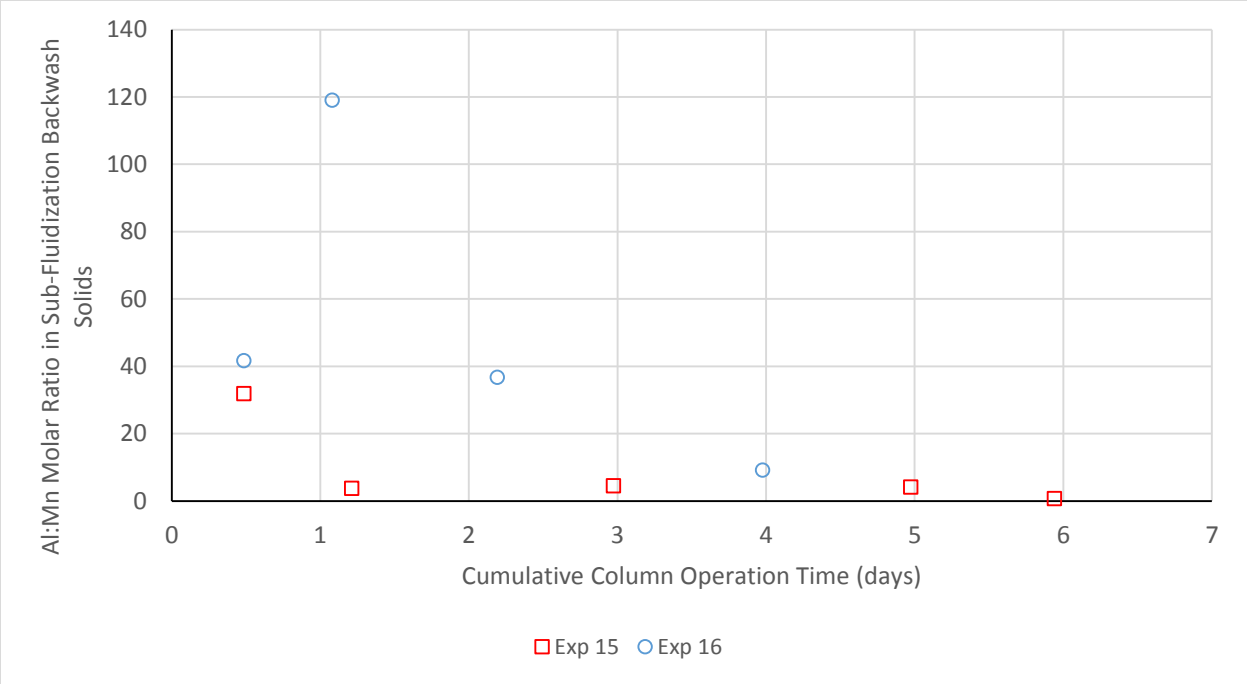

Figure 25: Al:Mn Molar Ratio of Sub-Fluidization Backwash Solids by Cumulative Operation Time

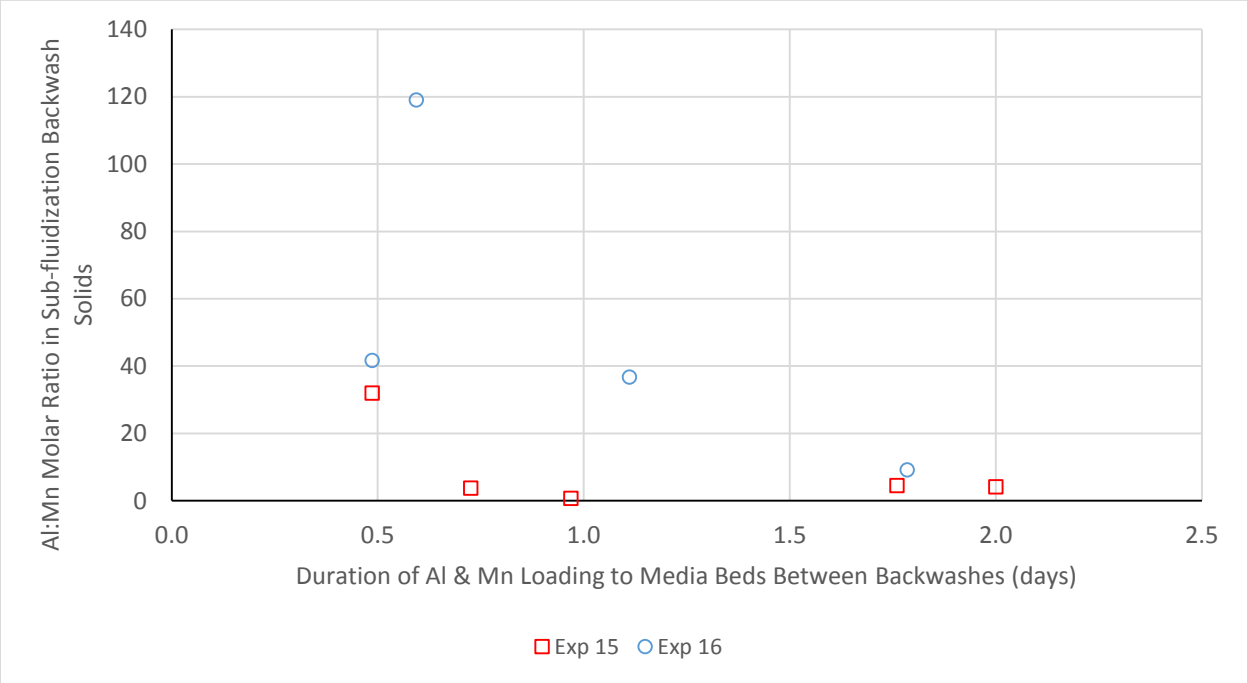

Figure 26: Al:Mn Molar Ratio of Sub-Fluidization Backwash Solids by Duration of Loading Between Backwashes

4.3.2 Full Backwash Rate Results

Solids were collected from full-rate backwashes for three Mn/Al experiments, including both of the experiments subjected to sub-fluidization backwashes. Full-rate backwashes were operated at approximately 25 gpm/ft^2, which was sufficient flow to fluidize the bed and expand it by 25% - 30% of its original depth. The scouring action of fluidization combined with the higher flow rate released captured particles from the bed which were not removed by sub-fluidization conditions, and likely resulted in some release of coating from the media.

Table 14 in Appendix A contains data for solids recovered from all full-rate backwashes. These backwashes tended to release significantly higher levels of both Mn and Al than the sub-fluidization backwashes, which is expected due to the enhanced bed cleaning gained from media fluidization. However, the cumulative Mn and Al from Experiment 15 and Experiment 16 are noticeably smaller than the totals from Experiment 10. These two experiments were noted previously to have been particularly effective at retaining Mn and Al in the top layers of the bed; this effect was reflected in the backwashes as well, where relatively small amounts of Mn and Al were recovered from the media.

The tendency of sub-fluidization backwashes to release greater amounts of Mn as the experiment progressed held true for the full-rate backwashes as well, and was even more pronounced. Figure 27 presents images of the backwash solids caught on glass fiber filters over the course of Experiment 15 and Experiment 16. Light brown coloration is visible on the second backwash filter for both experiments, and by the third backwash, the solids were dark brown in color. This trend is reflected in Figure 28, which displays the molar ratio of Al to Mn in the solids collected based on cumulative column operation time. Similar to the sub-fluidization backwash data, the ratios decreased to favor higher Mn content as the experiment progressed. It is expected that full-rate backwash should result in the detachment of some amount of $MnO_{x(s)}$ coating; since coating accumulated as the experiment progressed, backwashes that occurred later in each experiment would be expected to contain greater amounts of coating, which may account for this trend. The molar ratio is considered by time between backwashes in Figure 29. The trend of decreasing ratio with longer run time held true in this case as well. As noted previously, this could be the result of Mn sorption and oxidation on active sites present in Al floc formed pre-media. In general, the ratios yielded by full-rate backwashes were significantly smaller than those observed from sub-fluidization backwashes.

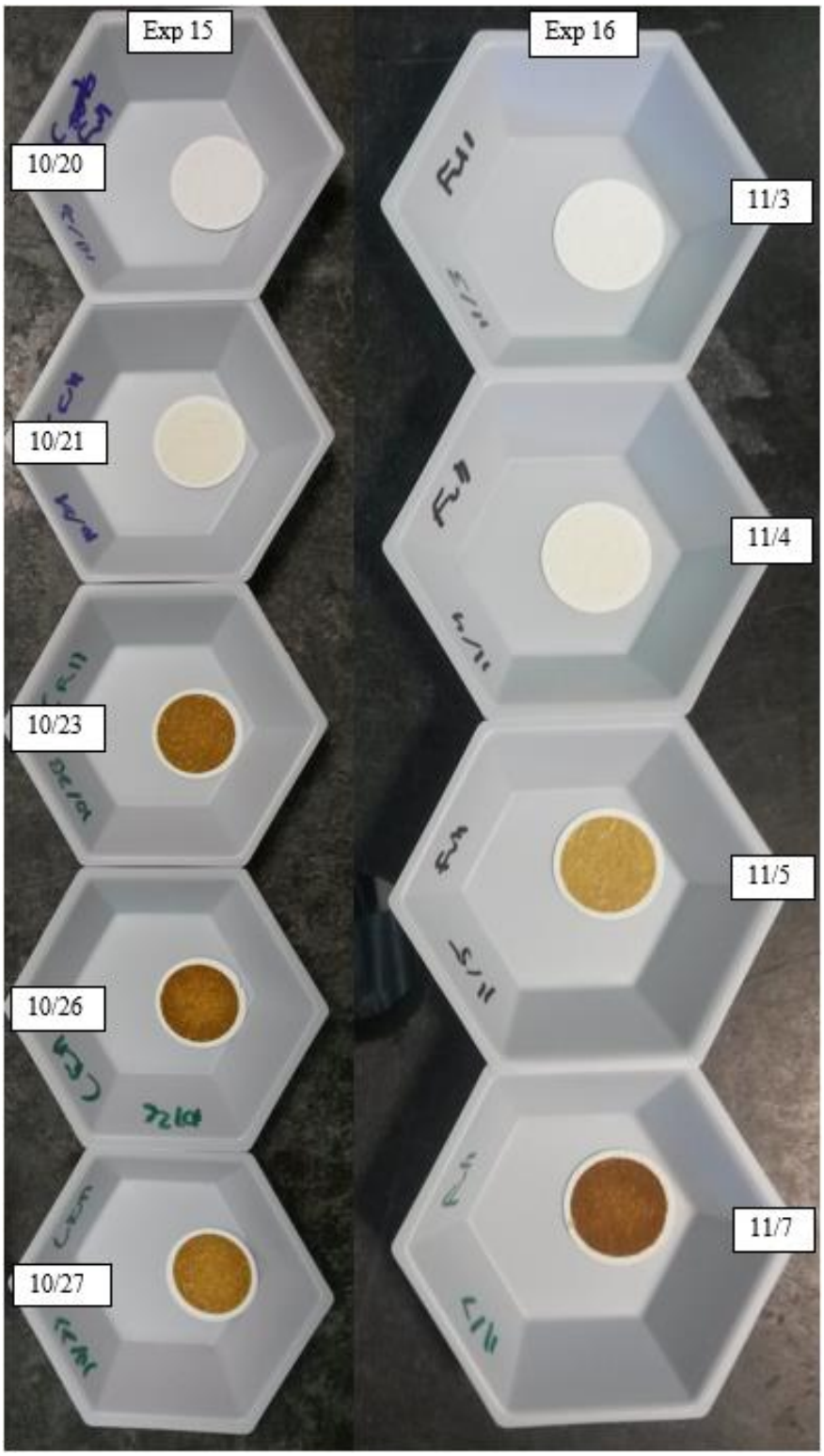

Figure 27: Glass Fiber Filters with Solids from Full-Rate Backwashes (Experiments 15 and 16)

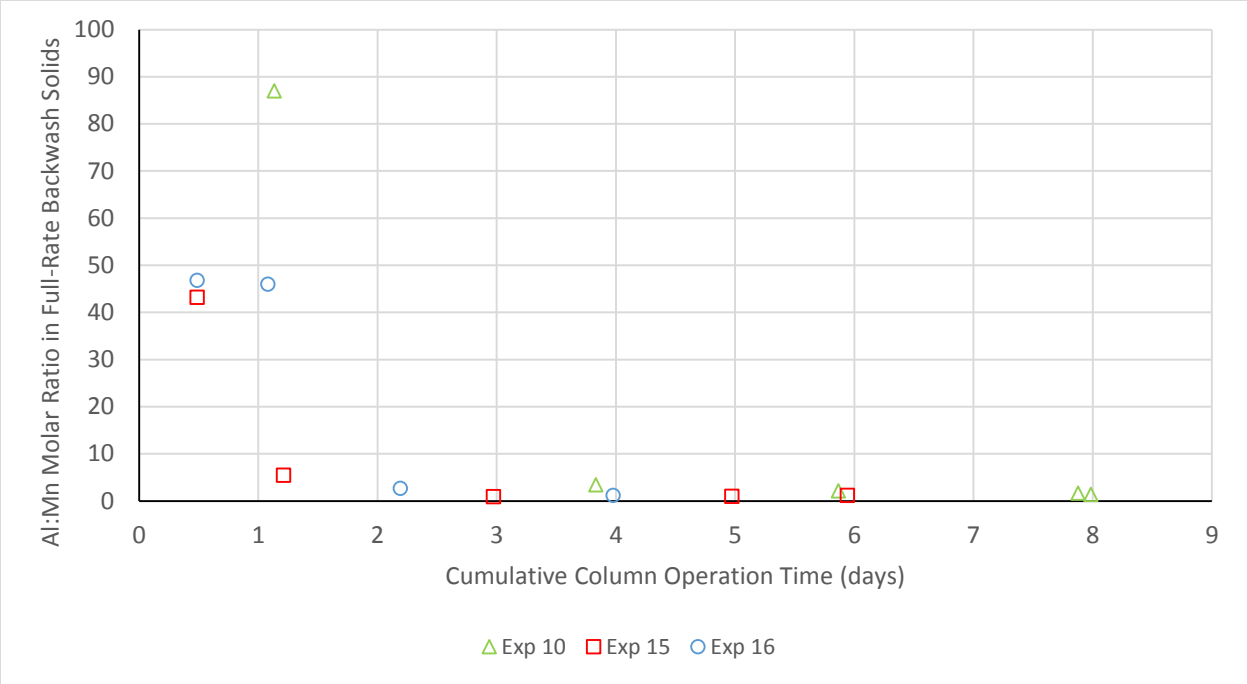

Figure 28: Al:Mn Molar Ratio of Full-Rate Backwash Solids by Cumulative Operation Time

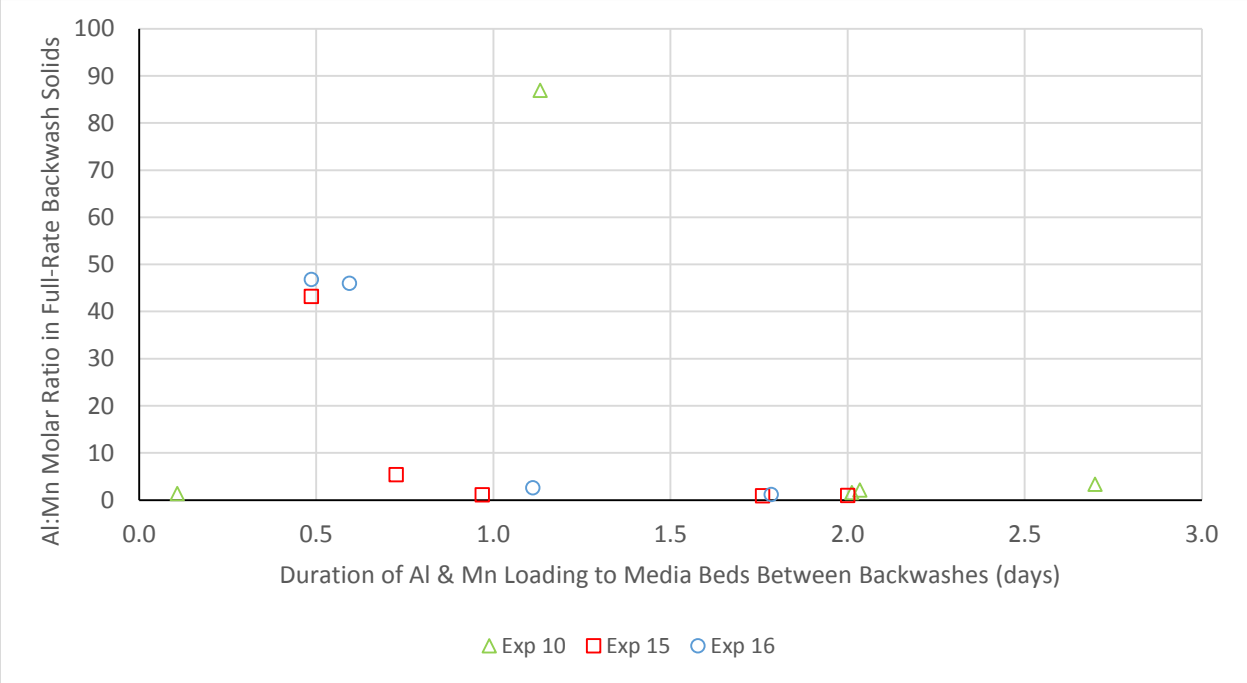

Figure 29: Al:Mn Ratio of Full-Rate Backwash Solids by Duration of Loading Between Backwashes

By subtracting the effluent Mn and Al concentrations from the influent Mn and Al concentrations during a given sampling event, an instantaneous estimate can be made of the molar ratio of Al to Mn being retained in each column at each sampling time. This ratio includes material incorporated into $MnO_{x(s)}$ coating on both media and column walls and fittings as well as particulate material captured which was subsequently released in backwashes. Figures 30 through 32 present the ratios of removed material alongside the ratios obtained from full-rate backwashes for Experiments 10, 15 and 16 respectively. The first backwash of each experiment, which as described previously tended to exhibit a relatively large Al to Mn ratio, far exceeded the ratios of material removed to that point for all three experiments. The fact that the first backwash yielded material composed of a higher Al to Mn ratio than the material removed to that point in the column indicates that a higher percentage of influent Mn was retained on the media surface through backwashes (likely as part of a permanent coating on the media) than influent Al. As the experiment progressed through multiple days, the ratio of Al to Mn in the backwash solids became very comparable to the ratio of cumulative mass removal of Al and Mn observed when the media was treating the applied water.

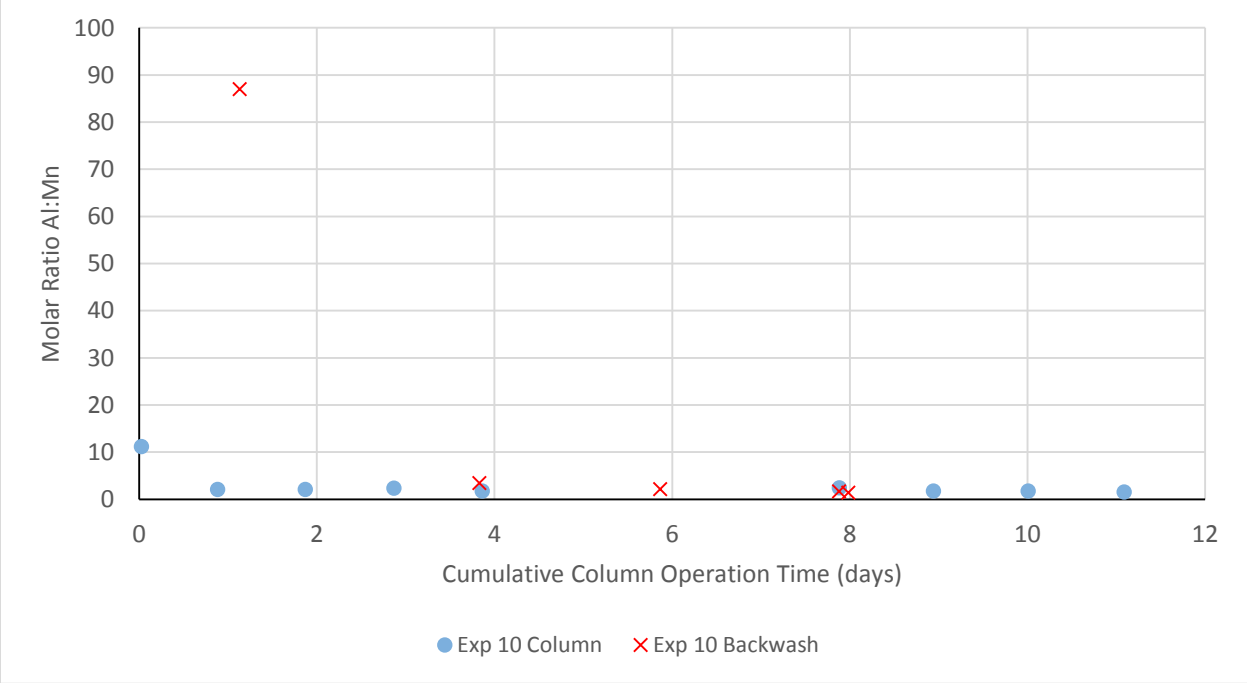

Figure 30: Molar Ratio of Al to Mn of Solids Retained in Column and of Solids Released in Backwash (Exp 10)

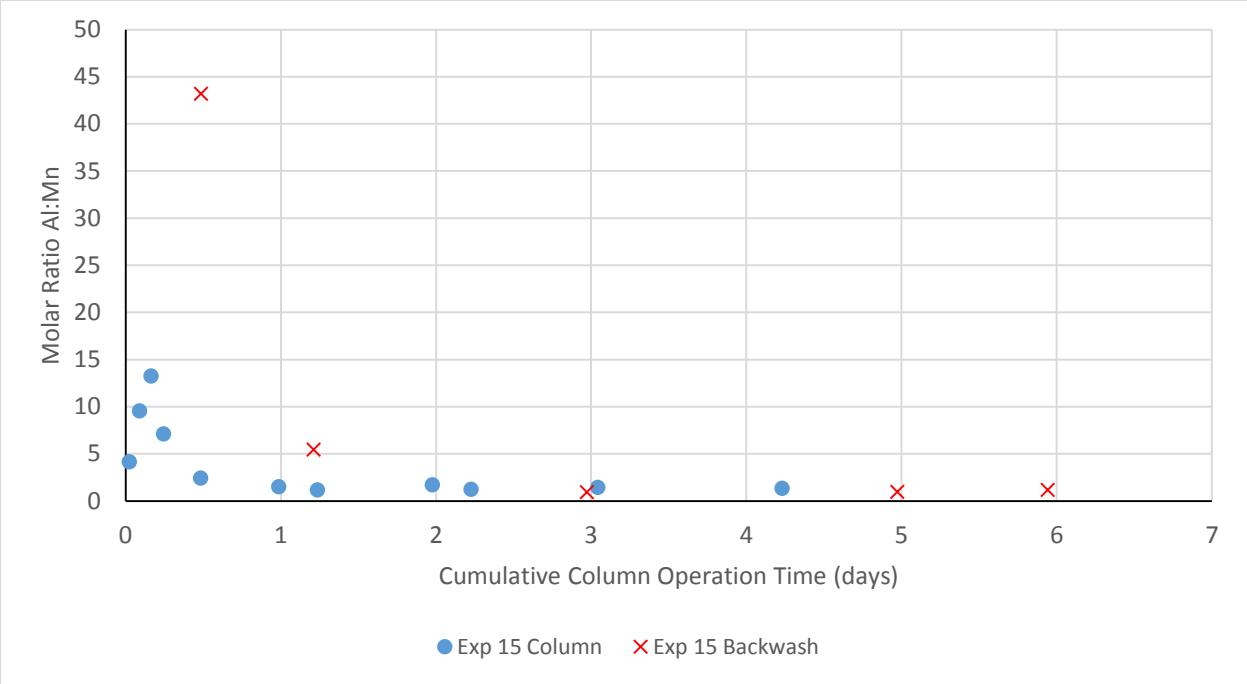

Figure 31: Molar Ratio of Al to Mn of Solids Retained in Column and of Solids Released in Backwash (Exp 15)

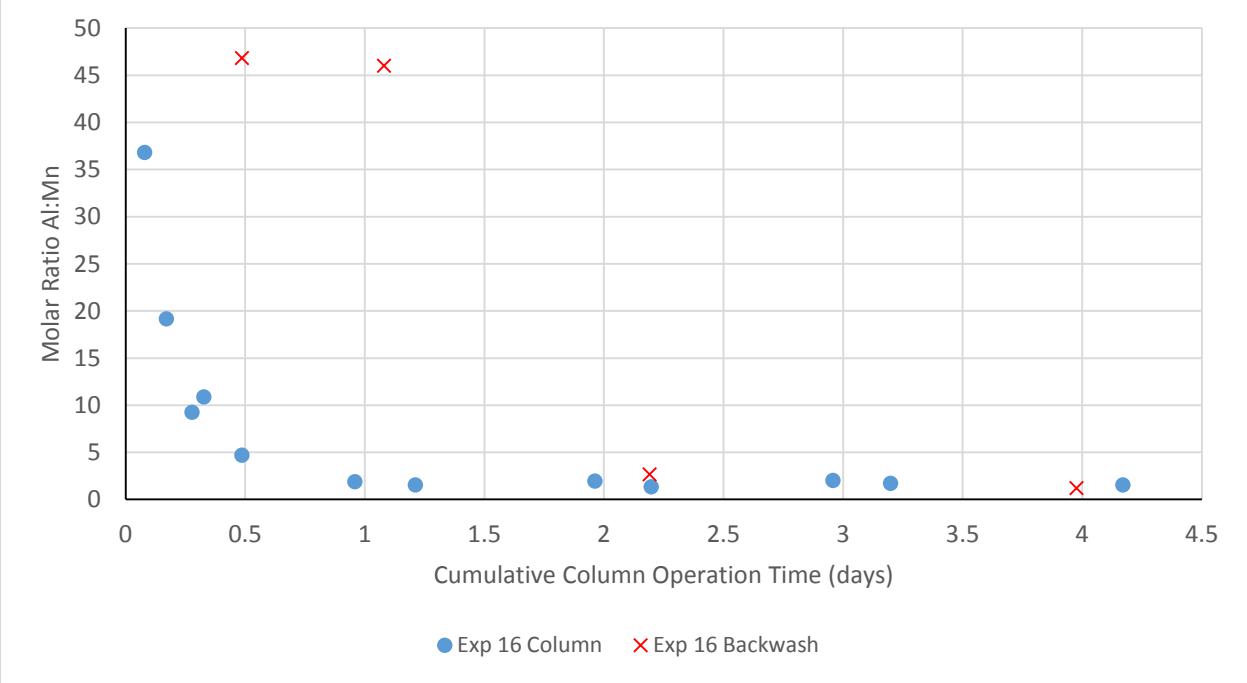

Figure 32: Molar Ratio of Al to Mn of Solids Retained in Column and of Solids Released in Backwash (Exp 16)

To better ascertain the relationship between the molar ratios of backwash material and captured material during the later parts of the experiments (which are difficult to see in Figures 30 through 32) the data are reproduced in Figures 33 through 35 with the y-axis scale expanded for easier viewing. These plots also include a dotted line which represents the average molar ratio of Al to Mn obtained from extractions of the top and bottom media samples for each experiment. All plots show that the material removed throughout the experiments contained higher Al content than the ultimate coating composition, which makes sense given that backwashes also tended to contain higher levels of Al relative to the coating. The material removed during Experiment 10, as seen in Figure 33, generally exhibited an Al to Mn ratio of approximately 2.0; material removed during both Experiment 15 and Experiment 16, on the other hand, generally yielded a ratio closer to 1.7. This result is consistent with previous data indicating that the beds in Experiment 15 and Experiment 16 were specifically adept at capturing Mn relative to other experiments.

The ratio data obtained from backwashes presented in these figures shows that as the experimental duration increased, Al to Mn ratios continued to decrease in favor of Mn and approached the average ratio obtained from media extractions. The fact that the molar ratio of the backwash solids closely matched the molar ratio of the extracted coatings later in the experiment suggests either that progressively larger amounts of coating were sheared off by each backwash until coating material dominated the ratio, or that the particulate material captured participated in adsorption-oxidation of Mn(II) without becoming strongly associated with the media coating. If captured particulate material contained active $MnO_{x(s)}$ sites (either through $MnO_{x(s)}$ nanoparticles integrated into Al floc or through growth of $MnO_{x(s)}$ coating onto deposited Al floc) and were capable of adsorption and oxidation, then during the course of a run the captured material would begin to resemble coating material closely but might not become fully encapsulated and integrated into the $MnO_{x(s)}$ coating on the media.

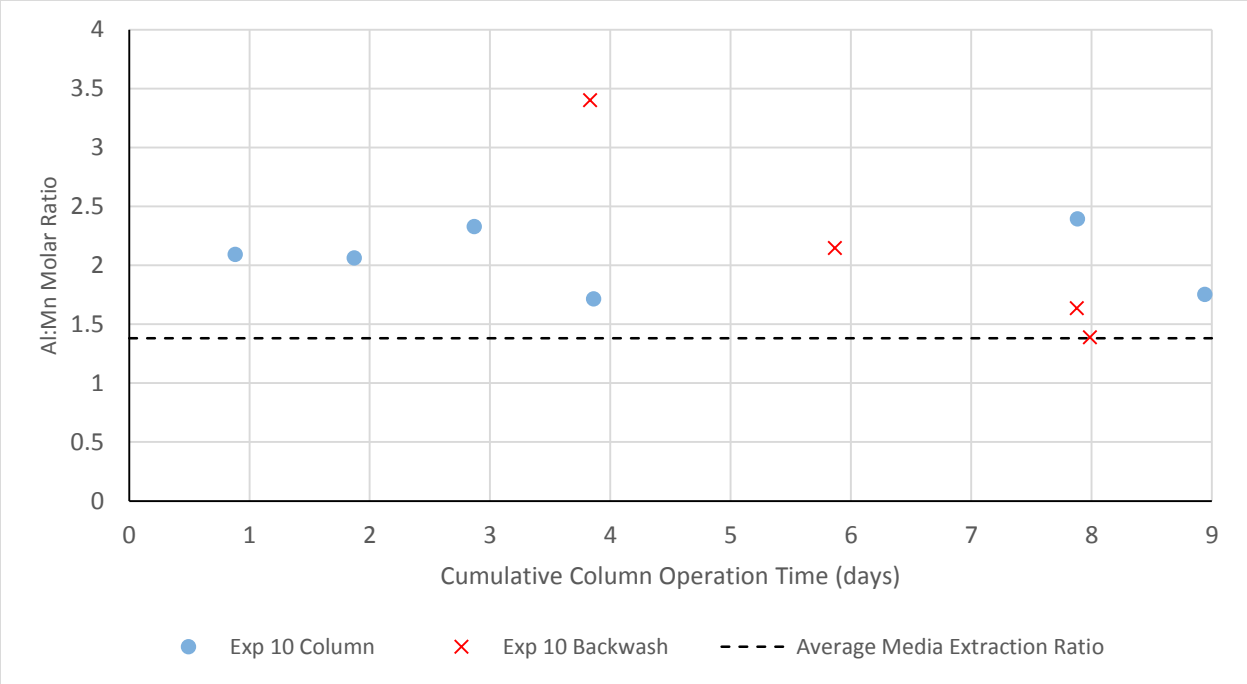

Figure 33: Molar Ratio of Al to Mn in Solids Retained in Column and Solids Released in Backwash (Exp 10: Initial Data Excluded, Average Media Extraction Ratio Included)

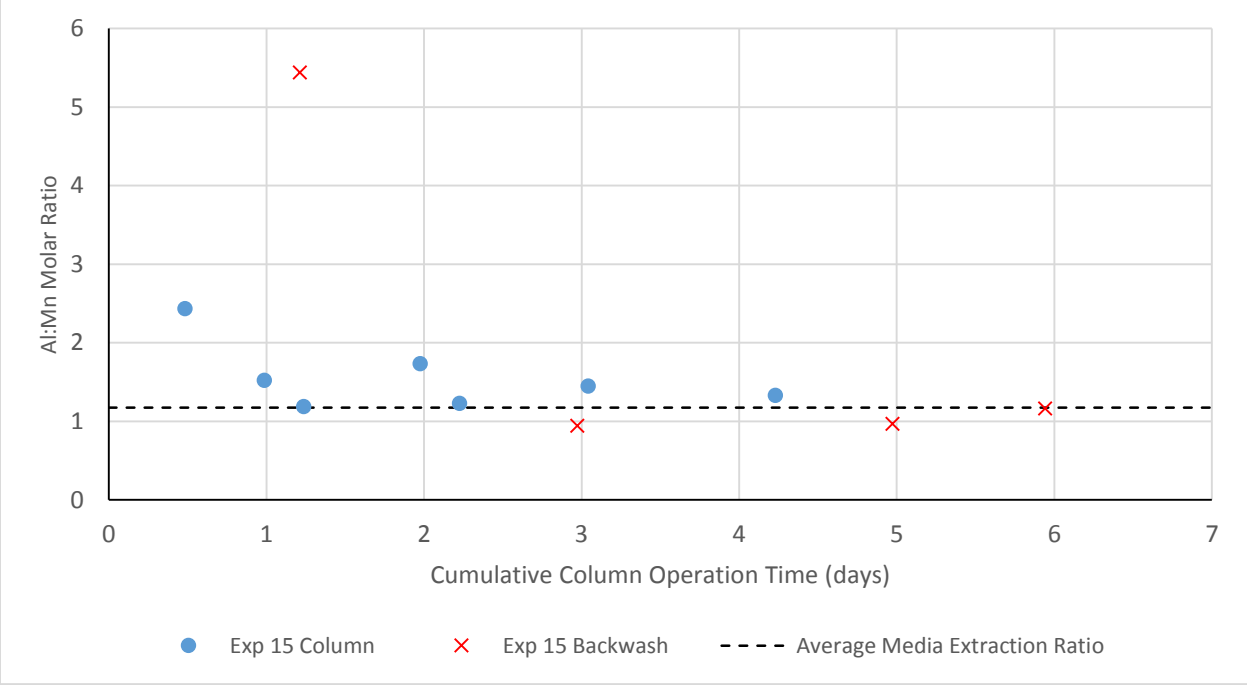

Figure 34: Molar Ratio of Al to Mn in Solids Retained in Column and Solids Released in Backwash (Exp 15: Initial Data Excluded, Average Media Extraction Ratio Included)

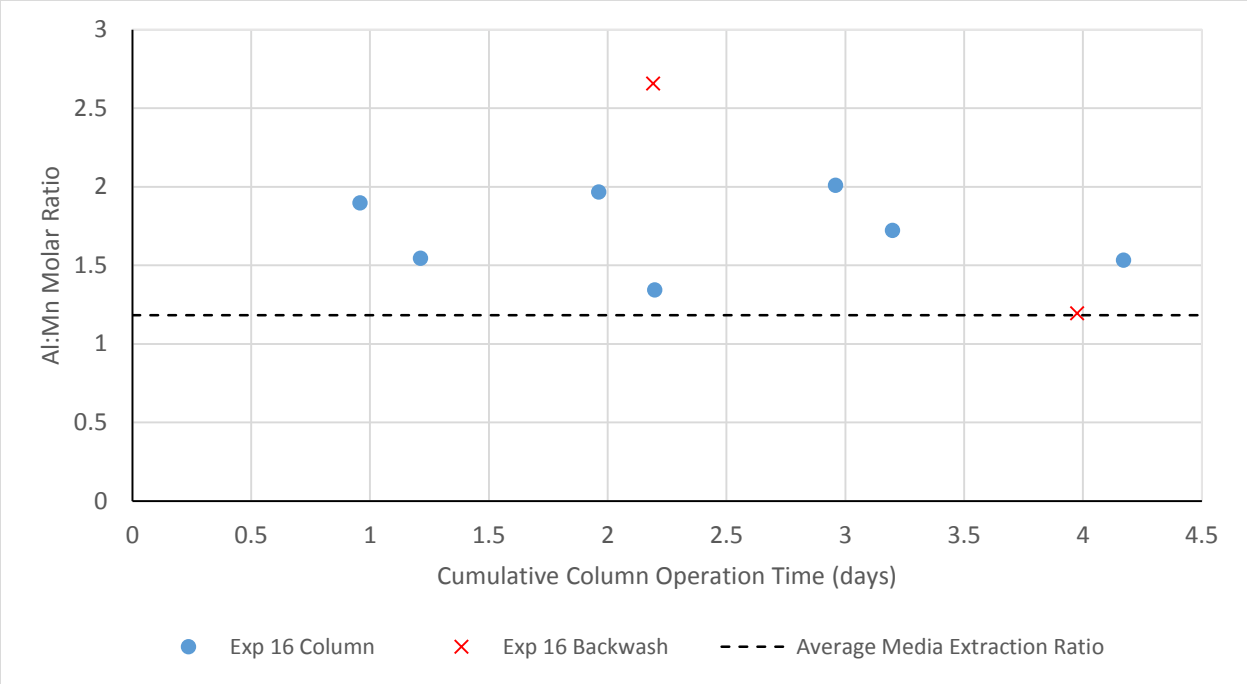

Figure 35: Molar Ratio of Al to Mn in Solids Retained in Column and Solids Released in Backwash (Exp 16: Initial Data Excluded, Average Media Extraction Ratio Included)

4.3.3 Discontinued Chlorination Experiment

In order to determine the source of the Mn present in full-rate backwash solids, an experiment was performed in which a $MnO_{x(s)}$ coating was developed in the presence of Al and after two days, free chlorine addition was discontinued. Although the coating continued to adsorb Mn(II) until all available sorption sites were occupied, this step should theoretically have eliminated the contribution of pre-media oxidized Mn and subsequent adsorption-oxidation of Mn to backwash solids. Any Mn found in solids recovered from the backwashes of this experiment could thus be considered to have come from sheared off coating.

Before examining the backwash solids produced in this experiment, the overall trends of Mn and Al removal were noted. Figure 36 presents the Mn removal curve for the discontinued chlorination experiment. Sampling began after the development of a full coating, when effluent Mn had already become undetectable. The dashed vertical line at 2.7 days represents the time when free chlorine addition was discontinued. After this point, effluent Mn levels began rising rapidly as the adsorption capacity of the media became exhausted. After one day of chlorine-free operation, effluent Mn had reached steady-state conditions with approximately 95% of influent

Mn passing through the bed. The additional 5% represented soluble influent Mn which was still being removed by the media.

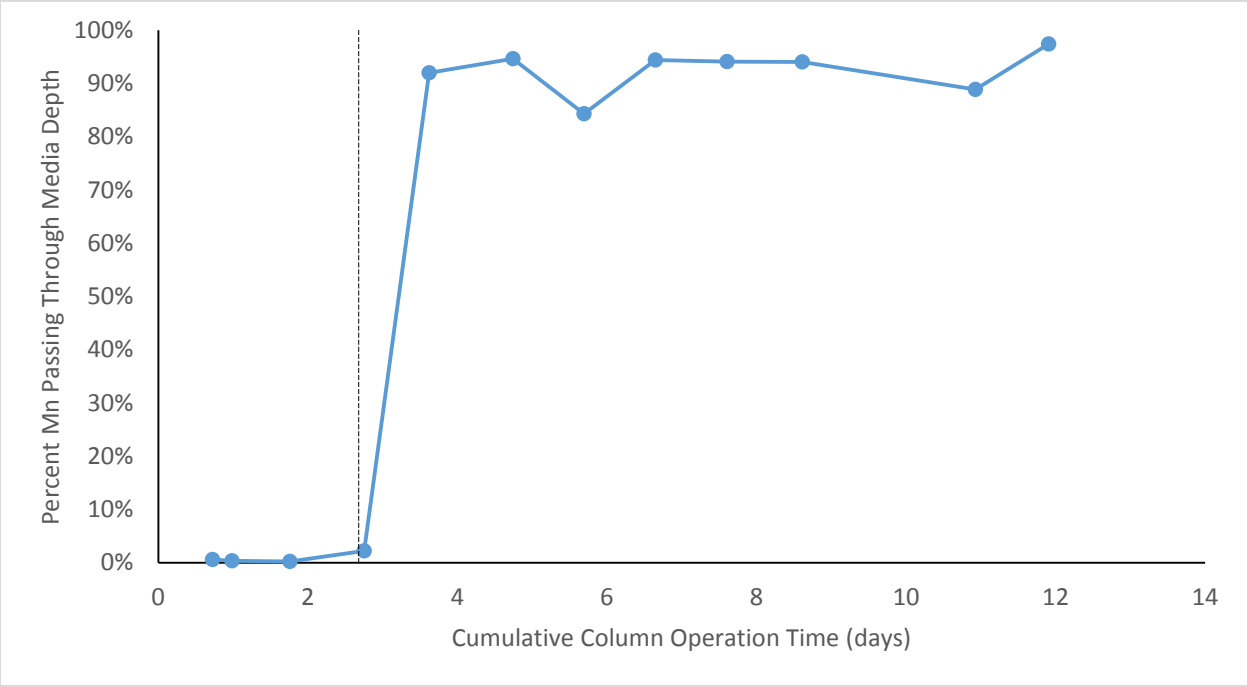

Figure 36: Mn Removal Curve for Discontinued Chlorination Experiment (Dashed Line Indicates Discontinuation of Free Chlorine; 200 µg/L Mn, 220 µg/L Al, pH 7.1-7.5)

This small removal could be the result of continued oxidation by dissolved oxygen, which would occur at a much slower rate than oxidation by free chlorine. Another explanation could be the slow diffusion of adsorbed Mn(II) deeper into the media coating. The $MnO_{x(s)}$ coatings contain additional adsorption capacity in the form of active sites below the surface of the coating, which are generally not accessed due to the rapid rate of oxidation of Mn(II) at the coating surface. Once oxidation at the surface stops, however, adsorbed Mn(II) may slowly diffuse into the coating to these sites, leaving available sites at the surface for small amounts of additional adsorption.

Figure 37 presents the Al removal curve for the discontinued free chlorine experiment. The point at which chlorination was discontinued is indicated by the dashed line. Prior to this point, approximately 20% - 30% of influent Al passed through, which was typical of previous Al/Mn experiments. However, once free chlorine was discontinued and deposition of Mn decreased significantly, effluent Al levels began to rise as well. Over the course of two to three days after

chlorine addition was stopped, effluent Al increased to approximately 60%-70% of influent Al levels. This trend may reflect breakthrough of particulate Al, the capture of which had previously been enhanced by the cementing effects of Mn deposition around captured floc during chlorinated operation. The net effect of chlorine discontinuation on Mn and Al removal resulted in a significant decrease in Mn removal (although not the complete elimination of Mn removal), and a decrease by approximately one half in the amount of Al captured and retained in the bed.

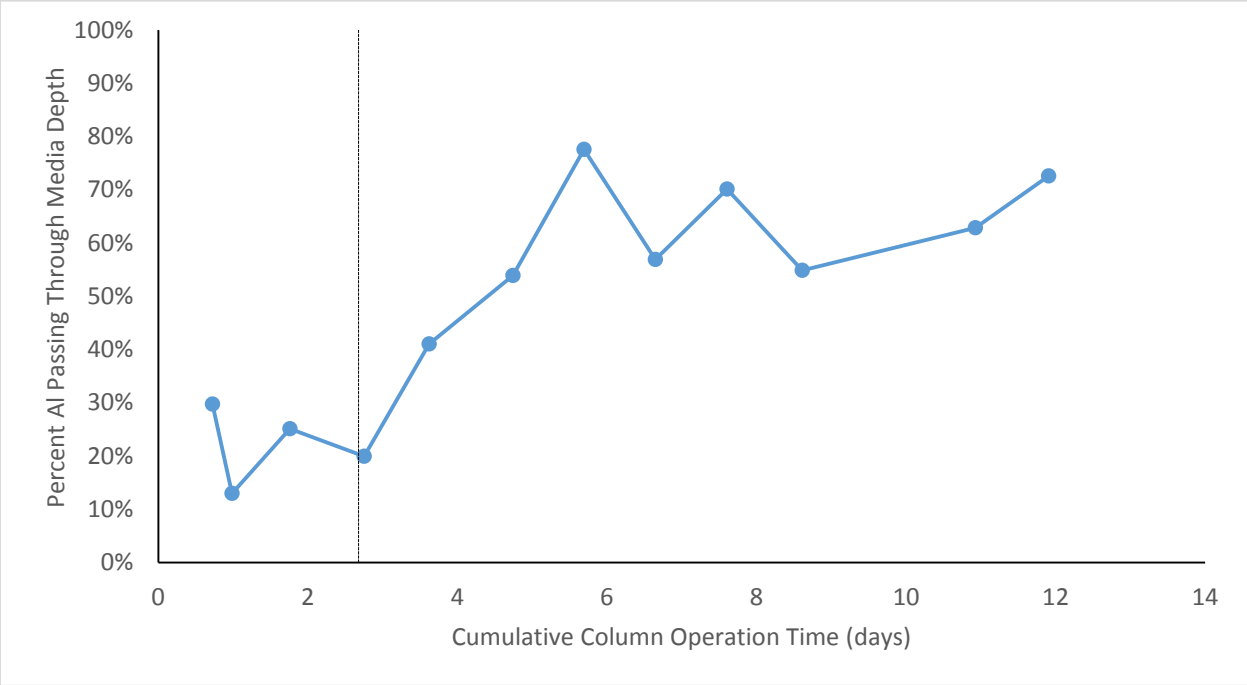

Figure 37: Al Removal Curve for Discontinued Chlorination Experiment (Dashed Line Indicates Discontinuation of Free Chlorine)

Table 15 (located in Appendix A) contains data for backwash solids released during the discontinued chlorine experiment. In order to see the effects of chlorine discontinuation on backwash content, the total mass of Al and Mn released in each backwash is plotted in Figure 38. The molar ratio of Al to Mn found in the solids for each backwash is presented in Figure 39**.** The first two backwashes yielded solids formed in the presence of free chlorine; addition of chlorine was stopped 30 minutes prior to the second backwash, to flush chlorine from feed tubes and from the column and ensure that the column would be exposed to minimal amounts of chlorine in the duration following this backwash.

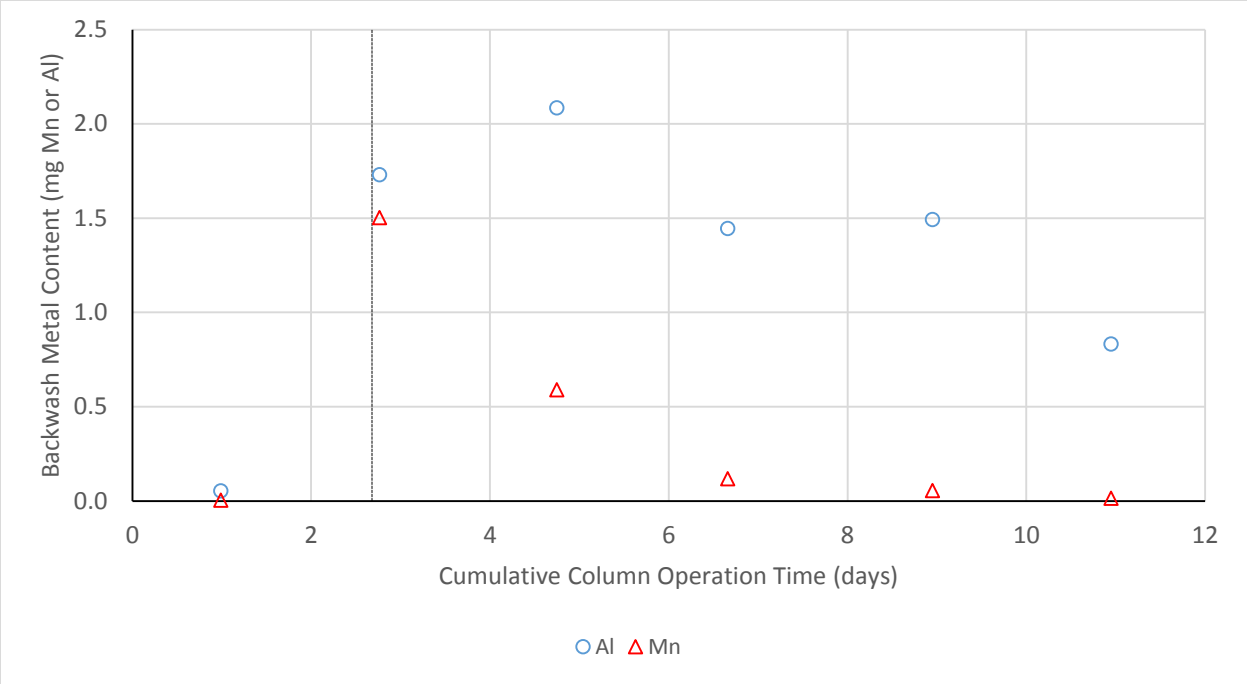

Figure 38: Total Mn & Al Content of Individual Backwashes, Discontinued Chlorination Experiment (Dashed Line Indicates Discontinuation of Free Chlorine)

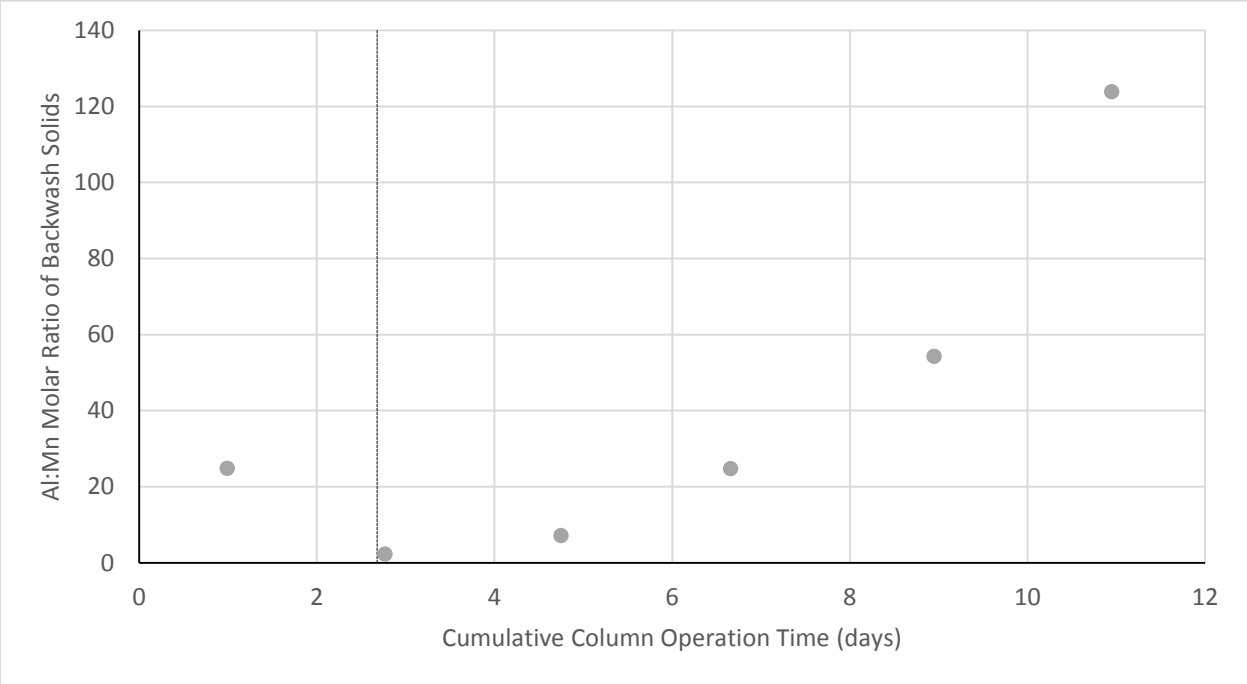

Figure 39: Al:Mn Molar Ratio of Backwash Solids, Discontinued Chlorination Experiment (Dashed Line Indicates Discontinuation of Free Chlorine)

As seen in the backwash solids recovered from previous experiments, much higher levels of both Al and Mn were released in the second backwash than the first backwash, and the Al to Mn ratio of this material decreased significantly from the first backwash to the second backwash. After chlorination was discontinued, each successive backwash yielded less Mn. This material likely originated either from pre-formed coating which sheared off in progressively smaller amounts, or from the small amounts of Mn removal which continued during the chlorine-free conditions. The amount of Al recovered in backwashes generally tended to decrease slightly as well after discontinuation of free chlorine; this trend can be attributed to the observed decrease in Al capture, as greater quantities of Al passed through the media bed. The net impact of these trends on Al to Mn ratio are apparent in Figure 39. The decreased amount of Mn recovered in each subsequent backwash caused the Al to Mn ratios to progressively increase as the experiment progressed.

Applying a mass-balance approach across the whole column, an estimate may be made of the total amount of Mn retained in the media bed over a given time period. The cumulative Mn capture of the bed can be estimated for a given run, and the results compared with the amount of Mn recovered from backwash solids. These data are presented in Figure 40 as the percent of cumulative Mn removed during a given run which was then recovered in the backwash solids (Mn content in backwash divided by total Mn removed during preceding run).

The first backwash yielded very little Mn, which represented an extremely small percentage of the cumulative Mn removal over that run. The second backwash yielded significantly more Mn, releasing approximately 20% of the cumulative Mn removed during that run (for which essentially all of the influent Mn was being removed by the column). The third backwash occurred following the first non-chlorinated period between backwashes, during which removal of influent Mn decreased from 100% to 5%. Although significantly less Mn was recovered in this backwash, this material represented a higher percentage (25%) of the influent Mn removed over this time period due to the decrease in Mn capture. Subsequent backwashes yielded progressively lower percentages; although an approximately constant 5% of influent Mn was removed over these runs, backwashes released a diminishing potion of captured Mn. It is likely that the Mn recovered from these backwashes originated from sheared off coating material.

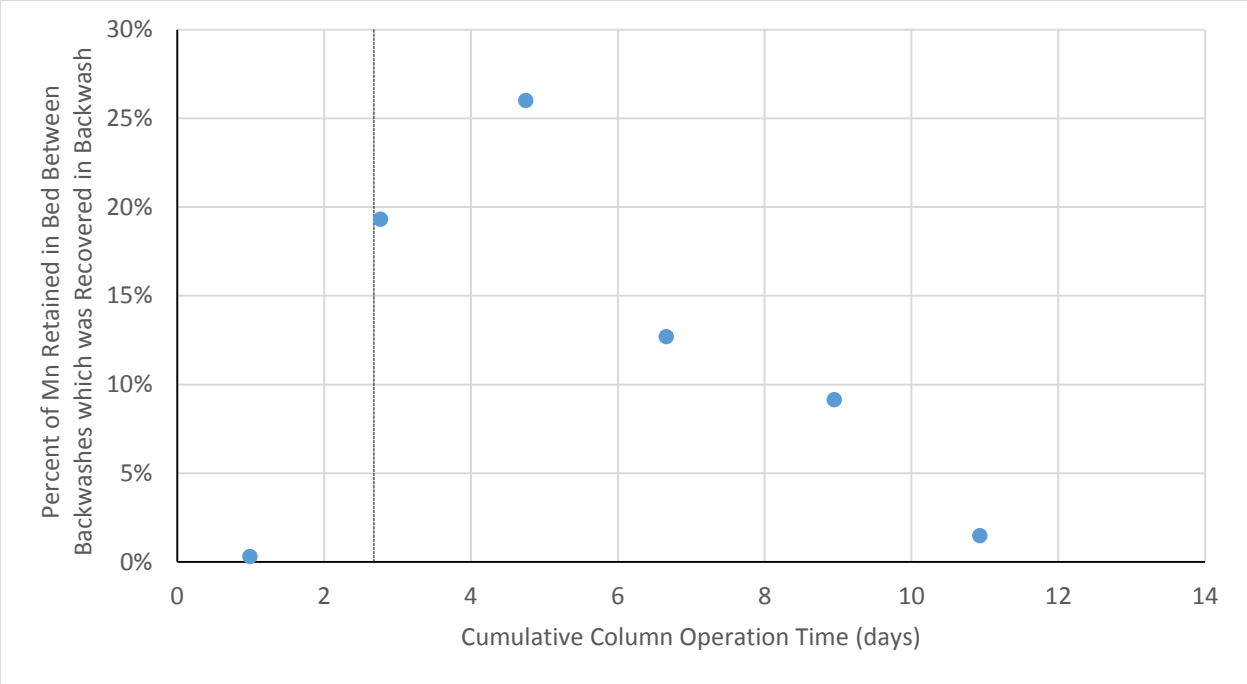

Figure 40: Percent of Mn Retained in Column During Run which was Recovered in Backwash Solids (Dashed Line Indicates Discontinuation of Free Chlorine)

The Mn removed during the chlorine-free period was more difficult to release in backwash than Mn removed in the presence of chlorine, indicating that the material captured during non-chlorinated conditions was more closely associated with the tightly-bound $MnO_{x(s)}$ coating on the media. If this material is considered to be the result of an adsorption-oxidation reaction (as noted previously, most likely by molecular oxygen) which occurs at a slower rate than the reaction with free chlorine, then it appears that the faster oxidation promoted by free chlorine tends to result in $MnO_{x(s)}$ material associated with Al floc which is relatively easy to backwash from the media coating. The fact that a significantly larger percentage of the chlorine-oxidized Mn was recovered in backwash solids supports the theory of pre-media oxidation of Mn(II) and subsequent integration into Al floc.

4.4 Centrifugation Experiments

Results from investigations of the backwash solids recovered from Mn/Al experiments indicated that Mn has the potential to become integrated into Al floc captured in media beds in the presence of free chlorine. The proposed mechanism by which this occurs is pre-media oxidation of a small amount of Mn, followed by destabilization and aggregation of $MnO_{x(s)}$ by

Al. In the centrifugation/UF experiments, pre-media conditions were reproduced in batches of prepared feed water and the solids produced were separated to determine whether any Mn truly existed in oxidized particulate form. A summary of centrifugation/UF experiments performed can be found in Table 16 in Appendix A. This section contains the results of these investigations.

4.4.1 Low-Speed Centrifuge

Experiments Cent/UF 1A and 1B were subjected to centrifugation at approximately 15,000 G in an IEC Centra machine. Batches of prepared feed water were dosed with chlorine, reacted for 30 minutes, and then quenched with thiosulfate. Duplicate samples of each batch were then centrifuged for 1 hour, 3 hours, and 6 hours with the expectation that longer centrifuge times should yield less Al and Mn in the supernatant until all particulate material was separated and truly soluble concentrations were reached. Both experiments were performed with a target pH of 7.0, free chlorine concentration of 2.5 – 3.0 mg/L, and initial soluble Mn concentration of 200 µg/L. Experiment 1A contained no Al, whereas Experiment 1B had a target Al value of 220 µg/L. Duplicate batches were created for both experiments; these batches, which were not chlorinated, acted as control for the chlorinated samples.

Low-speed centrifugation proved ineffective for separation of the solids formed. Supernatant Mn results from Experiment Cent/UF 1B, which contained added Al, are presented in Figure 41. The amount of Mn in the supernatant increases in the chlorinated samples between three and six hours. This experiment also yielded levels of Mn in the unchlorinated supernatants lower than what would be expected. These two unexpected results were typical of low-speed centrifugation data for all trials, suggesting that this process was not sufficient to detect the effects of free chlorine on supernatant Mn concentration.

The supernatant Al results from Experiment Cent/UF 1B are found in Figure 42. Unexpectedly high supernatant Al concentrations were observed in the six-hour samples, similar to the Mn results. The Al concentration never reached the theoretical solubility limit of approximately 40 µg/L, implying that this centrifugation process was ineffective at separating solids from solution. Al concentrations in these solutions should have been very comparable, since the presence of free chlorine should not have affected the formation of Al floc; however, the samples taken at one hour and three hours were not consistent with one another, further suggesting that this procedure did not adequately separate solids.

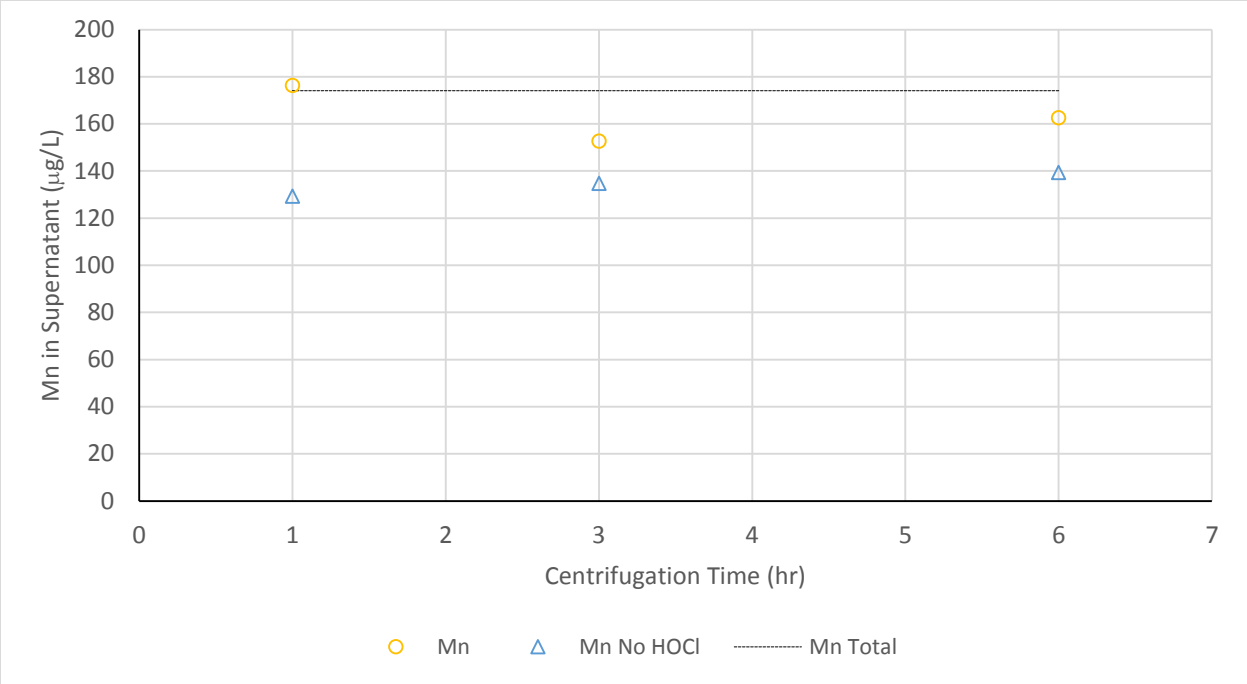

Figure 41: Supernatant Mn Following Low-Speed Centrifugation, Experiment Cent/UF 1B (Al/Mn)

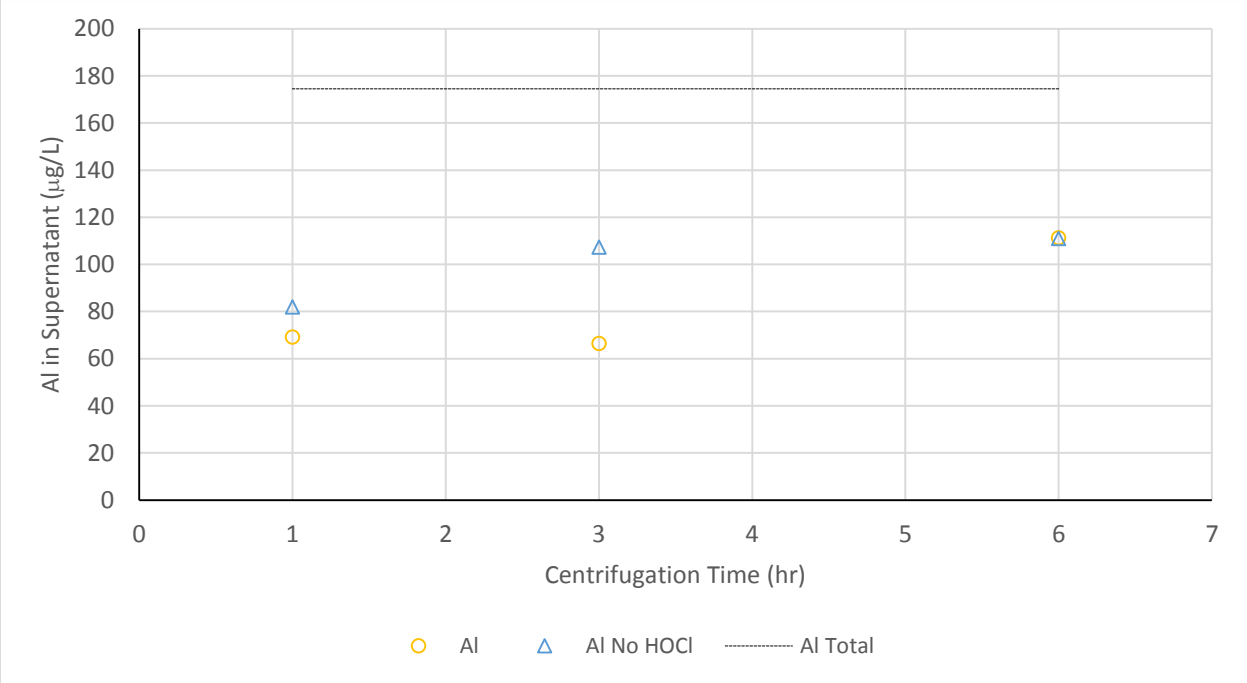

Figure 42: Supernatant Al Following Low-Speed Centrifugation, Experiment Cent/UF 1B (Al/Mn)

4.4.2 High-Speed Ultracentrifuge

The low-speed centrifuge experiment was repeated using a high-speed ultracentrifuge to attempt to enhance the separation of solids from solution. Duplicate chlorinated and unchlorinated batches were prepared with Mn only, Mn/Al, and Al only conditions, as detailed in Table 16 in Appendix A. Only one sample of each batch was run due to the capacity of the rotor; correspondingly, only one centrifuge time was used. Eight hours was selected to maximize solids removal, and samples were centrifuged at approximately 240,000 G. During centrifugation, the chlorinated Mn only tube was crushed; this sample was drawn out of the remaining supernatant as best as possible.

Similar to the low-speed centrifuge data, the results from this experiment were inconsistent with expectations. Figure 43 presents the control and supernatant concentrations of Mn and Al after centrifugation. Although significant removal of Mn was observed in the Mn only experiments (20% of initial level), almost no Mn removal was observed in the Mn/Al sample. Additionally, supernatant Al levels were significantly higher than the solubility limit of Al, suggesting that effective separation of solids was not achieved. It is possible that the high gravity effect of centrifugation damaged the structural integrity of floc, inhibiting removal of solids.

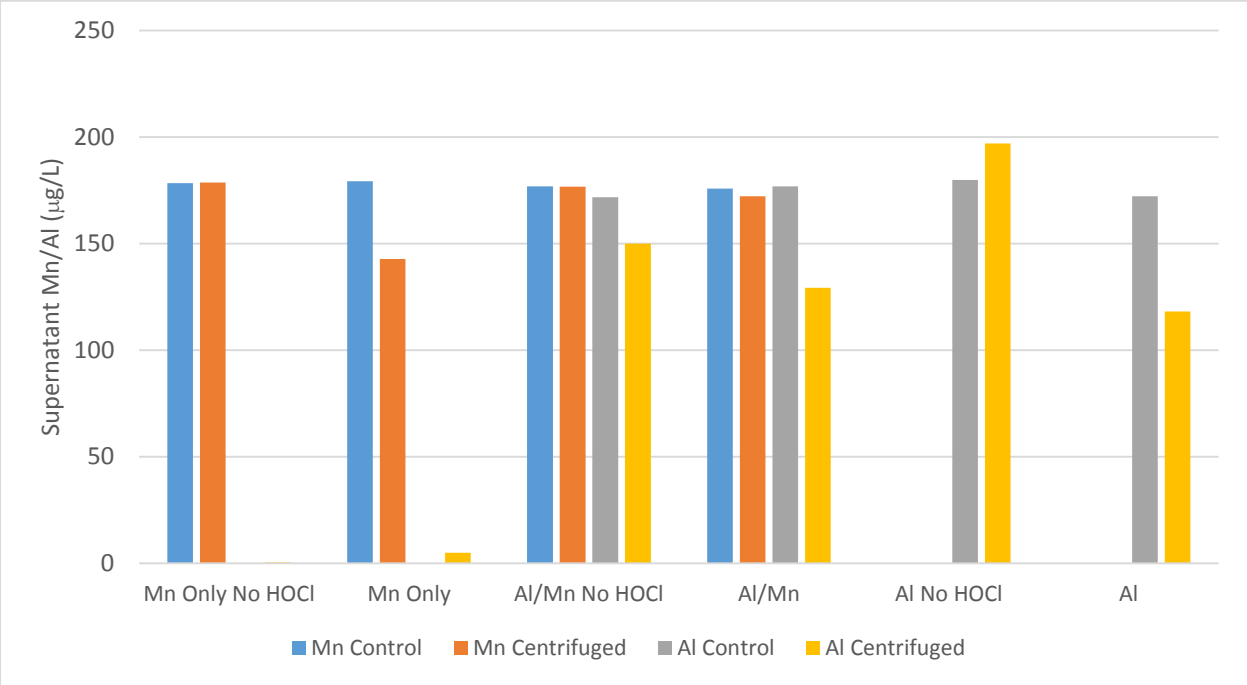

Figure 43: Supernatant Mn & Al Following Ultracentrifugation from Experiment Cent/UF 2A-C (240,000 G for 8 hours)

4.5 UF Experiments

Samples from all centrifugation/UF experiments were retained and filtered through a range of UF membranes to separate solids from solution. Filtrate was captured and analyzed for residual metals content. The five molecular weight cut-offs (MWCO) selected included 1 kDa (1k), 3k, 5k, 10k, and 30k. This range of membrane sizes yielded some insight into the size of solids produced.

4.5.1 Mn Only UF Results

Figure 44 presents results from Experiment Cent/UF 2A, which were typical of all Mn only UF experiments. Both the chlorinated and unchlorinated samples exhibited some relatively constant removal of Mn across the filter membranes. As seen in the low-speed centrifuge data for this experiment, the unchlorinated sample was removed more effectively than the chlorinated sample. This result does not make sense, but was commonly observed among Mn only samples. The removal of Mn from the unchlorinated sample might reflect the presence of oxidized Mn in this sample, but more likely is caused by either adsorption of soluble Mn to the UF cell walls or by complexation of soluble Mn with residual organics in the membrane itself. Although care was taken to soak and flush the membranes before each use to remove any organics, the presence of a small amount could result in the loss of some soluble Mn across the membrane.

4.5.2 Al/Mn UF Results

Results from the Mn/Al UF samples yielded some improvements, but were overall inconsistent with one another. Figure 45 presents the filtrate Mn and Al data for Experiment Cent/UF 1B, which yielded data consistent with expectations. This figure contains the filtrate concentration of both Mn and Al for the chlorinated and unchlorinated samples. The Al concentrations are very consistent between chlorinated and unchlorinated samples. This was expected since Al solubility and speciation are influenced mainly by pH, and these two sample had identical pH values. It can also be noted that UF was much more effective at separating particulate Al from solution than either of the centrifuges used; the Al concentration passing through the lowest two MWCO membranes used was approximately steady at 40 µg/L, which is close to the solubility limit for Al at a pH of 7.0.

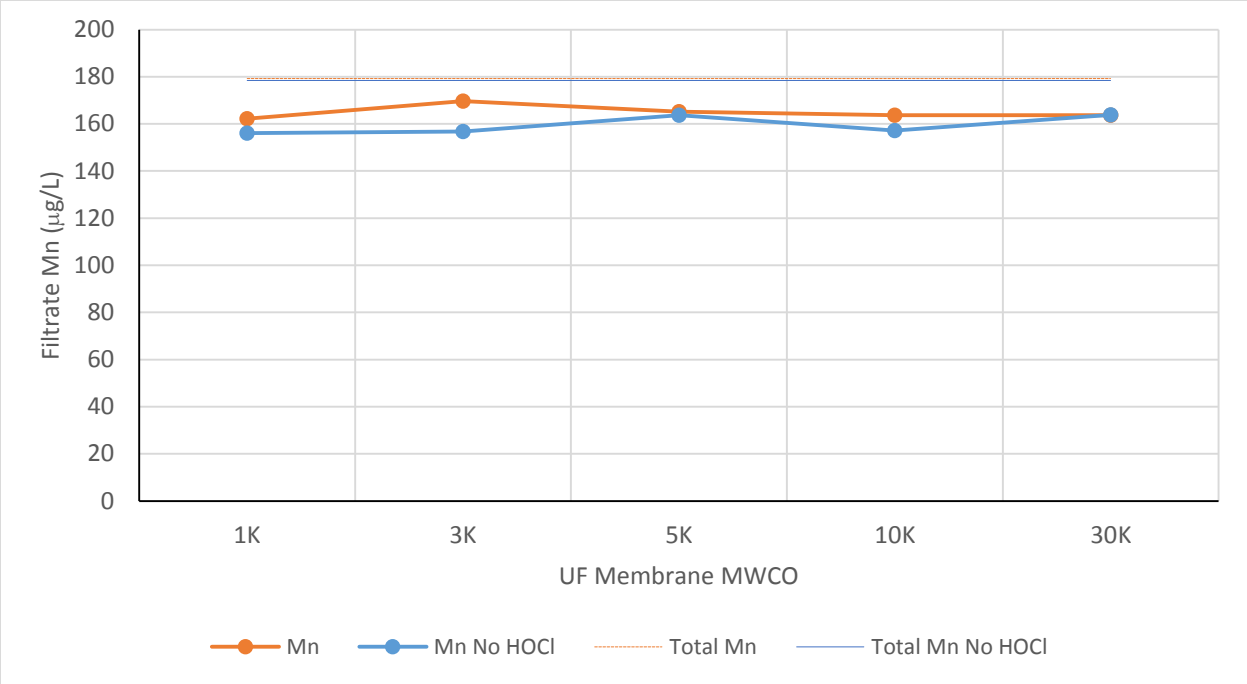

Figure 44: Filtrate Mn Following Ultrafiltration, Experiment Cent/UF 2A (Mn Only, pH 7.0, 30 min reaction)

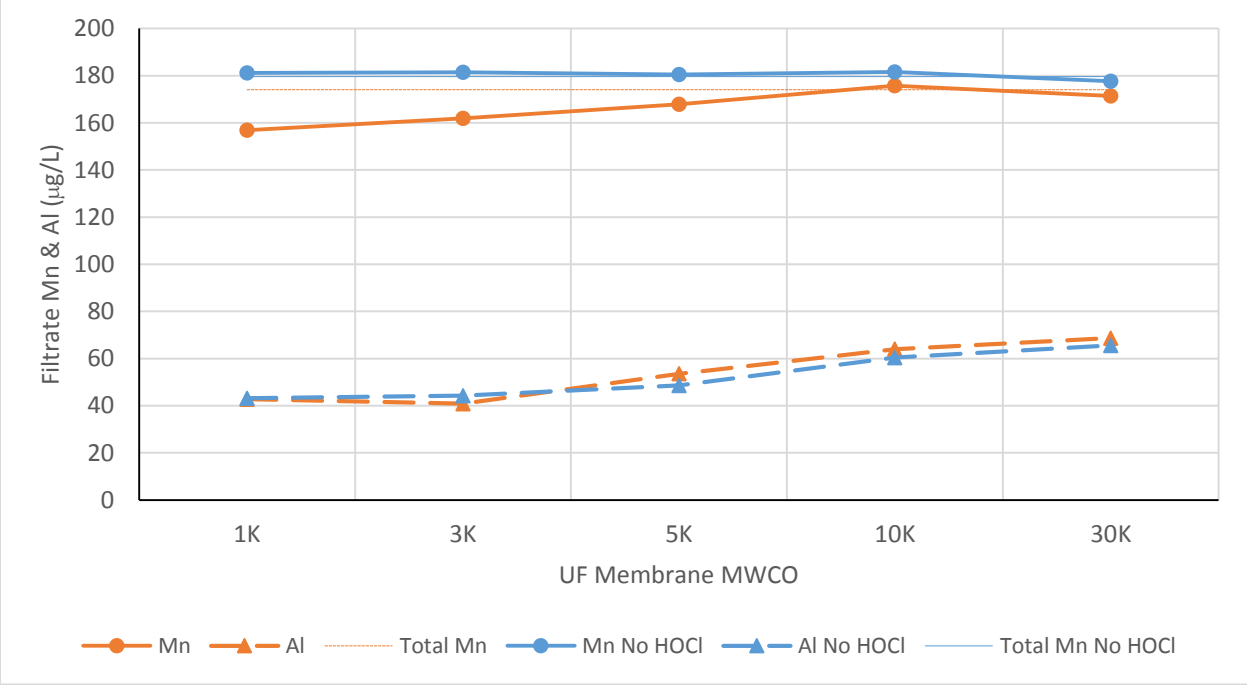

Figure 45: Filtrate Mn & Al Following Ultrafiltration, Experiment Cent/UF 1B (Mn/Al, pH 7.0, 30 min reaction)

The unchlorinated Mn results obtained from this experiment indicate that essentially all of the Mn in this sample was soluble. No appreciable Mn removal was noted across any of the filter sizes in the unchlorinated sample. However, the chlorinated sample demonstrated Mn removal for MWCO sizes smaller than 10k. Some additional removal was gained as membranes decreased in MWCO size, indicating that particulate material containing Mn was produced over a range of sizes. At least some of the Mn removal could not be attributed to corresponding Al removal; a decrease in filtrate Mn concentration was observed between the 3k and 1k filters, but no additional Al was removed between these two filters. It is possible that Mn solids became integrated into Al floc captured on the intermediate MWCO filters, but some of the oxidized Mn appeared to be free in solution as well.

Figure 46 presents the Mn and Al filtrate data for Experiment Cent/UF 2B. This experiment used almost identical conditions to Experiment Cent/UF 1B, although the pH was slightly lower. The pH difference may account for the lower Al levels observed in the filtrate of this experiment. At pH 6.9, the solubility of Al is less than the solubility at pH 7.0, which was reflected in the data. As with Experiment Cent/UF 1B, the unchlorinated sample of Experiment 2B yielded approximately 100% of the original Mn through all filter sizes. This result, which was expected and repeatable between these two experiments, contrasts sharply with the unexpected removal of unchlorinated Mn observed in the Mn only experiments. The reason for the difference is unknown.

The chlorinated sample showed the removal of some oxidized Mn at the higher MWCO filters, but this removal was not repeated across the smaller MWCO filters. Because the pH was slightly lower than Experiment 1B, less oxidation would be expected to occur during the reaction period, but why the lower MWCO filters were unable to capture material that was caught on the higher MWCO filters is unknown.

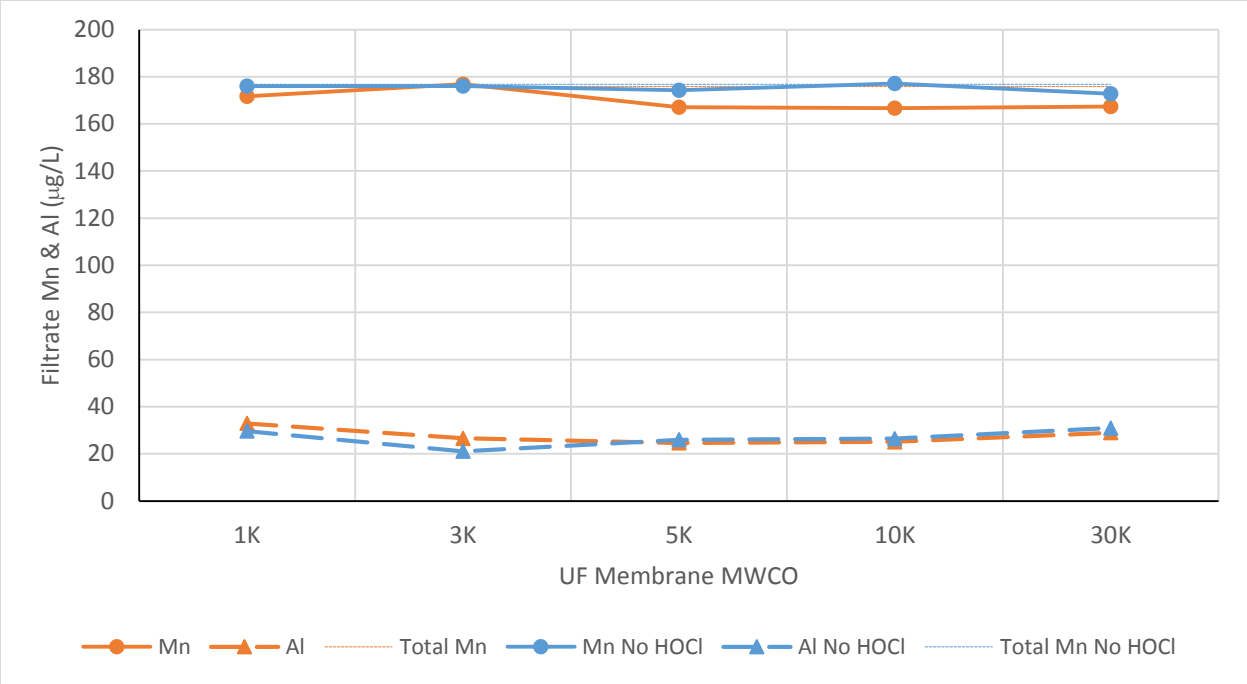

Figure 46: Filtrate Mn & Al Following Ultrafiltration, Experiment Cent/UF 2B (Mn/Al, pH 6.9, 30 min reaction)

5.0 DISCUSSION

5.1 Column Performance

The rapidity of $MnO_{x(s)}$ coating formation in the presence of particulate Al indicates that $MnO_{x(s)}$ coating initiation is improved by the addition of Al. Because the media used in the trials was initially uncoated, the initiation of $MnO_{x(s)}$ coating had to occur either by adsorption of Mn(II) ions to native features on the media surface and subsequent oxidation by free chlorine, or by capture of $MnO_{x(s)}$ particles formed prior to contact with the media bed which acted as a seed to initiate development of a $MnO_{x(s)}$ surface. It is unlikely that the retention of particulate Al alone in the media bed enhanced the adsorption of Mn(II) ions out of solution, since Mn(II) has been shown to adsorb very poorly onto $Al(OH)_{3(s)}$ floc (Jones 2012; Wang et al. 2012). The more likely explanation appears to be that some small amount of $MnO_{x(s)}$ particles were formed prior to contact with the media, and their retention on the media was enhanced by their destabilization and integration into $Al(OH)_{3(s)}$ floc and subsequent attachment to the media.

Figure 47 presents the Mn removal curves for representative experiments using Mn/Al, Mn only, soluble Al, and Fe feeds. The Mn removal performance of $MnO_{x(s)}$ coatings formed in the presence of particulate Al specifically was differentiated from the performance of coatings formed with no Al in two main respects: (a) the removal capacity of the six-inch bed, and (b) the rate of formation of $MnO_{x(s)}$ coatings. The addition of particulate Al into feed waters allowed for sufficient media coating to remove all influent Mn over the six-inch bed depth; furthermore, media extraction data indicated that most Mn removal actually occurred in the top inches of the bed. Conversely, beds coated in the absence of Al had the capacity to remove only 40 – 60% of influent Mn over the entire six-inch bed depth for the conditions studied. Figure 47 illustrates the difference in steady-state effluent Mn conditions between Mn only and Mn/Al experiments. The increased Mn removal observed in experiments with particulate Al was not dependent on continuous Al deposition; once a full coating was formed in the presence of Al, the enhanced capacity for Mn removal was maintained even after subsequent discontinuation of Al, as seen in Figure 19.

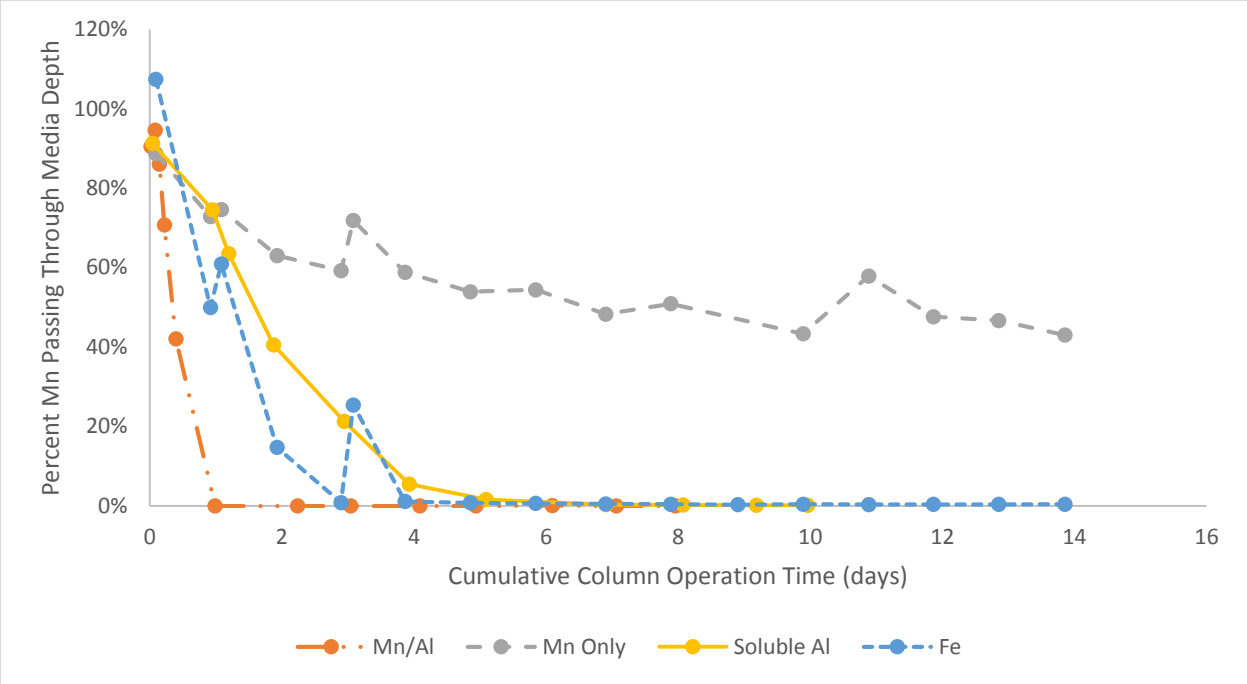

Figure 47: Comparison of Mn Removal Between Mn/Al, Mn Only, Soluble Al and Fe Experiments

It is possible that the enhanced Mn removal observed in the particulate Al experiments is caused partly by cementation and encasement of particulate Al species in growing $MnO_{x(s)}$ coatings, resulting in an increase in effective media surface area. Past work by Merkle (1996), Goodwill (2006), and Jones (2012) has indicated that $MnO_{x(s)}$ surfaces have the potential to grow around and encase particulate matter. Results from this research study corroborated findings by Jones (2012) who reported that deposition of Mn is associated with a corresponding improvement in the retention of particulate Al species in a media bed, which could be the result of cementation of Al floc into $MnO_{x(s)}$ coatings. Further, the enhanced Mn removal of the beds coated in the presence of Al would agree with findings by Goodwill (2006) correlating the presence of particulate matter in the influent to an oxide-coated media bed with increased apparent BET surface area.

SEM imaging of coatings formed in this research study, found in Figure 14, show that the general topography of the coating formed in the presence of particulate Al was significantly rougher and more porous in appearance than that of the Mn-only (no Al present) coating, which appeared to follow the surface topography of the media itself. The encasement of Al particles may be responsible for the alteration in topography. This assertion is supported by the fact that

application of Fe, which results in the formation of particulate hydroxide floc similar to Al floc, also resulted in enhanced removal of influent Mn.

The presence of Al in feed waters also resulted in a much more rapid rate of coating formation (as measured by the decrease in effluent Mn levels). Whereas columns exposed to Mn-only feeds tended to reach steady-state effluent Mn conditions within four to six days (with effluent Mn concentration asymptotically approaching a constant level), columns loaded with Al exhibited a swift and steady decrease in effluent Mn concentrations below detection limit within 24 hours of operation. The difference in the rate of Mn removal, which can be observed in Figure 47, may be attributed to the initiation mechanism of the coatings, as well as the more rapid accumulation of Mn into the media coating (especially in the upper few inches of the media bed).

In both Mn only and Mn/Al trials, $MnO_{x(s)}$ coating must have grown from initial seeding sites to cover the available surface area present on the media. The Mn/Al columns may have exhibited more rapid coating development compared with the Mn only columns because the capture of Al floc containing some Mn oxidized prior to media contact may have seeded the media in these columns with more coating initiation sites. As noted previously, in order for coating to begin forming on uncoated media, either soluble Mn(II) must sorb to native surface features or the media must capture pre-formed $MnO_{x(s)}$ to seed coating development. The presence of captured Al in a media bed is unlikely to improve adsorption of soluble Mn(II) (Jones 2012; Wang et al. 2012); however, Al would aid in the destabilization and capture of any $MnO_{x(s)}$ material formed prior to filtration, which might be colloidal in nature, negatively charged, and very unlikely to be retained in the media bed on its own. The retention of greater amounts of this material in the media bed results in a greater number of initial coating seed sites, and in more rapid formation of coating as observed in the Mn/Al columns. The net effect of improved capture of $MnO_{x(s)}$ particles formed pre-filter by Al and particulate Al cementation into $MnO_{x(s)}$ coatings could be responsible for the improved Mn removal performance of the Al/Mn columns compared with the Mn only columns.

The presence of both Fe and soluble Al in column feeds also resulted in more rapid coating formation than Mn only conditions, although development of coating was slower than observed in particulate Al experiments. Mn removal curves for these two experiments may be found in Figure 47. This can be attributed to the lower mass loading rate of coagulant (either Fe or Al) in these two experiments. Because the molar mass of Fe is approximately twice the molar mass of

Al, 220 µg/L of Fe is approximately half the molar concentration of 220 µg/L Al. Correspondingly, effluent Mn concentrations from the Fe experiment reached detection limit in approximately twice the time as the Mn/Al experiment. The soluble Al experiment, for which the lowest molar concentration of coagulant was added, resulted in the slowest $MnO_{x(s)}$ coating development rate of the three experiments with added coagulants. The fact that soluble levels of Al enhanced $MnO_{x(s)}$ coating development, and that increasing coagulant concentrations increased the rate of $MnO_{x(s)}$ coating development, strongly suggests that these coagulants were destabilizing and improving the retention of particulate $MnO_{x(s)}$ in the media bed. As noted previously, this effect would increase the development rate of $MnO_{x(s)}$ coating within the bed.

5.2 Media Extraction Data

Extraction data from the media used in column experiments provided substantiation for the enhanced ability of the media coated with Al to remove Mn. Samples were taken from the top and bottom of each bed in order to examine the effects of Al on coating distribution within a media bed. All extractions yielded more weight of coating from top samples than bottom samples, as anticipated since the top of the bed comes into contact with the highest concentrations of both Mn and free chlorine (and particulate Al, when present in feed water). Another common trend among experiments was that longer experiment durations resulted in greater amounts of coating on the media, which again makes sense since longer experiment duration results in more cumulative Mn and Al removal by the media.

Samples from Mn only columns proved to have coating distributed more evenly among the top and bottom layers of the bed than Mn/Al columns. Because a significant effluent level of Mn was constantly exiting Mn only media beds, the bottom layers of the beds were exposed to Mn and free chlorine at all times and so coating continued to form as the experiment progressed. In the Mn/Al columns, a small amount of coating initially developed in the bottom layers of the filter but beyond a certain point the vast majority of soluble Mn was being removed by the top layers of the bed and was not reaching the bottom layers any more. Consequently, extractions confirmed that the bottom samples from Mn/Al experiments tended not to accumulate much additional coating beyond about one day of operation. This result, which held true even when Al addition was discontinued after two days of operation, supports the idea that Al aids in the development of coating and improves the capture of Mn.

Extractions also yielded a relatively high degree of correlation between Mn and Al in the coatings. Columns generally had identical target conditions, so the incorporation of Al into coatings was very consistent between experiments. Figure 18 shows the correlation between extractable Mn and extractable Al for top and bottom samples from all experiments. Past work by Jones (2012) has indicated that the ratio of Al to Mn found in coatings depends on the relative loading of Mn and Al to the filter bed, so the consistency observed in the replicate experiments from this study was expected. The experiment conducted with soluble Al yielded a significantly lower ratio of Al to Mn than previous experiments, further supporting that the coating ratio is dependent on Al and Mn loading conditions.

5.3 Backwash Analysis

The observation that backwash material from the Mn/Al experiments tended to be brown-colored indicated that captured floc may have participated in adsorption and subsequent oxidation of Mn(II) by free chlorine. This prompted an investigation into the composition of backwash solids. There are four potential sources for Mn found in backwash solids. The first source is coating formed on the media which may shear off and wash out of the column with other solids during backwash, particularly at higher flow rates when media are partially fluidized. The second source is $MnO_{x(s)}$ formed prior to contact with the filter, which may be aggregated by Al floc and captured as particulate matter in the media bed. The third source is soluble Mn(II) which participates in adsorption-oxidation onto $MnO_{x(s)}$ material formed pre-media and aggregated into Al floc (as in the second source). The fourth source is adsorption of soluble Mn(II) onto Al floc; however, data by Jones (2012) and recorded from unchlorinated Mn/Al UF samples in this study indicate that little to no soluble Mn(II) adsorb to Al floc under the conditions of interest. If $MnO_{x(s)}$ particles were being formed prior to filtration, as the column performance data suggested, then the backwash analyses should show evidence of Mn from the second and third sources.

Sub-fluidization backwash rates (which were intended to flush captured particles from the bed without releasing any media coating) were used in an attempt to isolate Mn-containing solids which originated from pre-media oxidation. Solids recovered from these experiments yielded trace amounts of Mn, which may have been the result of pre-media oxidation. However, subsequent backwashes at sub-fluidization rates in media loading trials conducted with no free

chlorine present (where no pre-media oxidation could have taken place) yielded similar trace amounts of Mn, indicating that sub-fluidization backwash rates may actually result in the stripping of some Mn coating from the media. Thus, the trace Mn discovered in sub-fluidization backwash solids could not be definitely attributed to pre-media Mn oxidation by free chlorine.

Solids recovered from full-rate backwashes (sufficient to fluidize the bed by 30% of its original depth) were also analyzed for composition. These solids yielded far more cumulative Mn and Al than the sub-fluidization solids, and specifically were composed of a much lower Al to Mn ratio. Full-rate backwashes are expected to release greater amounts of solids, since these backwashes scour the bed of particles trapped deep within the bed and also result in the disruption of some media coating.

Solids recovered from both sub-fluidization and full-rate backwashes exhibited one common trend. In both sets of data, the Al to Mn ratio of solids tended to decrease as the operation time between backwashes increased. This trend can be observed in Figures 26 and 29. As the particulates which would eventually make up backwash solids were retained in the media beds longer, they tended to accumulate Mn. Since the Al to Mn ratio of solids applied to the media bed in the influent remained constant over time, this trend suggests that these solids were actively participating in adsorption-oxidation of Mn. This supports the case for $MnO_{x(s)}$ formed prior to media contact becoming incorporated into Al floc; once this material was captured in the media bed, it would act like $MnO_{x(s)}$-coated media to adsorb and catalyze oxidation of soluble Mn, shifting the Al to Mn ratio in favor of more Mn with longer operation times between backwashes.

The Al to Mn ratios of solids recovered from full-rate backwashes were also compared against the Al to Mn ratios of the material instantaneously being removed by the column at several points over the course of the experiment. Initial backwashes yielded material composed of a far higher Al to Mn ratio than the cumulative material removed to that point. As the experiments progressed, the Al to Mn ratio of backwash solids decreased and approached levels typical of the average coating ratio. This likely is caused partially by the presence of greater amounts of sheared-off coating in the backwash solids, but also may reflect the participation of $MnO_{x(s)}$ material captured in Al floc in adsorption-oxidation to form solids which more closely resemble coating than Al floc in composition.

5.4 Centrifugation/UF

The centrifugation and UF experiments were designed to replicate pre-media conditions from the column experiments (where some oxidation of Mn by free chlorine was hypothesized to occur), and to separate the solids formed under these conditions in an attempt to isolate some oxidized Mn. Low-speed centrifugation at approximately 15,000 G was not capable of reliably separating solids from solution, as evidenced by elevated and inconsistent levels of Mn and Al in the supernatant of the centrifuged samples. High speed centrifugation at approximately 240,000 G proved similarly incapable of removing solids from the sample supernatant. It is possible that the high gravity effect of centrifugation damages the structure of $Al(OH)_{3(s)}$ flocs and prevents their effective separation by centrifugation.

Samples in which soluble Mn was exposed to free chlorine for up to 30 minutes were also subjected to ultrafiltration through a range of membranes of different MWCO sizes. These membranes proved capable of removing particulate Al, resulting in filtrate Al levels close to the estimated solubility limit at the pH evaluated in each test. Mn removal was observed in some of these experiments; however, consistent results were not achieved across these UF experiments. Most of the Mn-only experiments exhibited a constant Mn removal across all filter sizes which was not observed in Mn/Al experiments, and in most cases the unchlorinated Mn-only samples registered more Mn removal across membranes than the corresponding chlorinated samples, which does not make sense. The Al/Mn experiments yielded results which were more closely aligned with expectations; Mn in the unchlorinated samples passed through membranes, indicating that it was soluble. Generally some Mn removal was observed in the chlorinated samples, specifically at lower MWCO sizes. However, the results were not consistent between experiments. The UF method shows potential for detection of the presence of oxidized Mn solids, but further development of this UF sample processing technique is required.

6.0 CONCLUSIONS

6.1 Conclusions

The impact of Al on the performance of $MnO_{x(s)}$ coatings, specifically regarding their initiation and formation, was examined in this research study. Bench-scale column tests were used to investigate the performance of media beds regarding soluble Mn capture with coatings developed in the presence and absence of Al. The coatings developed on the media in these studies were examined more closely using coating extraction and SEM imaging. Observations from these experiments resulted in subsequent experiments being designed to study the composition of backwash solids recovered from columns loaded with a combination of Mn and particulate Al. The potential for Mn oxidation by free chlorine prior to contact with media was examined in a series of experiments intended to replicate pre-media conditions and isolate the particulate matter formed under these conditions. The results of these studies led to several conclusions about the role played by Al in the development and performance of $MnO_{x(s)}$ coatings for Mn removal in drinking water treatment.

1. Al aids the development of $MnO_{x(s)}$ coating, resulting in the formation of more coating at a faster rate than similar experiments performed in the absence of Al.
2. The enhanced formation of $MnO_{x(s)}$ coating on media loaded with Al improves the ability of media to remove soluble Mn. The same effect was observed when particulate Fe was substituted for particulate Al, indicating that this effect is not unique to Al.
3. The improved Mn removal exhibited by media loaded with Al begins to take effect immediately upon introduction of Al into feed waters, and continues even after discontinuation of Al loading. This indicates that increased capacity for Mn removal is the result of increased deposition of coating onto media, and not a continuous interaction between Mn and Al in solution.
4. The growth of $MnO_{x(s)}$ coating on media surface has the ability to encapsulate particulate Al, which results in a much rougher and more porous surface than coatings formed without particulate Al.
5. Longer operation times between subsequent backwashes yield solids composed of a higher fraction of Mn, suggesting that solids retained in media beds participate in adsorption and oxidation of soluble Mn. The source of initial $MnO_{x(s)}$ sites in backwash solids necessary to seed adsorption and oxidation is hypothesized to be pre-media

oxidation of a small amount of Mn; this could not be confirmed by centrifugation and UF experiments in this study.

6.2 Future Research

This research study provided anecdotal evidence in support of the rapid formation of $MnO_{x(s)}$ nanoparticles by oxidation with free chlorine prior to contact with media. However, direct evidence of the formation of these particles was not obtained. Future research is needed to isolate and identify these particles. The UF experiments employed in this study showed promise for the detection of solid material formed by controlled oxidation reactions; this method should be further investigated to conclusively determine whether or not $MnO_{x(s)}$ particles form prior to contact with media beds under conditions representative of a water treatment plant, and whether these particles can become integrated into $Al(OH)_{3(s)}$ floc.

This study also raised questions about the potential for the release of coating from media by shear forces caused by flows typical of downward gravity filtration. Some experiments appeared to show $MnO_{x(s)}$ coating being released during the sub-fluidization rate backwash experiments, where the backwash superficial flow rate barely exceeded the forward flow rate used for operation of the column. If such small flows were truly capable of disrupting media coating, a continuous source of particulate oxidized Mn might be introduced into the distribution system under typical filtration conditions. Mn can be a difficult contaminant to control, and may have implications on human health which are only beginning to be realized by regulatory agencies. Continued research into NGE media for Mn treatment will be important as Mn control becomes a more prominent issue.

WORKS CITED

Agency for Toxic Substances and Disease Registry, 2012. *Toxicological Profile for Manganese*, Atlanta, GA.

AWWA, 2011. *Water Quality & Treatment: A Handbook on Drinking Water* 6th ed. J. K. Edzwald, ed., AWWA.

Bhang, S.-Y. et al., 2013. Relationship Between Blood Manganese Levels and Children's Attention, Cognition, Behavior, and Academic Performance--a Nationwide Cross-Sectional Study. *Environmental research*, 126, pp.9–16. Available at: http://www.ncbi.nlm.nih.gov/pubmed/23790803 [Accessed January 7, 2015].

Brandhuber, P. et al., 2013. *Guidance for the Treatment of Manganese*, Denver, CO.

Brezonik, P.L. & Arnold, W.A., 2011. *Water Chemistry*, New York, NY: Oxford University Press.

Casale, R.J., LeChevallier, M.W. & Pontius, F.W., 2002. *Manganese Control and Related Issues*, Denver, CO: AWWA.

Cerrato, J.M. et al., 2011. Application of XPS and solution chemistry analyses to investigate soluble manganese removal by MnO(x)(s)-coated media. *Environmental science & technology*, 45(23), pp.10068–74. Available at: http://www.ncbi.nlm.nih.gov/pubmed/22040038.

Cerrato, J.M. et al., 2010. Manganese-oxidizing and -reducing microorganisms isolated from biofilms in chlorinated drinking water systems. *Water research*, 44(13), pp.3935–45. Available at: http://www.ncbi.nlm.nih.gov/pubmed/20605183 [Accessed September 4, 2014].

El Araby, R., Hawash, S. & El Diwani, G., 2009. Treatment of iron and manganese in simulated groundwater via ozone technology. *Desalination*, 249(3), pp.1345–1349. Available at: http://linkinghub.elsevier.com/retrieve/pii/S0011916409008066 [Accessed October 20, 2014].

EPA, 1979. National Secondary Drinking Water Regulations, *143.3*

Goldstein, J.I. et al., 1981. *Scanning Electron Microscopy and X-Ray Microanalysis*, New York, NY: Plenum Publishing Corporation.

Goodwill, J., 2006. *Characterization of Manganese Oxide Coated Filter Media*. Master's Thesis, University of Massachusetts Amherst

Gregory, D. & Carlson, K., 2003. Effect of Soluble Mn Concentration on Oxidation Kinetics. *Journal (American Water Works Association)*, 95(1), pp.98–108.

Hao, B.O.J. et al., 1991. Kinetics of Manganese (II) Oxidation with Chlorine. *Journal of Environmental Engineering*, 117(3), pp.359–374.

Hargette, A.C. & Knocke, W.R., 2001. Assessment of the Fate of Manganese in Oxide-Coated Filtration Systems. *Journal of Environmental Engineering*, 127(December), pp.1132–1138.

Hem, J.D., 1992. *Study and Interpretation of the Chemical Characteristics of Natural Waters*,

Islam, Anjuman et al., 2010. Characterization of Filter Media MnOx(s) Surfaces and Mn Removal Capability. *Journal (American Water Works Association)*, 102(9), pp.71–83.

Jones, A., 2012. The Role of Aluminum within MnOx(s) - Coated Filtration Media in Drinking Water Treatment.

Junta, J.L. & Hochella, M.F., 1994. Manganese(II) Oxidation at Mineral Surfaces : A Microscopic and Spectroscopic Study. , 58(22), pp.4985–4999.

Khan, K. et al., 2012. Manganese exposure from drinking water and children's academic achievement. *Neurotoxicology*, 33(1), pp.91–7. Available at: http://www.pubmedcentral.nih.gov/articlerender.fcgi?artid=3282923&tool=pmcentrez&rendertype=abstract [Accessed September 8, 2014].

Knocke, W.R. et al., 2010. Adsorptive Contactors for Removal of Soluble Manganese during Drinking Water Treatment. *Journal (American Water Works Association)*, 102(8), pp.64–75.

Knocke, W.R. et al., 1991. Kinetics of Manganese and Iron Oxidation by Potassium Permanganate and Chlorine Dioxide. *Journal (American Water Works Association)*, 83(6), pp.80–87.

Knocke, W.R., Hoehn, R.C. & Sinsabaugh, R.L., 1987. Using Alternative Oxidants to Remove Dissolved Manganese From Waters Laden With Organics. *Journal (American Water Works Association)*, 79(3), pp.75–79.

Knocke, W.R., Ramon, J.R.. & Thompson, C.P.., 1988. Soluble Manganese Removal on Oxide-Coated Filter Media. *Journal (American Water Works Association)*, 80(12), pp.65–70.

Kohl, P.M. & Medlar, S.J., 2006. *Occurrence of Manganese in Drinking Water and Manganese Control*, Denver, CO.

Kothari, N., 1988. Groundwater , Iron and Manganese: An Unwelcome Trio. *Water Engineering & Management*, 135(2).

Ljung, K. & Vahter, M., 2007. Time to re-evaluate the guideline value for manganese in drinking water? *Environmental health perspectives*, 115(11), pp.1533–8. Available at:

http://www.pubmedcentral.nih.gov/articlerender.fcgi?artid=2072823&tool=pmcentrez&rendertype=abstract [Accessed September 8, 2014].

Merkle, P.B., Knocke, W.R. & E, D.L.G.P., 1997. Method for Coating Filter Media with Synthetic Manganese Oxide. *Journal of Environmental Engineering*, 2(6), pp.642–649.

Merkle, P.B., 1996. Characterizing Filter Media Mineral Coatings. *Journal (American Water Works Association)*, 88(12).

Missouri Department of Natural Resources, 2007. *Total Maximum Daily Load Information Sheet: Fox River*,

Morgan, J.J. & Stumm, W., 1964. Colloid-Chemical Properties of Manganese Dioxide. *Journal of Colloid Science*, 359, pp.347–359.

National Academy of Sciences, 1973. *Manganese In the Ecosystem. In: Medical and Biological Effects of Environmental Pollutants: Manganese*, Washington DC: National Academy of Sciences.

Peng, C.-Y. et al., 2010. Characterization of Elemental and Structural Composition of Corrosion Scales and Deposits Formed in Drinking Water Distribution Systems. *Water research*, 44(15), pp.4570–80. Available at: http://www.ncbi.nlm.nih.gov/pubmed/20576284 [Accessed September 8, 2014].

Sly, L.I., Hodgkinson, M.C. & Arunpairojana, V., 1990. Deposition of Manganese in a Drinking Water Distribution System. *Applied and Environmental Microbiology*, 56(3).

Subramanian, Archana. Unpublished Data

Tobiason, J.E. et al., 2008. *Characterization and Performance of Filter Media for Manganese Control*, Denver, CO: AWWA Research Foundation.

USGS, 2011. *Trace Elements and Radon in Groundwater Across the United States, 1992-2003: U.S. Geological Survey Scientific Investigations Report 2011-5059*,

Wang, W. et al., 2012. Laboratory Study on the Adsorption of Mn on Suspended Al(OH)3(s). *Water Research*, 46.

Weng, C., Hoven, D.L. & Schwartz, B.J., 1986. Ozonation : An Economic Choice for Water Treatment. *Journal (American Water Works Association)*, 78(11), pp.83–89.

WHO, 2011. *Manganese in Drinking-Water*, Geneva, Switzerland.

Wilczak, A. et al., 1993. Manganese Control During Ozonation of Water Containing Organic Compounds. *Journal (American Water Works Association)*, 85(10), pp.98–104.

APPENDIX A: EXPERIMENTAL DATA

Benchtop Column Data

Table 7: Summary of Experimental Conditions

Experiment ID	Dates	Experimental Duration (days)	Conditions	Effleunt Free Chlorine (mg/L as Cl_2)	Mn (µg/L)	Al (µg/L)	pH
Exp 2	8/9/13 - 8/24/13	12.9	Mn Only	2.2-2.5	185	0	7.1-7.3
Exp 5	12/2/13 - 12/15/13	7.4	Mn Only	2.5-2.8	205	0	7.3-7.4
Exp 6 (Mn)	1/10/14 - 1/19/14	8.2	Mn Only	2.0-2.5	183	0	7.5-7.7
Exp 7 (Mn)	2/21/14 - 3/7/14	13.9	Mn Only	2.4-2.7	199	0	7.0-7.3
Exp 10 (Mn)	6/16/14 - 6/30/14	13.2	Mn Only	2.5-3.0	201	0	7.0-7.3
Exp 16 (Mn)	11/3/14 - 11/9/14	6	Mn Only	2.5-3.0	196	0	7.0-7.2
Exp 3	10/15/13 - 10/20/13	4.9	Particulate Al/Mn	2.5-3.0	215	320	7.3-7.5
Exp 4	11/12/13 - 11/18/13	6.2	Particulate Al/Mn	2.5-3.0	194	315	7.2-7.3
Exp 6 (Mn/Al)	1/10/14 - 1/19/14	8.2	Particulate Al/Mn	2.0-2.5	179	203	7.5-7.6
Exp 10 (Mn/Al A)	7/21/14 - 8/5/14	8	Particulate Al/Mn	2.2-2.3	205	236	7.0-7.3
Exp 10 (Mn/Al B)	7/21/14 - 8/5/14	8	Particulate Al/Mn	2.0-2.5	225	229	7.0-7.3
Exp 11 (Mn/Al)	8/18/14 - 8/28/14	9.8	Particulate Al/Mn	2.2-2.5	197	177	7.0-7.3
Exp 15	10/20/14 - 10/27/14	5.9	Particulate Al/Mn	2.5-3.0	170	150	7.0-7.3
Exp 16 (Mn/Al)	11/3/14 - 11/9/14	6	Particulate Al/Mn	2.4-2.6	205	208	7.0-7.2
Exp 13	9/16/14 - 9/29/14	11.9	Particulate Al/Mn, Discontinue HOCl	Varies	190	175	7.1-7.5
Exp 7 (Fe)	2/21/14 - 3/7/14	14	Particulate Fe/Mn	2.1-2.5	197	200 (Fe)	7.0-7.3
Exp 11 (Al Sol)	8/18/14 - 8/28/14	9.8	Soluble Al/Mn	2.5-2.7	180	10	7.3-7.5
Exp 9	5/6/14 - 5/21/14	9.3	Alternating Feed	2.4-2.7	195	Varies	7.0-7.3

Table 8: Extractable Mn, All Mn Only Experiments

	Operation Time (days)	Top Mn (mg/g)	Bottom Mn (mg/g)	Ratio Mn (Top:Bottom)
Exp 2	12.9	1.1	0.83	1.36
Exp 5	7.4	0.68	0.44	1.56
Exp 6 (Mn)	8.2	0.58	0.40	1.44
Exp 7 (Mn)	13.9	0.92	0.59	1.55
Exp 16 (Mn)	6	0.44	0.21	2.07
			Average	1.60

Table 9: Media Extraction Data for All Mn/Al Experiments

	Operation Time (days)	Top		Bottom		Ratio			
						Al:Mn Molar		Top:Bottom	
		Mn (mg/g)	Al (mg/g)	Mn (mg/g)	Al (mg/g)	Top	Bottom	Mn	Al
Exp 3	4.9	0.20	0.21	0.20	0.26	2.13	2.67	1.02	0.81
Exp 4	6.2	0.37	0.30	0.23	0.20	1.68	1.75	1.60	1.53
Exp 6 (Mn/Al)	8.2	0.73	0.72	0.13	0.14	2.01	2.21	5.50	5.00
Exp 10 (Mn/Al A)	8	1.89	1.20	0.33	0.24	1.29	1.47	5.64	4.97
Exp 11 (Mn/Al)	9.8	2.09	1.26	0.39	0.27	1.22	1.41	5.34	4.63
Exp 15	5.9	1.40	0.87	0.20	0.11	1.26	1.09	7.09	8.17
Exp 16 (Mn/Al)	6	1.55	0.97	0.09	0.05	1.28	1.09	16.87	19.82
					Average	1.55	1.67	6.15	6.42

Table 10: Media Extraction Data from Alternating Feed Experiment

	Operation Time (days)	Top		Bottom		Ratio	
						Top:Bottom	
		Mn (mg/g)	Al (mg/g)	Mn (mg/g)	Al (mg/g)	Mn	Al
Exp 9 Column A	9.3	0.74	0.093	0.50	0.045	1.49	2.08
Exp 9 Column B	9.3	3.31	0.19	0.18	0.083	18.69	2.30

Table 11: Media Extraction Data for Soluble Al Experiment

	Operation Time (days)	Top		Bottom		Ratio	
						Top:Bottom	
		Mn (mg/g)	Al (mg/g)	Mn (mg/g)	Al (mg/g)	Mn	Al
Exp 11 (Al Sol)	9.8	2.17	0.07	0.50	0.01	4.37	6.75

Table 12: Media Extraction Data from Fe Experiment

					Top:Bottom	
	Operation Time (days)	Mn (mg/g)	Al (mg/g)	Fe (mg/g)	Mn	Fe
Exp 7 (Fe) Top	14	6.6	0.088	1.63	14.19	28.09
Exp 7 (Fe) Bot	14	0.46	0.008	0.058		

Backwash Solids Data

Table 13: Sub-Fluidization Backwash Solids Analysis

Exp	Date	Run Time (days)	Cumulative Operation Time (days)	Al (mg)	Mn (mg)	Al:Mn Molar Ratio
15	20-Oct	0.5	0.5	0.042	0.003	32
	21-Oct	0.7	1.2	< 0.001	< 0.001	-
	23-Oct	1.8	3	< 0.001	< 0.001	-
	26-Oct	2	5	< 0.001	< 0.001	-
	27-Oct	1	6	0.001	0.003	0.74
16	3-Nov	0.5	0.5	0.050	0.002	42
	4-Nov	0.6	1.1	0.036	< 0.001	-
	5-Nov	1.1	2.2	0.037	0.002	37
	7-Nov	1.8	4	0.061	0.013	9.1

Table 14: Full-Rate Backwash Solids Analysis

Exp	Date	Run Time (days)	Cumulative Operation Time (days)	Al (mg)	Mn (mg)	Al:Mn Molar Ratio
10	22-Jul	1.1	1.1	2.3	0.054	86
	25-Jul	2.7	3.8	3.9	2.3	3.4
	30-Jul	2	5.9	5.0	4.8	2.2
	1-Aug	2	7.9	4.0	5.0	1.6
	5-Aug	0.1	8	0.11	0.16	1.4
15	20-Oct	0.5	0.5	0.17	0.008	43.2
	21-Oct	0.7	1.2	0.0049	0.0018	5.4
	23-Oct	1.8	3	0.019	0.042	0.9
	26-Oct	2	5	0.0053	0.011	1
	27-Oct	1	6	0.31	0.54	1.2
16	3-Nov	0.5	0.5	0.24	0.011	46.8
	4-Nov	0.6	1.1	0.41	0.018	46
	5-Nov	1.1	2.2	1.0	0.79	2.7
	7-Nov	1.8	4	0.18	0.30	1.2

Table 15: Discontinued Chlorine Backwash Solids Analysis

Exp	Date	Run Time (days)	Cumulative Operation Time (days)	Al (mg)	Mn (mg)	Al:Mn Molar Ratio
13	17-Sep	1	1	0.05	0.00	24.9
	19-Sep	1.8	2.8	1.73	1.50	2.3
	21-Sep	2	4.8	2.09	0.59	7.2
	23-Sep	1.9	6.7	1.44	0.12	24.8
	26-Sep	2.3	9	1.49	0.06	54.3
	28-Sep	2	11	0.83	0.01	124

Centrifugation/UF Data

Table 16: Summary of Centrifugation/UF Experiments

Exp ID	Date	Mn (ug/L)	Al (ug/L)	pH	Free Chlorine (mg/L as Cl2)	Separation Process
Cent/UF 1A	8/18/2014	180	0	7.05	3.00	Low-speed centrifugation Ultrafiltration
Cent/UF 1B	8/19/2014	175	175	7.00	3.00	Low-speed centrifugation Ultrafiltration
Cent/UF 2A	9/25/2014	180	0	6.91	2.50	High-speed centrifugation Ultrafiltration
Cent/UF 2B	9/25/2014	175	175	6.90	2.46	High-speed centrifugation Ultrafiltration
Cent/UF 2C	9/25/2014	0	180	6.90	2.50	High-speed centrifugation
Cent/UF 3A	10/2/2014	200	0	7.55	2.5 - 3.0	Ultrafiltration
Cent/UF 3B	10/3/2014	195	210	7.50	2.5 - 3.0	Ultrafiltration
Cent/UF 3C	10/3/2014	200	215	React: 7.50 Filter: 6.75	2.5 - 3.0	Ultrafiltration